

1<sup>st</sup> Colloquium Paper:

# **ADVANCED MATERIALS AND MECHANICAL ENGINEERING RESEARCH (CAMMER'18)**

Organized by:

Advanced Materials Characterization Laboratory  
Center for Advanced Research on Energy  
Faculty of Mechanical Engineering  
Universiti Teknikal Malaysia Melaka

Mohd Azli bin Salim  
Choong Chee Guan  
Ghazali bin Omar  
Mohd Nur Azmi bin Nordin  
Mohd Zaid bin Akop  
Muhd Ridzuan bin Mansor  
Nor Azmmi bin Masripan

1st Colloquium Paper:  
**ADVANCED  
MATERIALS AND  
MECHANICAL  
ENGINEERING  
RESEARCH  
(CAMMER'18)**

Organized by:  
Advanced Materials Characterization Laboratory  
Center for Advanced Research on Energy  
Faculty of Mechanical Engineering  
Universiti Teknikal Malaysia Melaka

Editor-in-Chief  
Mohd Azli bin Salim

Editors  
Choong Chee Guan  
Ghazali bin Omar  
Mohd Nur Azmi bin Nordin  
Mohd Zaid bin Akop  
Muhd Ridzuan bin Mansor  
Nor Azmmi bin Masripan

Penerbit Universiti  
Universiti Teknikal Malaysia Melaka

**©FIRST PUBLISHED 2018**  
Universiti Teknikal Malaysia Melaka

ISBN: 978-967-2145-13-4

All right reserved. No part of this publication may be reproduced, stored in a retrieval system, or transmitted, electronic, mechanical photocopying, recording or otherwise, without the prior permission of the University Press,  
Universiti Teknikal Malaysia Melaka

Perpustakaan Negara Malaysia

Cataloguing-in-Publication Data

Mohd Azli bin Salim, Choong Chee Guan, Ghazali bin Omar, Mohd Nur Azmi bin Nordin, Mohd Zaid bin Akop, Muhd Ridzuan bin Mansor, Nor Azmmi bin Masripan  
1st Colloquium Paper:  
Advanced Materials and Mechanical Engineering Research  
(CAMMER'18) / MOHD AZLI BIN SALIM  
ISBN: 978-967-2145-13-4

**Published and Printed in Malaysia**  
Penerbit Universiti  
Aras Bawah, Perpustakaan Laman Hikmah  
Universiti Teknikal Malaysia Melaka  
Hang Tuah Jaya, 76100 Durian Tunggal  
Melaka, Malaysia

# **Editorial Board and Reviewers**

**CAMMER18 Vol. 1 No. 1 (March, 2018)**

## **Editor-in-Chief**

Mohd Azli bin Salim

## **Editors:**

Choong Chee Guan

Ghazali bin Omar

Mohd Nur Azmi bin Nordin

Mohd Zaid bin Akop

Muhd Ridzuan bin Mansor

Nor Azmmi bin Masripan

## **Reviewers:**

Adzni bin Md. Saad

Anita Akmar binti Kamarolzaman

Noreffendy bin Tamaldin

Siti Hajar binti Sheikh Md. Fadzullah

## Table of Contents

Title and Authors	Page
Sheet resistivity and morphological analysis of silver nanoparticles-filled epoxy conductive ink By: R. Hamidi, M.A. Salim and G. Omar	1
Measurement of sheet resistivity on silver nanoparticles-filled epoxy conductive ink using thermoplastic polyurethane By: N.A.S. Mahamad Kamel, M.A. Salim and G. Omar	5
Modelling and simulation of assembled components of an integrated diffusion method By: A.N. Yusoff and M.A. Salim	8
Investigation of silver nanoparticles ink resistivity on polyethylene terephthalate By: N.A. Abd Rahim and M.A. Salim	10
Design of experiment on energy conservation using solar energy By: Choong Chee Guan, Koh Foo Hin and Saw Chun Lin	12
Product development of a fertilizer dispensing machine By: Choong Chee Guan, Robert @ Kerk Swee Tian, Saw Chun Lin and Salvinder Singh Karam Singh	14
Design of an eco-charger using wind turbine concept By: C.C. Guan, R. Yusof and S.W. Lin	16
Data extraction from impulsive muscle under preplanned gesture By: A.Y. Bani Hashim, Z. Fu, Z. Jamaludin and I.S. Mohamad	18
Electrically tested nanofluids on printed mini channels By: A.Y. Bani Hashim, I.S. Mohamad, Z.A. Syazwani, and A. Abdullah	21
Conversion of plastic waste to fuel oil using pyrolysis process By: S. Ahmad and M. Shafie	25
Effective maintenance engineering and management in welding industry By: C.G. Choong and L.F. Zakaria	27
Development of an oil trap system for wastewater handling By: Zulkifli Sulaiman, Sahrijan Ahmad and Mohd Fadhli Ahmad	30
Enriched laboratory experiments with interactive simulation By: N. I. Haris and A. Talip	32

Effects of engine sizing on battery state-of-charge for hybrid electric vehicle By: A. Md Saad, M.A. Salim, M.R. Mansor and M.Z. Akop	34
Effect of coconut shell powder in brake friction materials By: M.A.M. Daud, N. F. Bayanuddin, M. Z. Selamat and D.M. Sivakumar	36
Effect of temperature on reliability performance of electrically conductive nano – composites By: M.A. Othman and S.H.S.M. Fadzullah	38
Effects of carbon nanotube aspect ratio on the functional properties of electrically conductive adhesive By: A.M.A Raheem and S.H.S.M. Fadzullah	40
Fabrication of hybrid oil palm empty fruit bunch and kenaf reinforced epoxy composite panels at varying fiber layering sequence By: M.R. Mansor, M.A.A. Hadi, M.J. Taufiq, M.A. Salim and A. Md. Saad	42
Effect of Line Thickness Cross-Sectional Geometry to Stretchable Printed Circuit By: M.A. Suhaimi, M.Z. Azmi, N.S. Rozali, N.H. Sobri and M.Z. Akop	44
The effect of substrate surface conditions on mechanical performance of electrically conductive adhesive By: W.A.W.A. Rahman, S.H.S.M. Fadzullah and M.M. Nasaruddin	46
Thermal conductivity and heat transfer of MWCNT-OH ethylene glycol based nanofluids By: A. Abdullah, I.S. Mohamad, A.Y. Bani Hashim, M.H. Mohd Husin and S. Zainal Abidin	48
A study of ultimate load of a beam under bending By: Masniza Yusof	50
Specific heat capacity of carbon nanofiber nanocoolant By: S. Zainal Abidin, I.S. Mohamad, A.Y. Bani Hashim, N. A. B. Masripan and A. Abdullah	52
Electrical performances of graphene with different filler loading as conductive ink By: M. Mokhlis, M.A. Salim and N.A. Masripan	54
Fabrication of uniaxially aligned electrospun nanofibre using a rotating collector By: M. N. A. Hamzah and A. H. Nurfaizey	56

Effects of carbon black to electrical properties on stretchable printed circuit By: N.S. Rozali, N.H. Sobri, M.A. Suhaimi, M.Z. Azmi and M.Z. Akop	58
Conceptual design of stretching test rig for stretchable conductive ink By: M.Z. Azmi, N.H. Sobri, M.A. Suhaimi, N.S. Rozali and M.Z. Akop	61
Electrothermal performance of Ag-filled stretchable conductive ink By: A.A. Ashikin, G. Omar, N. Tamaldin, M.A. Nordin, M. Z. Akop, S.H.S.M Fadzullah, F. Che Ani Fadzullah and S. Jasmee	63
Hydrophobicity performance of thermoplastic polyurethane coated with TiO <sub>2</sub> under thermal aging effect By: S. Jasmee, G. Omar, M.N.A. Nordin, N.A.B. Masripan and A. A. Kamarolzaman	65
The effects of line width cross-sectional geometry to stretchable printed circuit By: N.H. Sobri, N.S. Rozali, M.A. Suhaimi, M.Z. Azmi and M.Z. Akop	67
The preparation and morphological investigation of polyacrylonitrile electrospun nanofibre with different loading of carbon nanotube By: N.A. Munajat, A.H. Nurfaizey and S.H.S.M. Fadzullah	69
Effect of the contact angle between mass and finite rod in transverse vibration using laminated rubber-metal spring model for automotive absorber By: S.R. Ruslan and M.A. Salim	71

# Sheet resistivity and morphological analysis of silver nanoparticles-filled epoxy conductive ink

R. Hamidi<sup>1</sup>, M.A. Salim<sup>1,2,\*</sup> and G. Omar<sup>1,2</sup>

<sup>1</sup> Faculty of Mechanical Engineering, Universiti Teknikal Malaysia Melaka, Hang Tuah Jaya, 76100 Durian Tunggal, Melaka, Malaysia

<sup>2</sup> Centre for Advanced Research on Energy, Universiti Teknikal Malaysia Melaka, Hang Tuah Jaya, 76100 Durian Tunggal, Melaka, Malaysia

\*Corresponding e-mail: azli@utem.edu.my

**Keywords:** Silver nanoparticles; conductive ink; sheet resistivity

**ABSTRACT** – This paper presents measurement of sheet resistivity of silver nanoparticles-filled conductive ink with Four-Point probe. The Four-Point probe was used to measure the sheet resistance value of the silver nanoparticle-filled epoxy conductive ink sample in ohms-per-square, then the resistivity volume is in ohms-cm, and finally the thickness of sample also be measured too. Based on the results, some percentage of conductive ink was detected the presence of the resistivity value. The highest resistivity value was detected in low percentage of conductive ink loading, while the lowest resistivity was founded in high percentage of conductive ink loading, respectively. On the other hand, the dispersion of silver nanoparticles-filled epoxy also been investigated in morphological study through light microscopy analysis. The dark spot was presumed as a silver nanoparticles, and the rest were presumed the filled epoxy

## 1. INTRODUCTION

Conductive ink, which is an ink printed to conduct electricity have been in some talk for a few years for their applications in printed electronics (PE) and flexible electronics (FE), respectively. It has the ability to print circuits on paper or some form of flexible surface through the inkjet printing technology. Although the early growth of the printed electronics industry is not as drastic as expected, there are some great demands to use these products (conductive inks) in daily activities such as cell phones, displays, smart wearable, lighting, small packaging, labels, shipping, storage or any else.

Choosing the right ink loading is a crucial successful factor for quick, simple and affordable production of PE prototypes and electronically functional prints. It is mainly based on the electrical properties of the conductive ink itself. In this experiment, the investigation in the characterization of conductive ink is related to the formulation of ink loading and preparation method of the ink samples.

The objective of this study is to investigate the sheet resistivity measurement of silver nanoparticles-filled epoxy conductive ink with Four-Point probe, and evaluate the morphological study of the conductive ink through the light microscopy analysis.

## 2. RESEARCH METHODOLOGY

### 2.1 Samples preparation

Firstly, samples of silver nanoparticles-filled epoxy conductive ink was fabricated. The silver nanoparticles acted as the filler element, epoxy as the binder and hardener were used. The materials were weighed based on the values of weight in Table 2.1. The loading of hardener was 30% of amount of binder loading while the total value in the table only included the total sum of amount of filler loading and binder loading. The total value was set at the beginning of experiment.

Table 2.1 Composition of ink loading.

Sample	Filler		Binder		Hardener (g)	Total (g)
	(%)	(g)	(%)	(g)		
1	10	0.2	90	1.8	0.54	2
2	20	0.4	80	1.6	0.48	2
3	30	0.6	70	1.4	0.42	2
4	40	0.8	60	1.2	0.36	2
5	50	1.0	50	1.0	0.30	2
6	60	1.2	40	0.8	0.24	2
7	70	1.4	30	0.6	0.18	2
8	80	1.6	20	0.4	0.12	2
9	90	1.8	10	0.2	0.06	2

After they were weighed, all three materials were mixed in a beaker and stirred for 10 minutes by using glass rod in the same direction and consistent speed. After stirring process completed, the mixture was deposited onto the glass slide by applying doctor-blading method with 0.5 cm of width gap. Then, the sample was placed in an oven with the setup of 160 °C for 60 minutes in order to preserve the adhesion between ink and the substrate. The sample was put aside until it fully dried.

### 2.2 Sheet resistivity measurement

The study of resistivity was carried on by using Four-Point probe after the ink was fully dried. For the purpose of this study, three readings of sheet resistance were taken at each constructed points of the ink track. The average values of resistivity were recorded.



### 2.3 Morphological study

This study was conducted using light microscope with 100  $\mu\text{m}$  and the magnification 5X, 10X and 20X, while the magnifications were 5x, 10x and 20x. All the results have been recorded to predict the silver nanoparticles and filled epoxy dispersion.

## 3. RESULTS AND DISCUSSION

### 3.1 Results of sheet resistivity

The Four-Point probe was been used to evaluate the sheet resistivity of the silver nanoparticles-filled epoxy conductive ink. Table 3.1 shows the values of sheet resistivity of conductive ink for sample A and sample B. These two samples basically have same filler loading and same binder. At 60% of filler, the resistivity were recorded at 150.54  $\Omega/\text{sq}$  and 369.63  $\Omega/\text{sq}$ , but by increasing the filler value, the sheet resistivity were decreased to 0.06  $\Omega/\text{sq}$  and 0.10  $\Omega/\text{sq}$  for sample A and sample B, respectively. Based on this results, the value of sheet resistivity is inverse proportional with filler loading.

Table 3.1 Total average sheet resistivity based on filler loading percentage.

Filler (%)	Average Resistivity ( $\Omega/\text{sq}$ )	
	Sample A	Sample B
60	150.54	369.63
70	37.37	36.52
80	7.77	4.29
90	0.06	0.10

At 60 % of filler loading, the average of sheet resistivity was identified. By increasing the filler loading at 70%, the sheet resistivity was recorded lower compared the previous one. The value is too different by comparing 60 % of filler. For filler loading at 80 % and 90 %, their average values of resistivity were rapidly decreased; being linked to the high amount of conducting materials composition in the ink. For the filler with highest percentage of 90 % filler loading, it was produced the highest conductivity among all the filler percentages.

Figure 3.1 indicated the percentage of filler loading from 60 % until 90 % of filler loading, the average resistivity alternately decreased as the amount of conducting materials in the sample increased. In addition, the graph illustrate the formulation of ink in term of filler loading was used in sample A and sample B which are the composition of filler and binder are same, but the sheet resistivity value is slightly different. These differences was caused by two reasons, which are printing technique and Four-Point probe measurement.

In order to produce fewer flaws of conductive tracks with good resolution, there is a need to alter the silver ink composition and some printing states. It relates to the speed of printing, which is linked to the firing frequency, the temperature of substrate and the inter-spacing interval among the dots [1].

In this case, the difference was due to the printing

technique; doctor-blading method. During the printing process, the ink was not well-distributed all over the gap between the Scotch tape on the glass slide when the blade moved across the gap due to the speed or the viscosity of ink. When the speed of blade was high, the ink may lose and not cover all over the gap region. As for the viscosity of ink, it increased as the filler content was getting higher. Ink with high viscosity was hard to print in compliance to the texture of ink; more concentrated texture.

Thus, it affected the thickness of ink tracks printed on the glass slide. Some regions may have different thickness; either thin or thick which led to the different spreads of conducting material. Silver nanoparticles on the substrate where region with high content of silver had low resistivity and vice versa.

Another factor of the difference in resistivity values was the time condition while taking the measurement by using the 4-point probe. The error happened because there was no adequate time in taking the data. Longer time was needed due to RC (resistance-capacitance) delay in the highest resistive samples. It was because, the current required more time to climb up to the value of saturation. Once the data was stable, only then a certain point of measurement can be taken and the average value can be obtained. The inconsistency of measurement time caused the resistivity values to be unstable too.

For the filler composition of 10 % until 50 %, Four-Point probe did not detect any presence of resistivity value of the printed ink as it may lack of conducting materials in the ink. It proved that by lowering the percentage of conductor filler, it reduced the conductivity and increased the resistivity as can be seen in the same figure. Therefore, they were not included in data tabulating for this analysis.

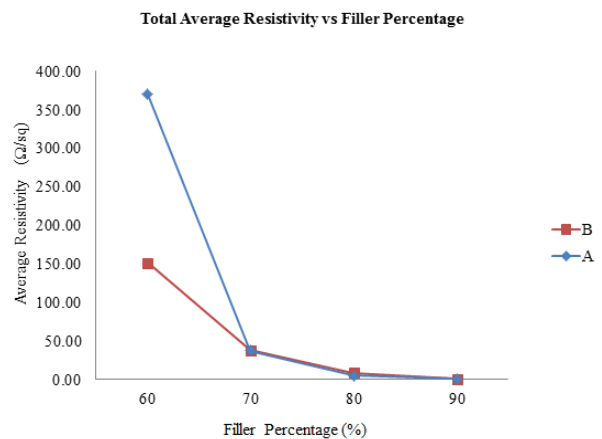


Figure 3.1 Total average resistivity versus filler percentage.

### 3.2 Comparison of standard deviation between filler percentage

There is no standard benchmarking in determining the standard deviation, but it can be determined by having the lowest value. It presents how tightly the data is gathered around the mean or average or how far the data is spread out from the mean or average.

From the table above, the data of 60 % of filler

has a very large standard deviation. It means that the data is spread out widely from the average, which indicates the highest average resistivity. The high range of values at 60 % is expected to be followed by 70 % of filler but, it shows significant difference. It has one of the lowest values among the other filler loadings. While for filler at 80 % and 90 %, the data has a small standard deviation, which tells that the data is gathered closely around the average. It proves that 80 % and 90 % of filler have the lowest and stable average resistivity

Table 3.2 Standard deviation between filler percentage.

Standard Deviation				
Sample	Filler (%)			
	60	70	80	90
A	77.82	2.69	5.29	0.08
B	289.86	7.20	1.04	0.03

### 3.3 Morphological analysis

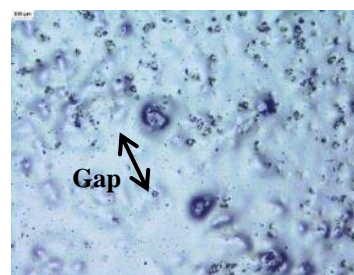
In this section, results for morphological study will be discussed in detail. The filler loading in the range of 10 % until 50 % showed no presence of conductivity while for 60 % to 90 % of filler loading exhibited the presence of conductivity. For the first assumption, the dark spot was presumed as a silver nanoparticles while the rest is the filled epoxy.

At 10 % of filler loading, the microstructure showed no appearance of silver nanoparticles element that could be traced due to lack of filler loading compared to the amount of binder and hardener. Binder and hardener conquered all over the ink track and if the conductor materials are in low quantity [2], there is no conductivity at all. Overall, the 10 % filler loading only created the formation of voids as shown in Figure 3.2.

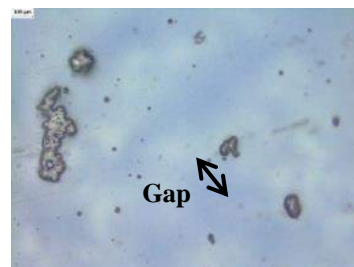


Figure 3.2 Morphological image of 10 % of filler loading on silver nanoparticles-filled epoxy.

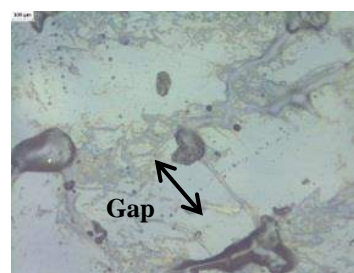
At 20 %, 30 % and 40 % of filler loadings, it showed the existence of gaps between the dark spot. The frequency of gaps was presumed gave an affected the sheet resistivity properties of the conductive ink. By increasing dark spot gap, it caused the higher resistance due to high voltage and it was required to ensure the flowing of current among the filler loading [2]. The percentage of filler loading at 50 % showed the presence of dark spot is a very minimum quantity due to the same amount of filler to binder, respectively. All the results showed in Figure 3.3.



(a)



(b)



(c)



(d)

Figure 3.3 Morphological image of (a) 20%, (b) 30%, (c) 40% and (d) 50% of filler loading.

At 60 %, 70 % and 80 % of filler loadings, it were illustrated no outstanding differences between each other either in shape of particle or size of particle compared with the filler loading at 90 %. The ink layer had the presence of granular-like particle. In order become a conductive ink, the granular particle should contain a 3-D connection of conduction that led to the existence of particle necking [3].

The necking growth provided a continuous connection and once the inter particle neck was produced, the granular-like particle became conductive although it was still porous [3-4]. All the results for 60 % to 80 % showed in Figure 3.4.

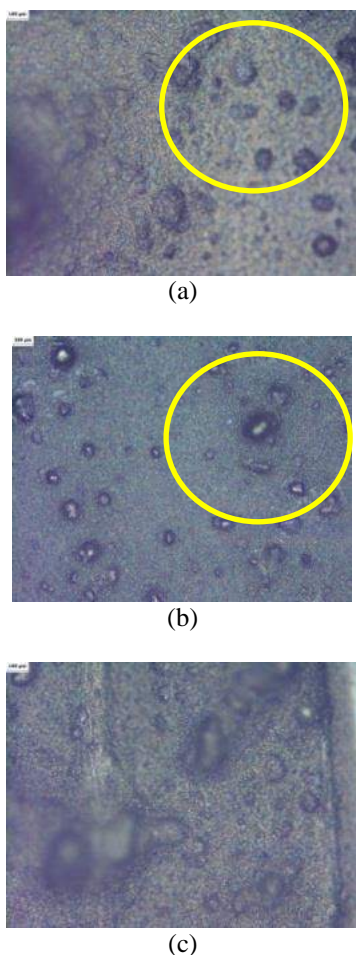


Figure 3.4 Granular-like particles in (a) 60%, (b) 70% and (c) 80% of filler loading.

At 90 % of filler loading, the dark spot in the morphological imaging represented the presence of silver nanoparticles while the rest is filled by the epoxy. Major change that could be noticed was the vanished barriers between particles [4-5]. This indicated that the ink layers had a close-packed structure where the particles created a strong bonding between each other. Once the silver nanoparticles were in contact between each other, the particles became more continuous rather than being in the shape of discrete and spherical, thus the contact area between particles became bigger.

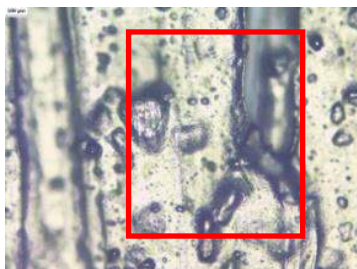


Figure 3.5 Continuous particles in 90% of filler loading.

#### 4. SUMMARY

This study was examined the sheet resistivity and morphological study on silver nanoparticles-filled epoxy conductive ink. The Four-Point probe was used to measure the sheet resistance value of the sample in ohms-per-square, the resistivity volume in ohms-cm and the thickness of sample, and light microscope was used in microscopy analysis.

From the results obtained from Four-Point probe measurement, only some percentage of filler loadings detected the presence of resistivity. The highest average resistivity of 369.63  $\Omega$ /sq was detected in 60 % of filler loading while the lowest of 0.06  $\Omega$ /sq was found in 90 % of filler loading, respectively. The characterization of silver nanoparticles-filled epoxy conductive ink in terms of sheet resistivity can be identified through the results obtained from the Four-Point probe.

Light microscope was used to visualize the morphological study of the silver nanoparticles-filled epoxy conductive. The presented results showed that ink loading with high percentage of silver nanoparticles had conductivity while low percentage had no conductivity. At low percentage, the microstructure image showed no appearance of dark spot element while for high percentage; the image showed the content of dark spot, respectively. The dark spot basically inversely proportional relationship with the sheet resistivity value.

#### REFERENCES

- [1] Kim, D., Jeong, S., Moon, J., & Kang, K. (2006). Ink-jet printing of silver conductive tracks on flexible substrates. *Molecular Crystals and Liquid Crystals*, 459(1), 45-325.
- [2] Nash, C., Spiesschaert, Y., Amarandei, G., Stoeva, Z., Tomov, R. I., Tonchev, D., & Glowacki, B. A. (2015). A comparative study on the conductive properties of coated and printed silver layers on a paper substrate. *Journal of Electronic Materials*, 44(1), 497.
- [3] Ghahremani, M., Babaei, M., & Latifi, M. (2016). Evaluating silver tracks conductivity on flexible surfaces. *Journal of Industrial Textiles*, 46(2), 530-548.
- [4] Matsuhisa, N., Inoue, D., Zalar, P., Jin, H., Matsuba, Y., Itoh, A., ... & Someya, T. (2017). Printable elastic conductors by in situ formation of silver nanoparticles from silver flakes. *Nature materials*, 16(8), 834.
- [5] Zulkarnain, M., Fadzil, M. A., Mariatti, M., & Azid, I. A. (2017). Effects of silver microparticles and nanoparticles on thermal and electrical characteristics of electrically conductive adhesives. *Journal of Electronic Materials*, 46(11), 6727-6735

# Measurement of sheet resistivity on silver nanoparticles-filled epoxy conductive ink using thermoplastic polyurethane

N.A.S. Mahamad Kamel<sup>1</sup>, M.A. Salim<sup>1,2,\*</sup> and G.Omar<sup>1,2</sup>

<sup>1</sup> Faculty of Mechanical Engineering, Universiti Teknikal Malaysia Melaka, Hang Tuah Jaya, 76100 Durian Tunggal, Melaka, Malaysia

<sup>2</sup> Centre for Advanced Research on Energy, Universiti Teknikal Malaysia Melaka, Hang Tuah Jaya, 76100 Durian Tunggal, Melaka, Malaysia

\*Corresponding e-mail: azli@utem.edu.my

**Keywords:** Silver nanoparticles; thermoplastic polyurethane

**ABSTRACT** – This paper investigate the measurement of sheet resistivity in silver nanoparticles-filled epoxy conductive ink using thermoplastic polyurethane. Firstly, this study was conducted by formulating the conductive ink samples and then carried by experimental testing. The Jandel's Four-Point probe was used to measure the sheet resistivity of silver nanoparticles-filled epoxy conductive ink. The 60 % of filler loading was chosen accordingly to the resistivity behavior and also the economic criteria. Nevertheless, the microscopy study was added to check the dark spot of the silver nanoparticle-filled epoxy conductive ink.

## 1. INTRODUCTION

Recently, there is an increased attention given on the development of conductive ink. Conductive ink is printed by using inkjet printing that can conduct electricity. Conductive inks have various applications such as in solar cells, organic light-emitting diodes (OLED), radio-frequency identification (RFID) antennas, and electronic circuits. Traditional production of circuit boards is highly time-consuming and uses too much copper. According to Lee, 2016, the traditional method has technical difficulties when applying in large area and flexible-device manufacturing process. Inkjet printing is an attractive technology for flexible devices manufacturing process. Among all the substrates, polymer has low surface energy and hydrophobic [1-2].

The substrates that is used in this study is thermoplastic polyurethanes (TPU). The TPU is thermoplastic elastomers that have many properties such as flexibility, transparency and low temperature performance. TPU is consist of soft and hard segment, which makes it a very flexible material and can be accustomed to many applications [3]. Soft segment consists of polyester or polyether type while hard segment consists of aromatic or aliphatic.

The difference in electric potential (voltage) throughout the metal in the electric field causes the electron to float towards the positive terminal. From the Ohm's law, the voltage difference across a conductor is corresponding to flow of electric current through a conductor.

The correlation between resistivity and resistance needs to be understood in describing the conductor that can be printed out [3]. Resistance can be defined as measurements for objects which opposed the electric current flow through it. The unit for resistance is ohm.

The thin and long wire has more resistance than the thick and short wire. Furthermore, resistivity is the measure of the resistance of electrical conduction for different size and material used. The shape and pattern influence the resistance, while the nature of the material influences the resistivity [3]. The correlation between resistivity and resistance is demonstrated in following equation. The measurement for the ability of substance to transmit or carry electric current is defined as electrical conductivity. The higher conductivity means the lower resistivity.

The aims of this study is to investigate the sheet resistivity of silver nanoparticles-filled epoxy conductive using TPU substrate.

## 2. RESEARCH METHODOLOGY

This section explains in details the methodology that involves in this study to achieve the research objectives. It includes the formulation preparation and testing process. This section describes how the experimental sample process is obtained.

### 2.1 Formulation preparation

The first phase for the process was selected the material and the apparatus for the experimental works. Materials used in this study are silver nanoparticles as a filler, epoxy as the binder, and finally hardener as the solvent.

The apparatus was used in this experiment are beaker, glass rod, measuring balance, spoon, glove, mask, blade, thermoplastic polyurethane and scotch tapes. Then all materials were measured by using measuring balancer according to the value recorded in Table 2.1. The total mass of silver nanoparticles is 2 g and the percentage of filler is 60 %.

Table 2.1 Composition of ink loading

Filler		Binder		Hardener (30% from binder) (g)	Total (g)
(%)	(g)	(%)	(g)		
60	1.2	40	0.8	0.24	2

The second phase was cured and printed processes. All materials were mixed slowly into a beaker and stirred by using glass rod until the filler were completely dissolved around 10 minutes. Then, the mixture was printed by using manual deposition method on TPU substrates. In addition, the printed conductive ink was pre-heated in oven for 60 minutes

at 160 °C. After that, the conductive ink was cold down at ambient temperature for two days until it was fully dried.

## 2.2 Testing

The third phase of this study is a testing works. It was carried out by taking the measurement of sheet resistance by using Jandel's Four-Point probe. At first, the Four-Point probe was calibrated before measuring the conductive ink samples. The calibration process is necessary before start the measurement, and it is defined as comparison between the standard measurement and the measurement by using the instrument. The purpose of this calibration process is to check the precision of the instrument. The following step was measured the conductive samples by placing the TPU substrates under the metal tips of Jandel's Four-Point probe.

Data readings were taken three times for each sample at different locations, and the average amount of data was calculated and recorded. Figure 2.2 shows the Jandel's Four-Point probe instrument has been used in this study.

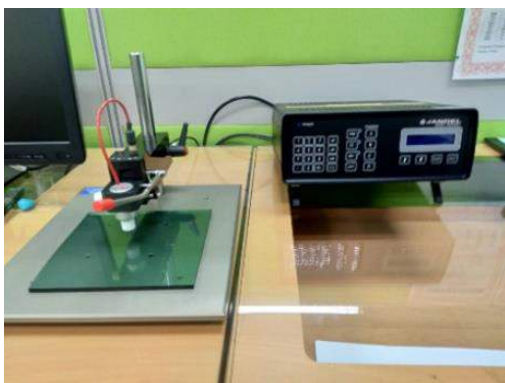


Figure 2.2 Jandel's 4-Point Probe

## 2.3 Printing method

Manual deposition method had been used to print conductive ink on substrates. TPU has been used as substrates in this study. For this method, spoon was used to apply conductive ink on the uncovered area. Then, the blade coated the substrate in upward to downward motions until the ink was evenly distributed on the substrate. The essential process after printing process was curing process. The conductive inks that had been printed on substrates were heated in the oven at 160 °C for 60 minutes. The curing temperature was set based on previous research. In previous research, silver nanoparticles based ink were heated at curing temperature over 150 °C [2]. After 60 minutes, the conductive ink was dried at room temperature for 2 days.

## 2.4 Morphological study

Morphological study is a one option to investigate the dispersion of filler and binder in conductive ink sample. First of all, the assumption is necessary which is the dark spot represents the filler and the rest presents the epoxy and hardener. The microscope scale is around 100 μm and the magnifications are from 5x

to 20x, respectively.

## 3. RESULTS AN DISCUSSION

### 3.1 Resistivity

This section discussed the data was obtained in this study. Silver nanoparticles-filled epoxy conductive ink should have good conductivity which is proportional with low resistivity to make the better. After analyzing the data, 60 % of filler for silver nanoparticles conductive ink had low resistivity and economic criteria. Table 3.1 shows the value of estimation error that had been calculated between sample A and B.

Estimation of error between true value and estimated value was examined. The formula for estimation error is shown, and the summary of estimation error is shown in Table 3.1, respectively,

$$\text{Estimation error} = \frac{Y - Z}{Z} \times 100\%$$

where, Y is a theoretical value and Z is an experimental value. Example of calculation is demonstrated as below:

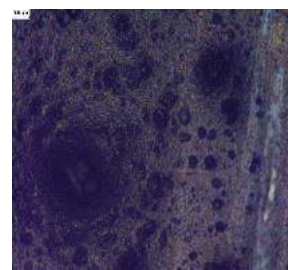
$$\text{Estimation error} = \left| \frac{108.36 - 119.89}{119.89} \right| \times 100\%$$

Table 3.1 Summary of estimation error.

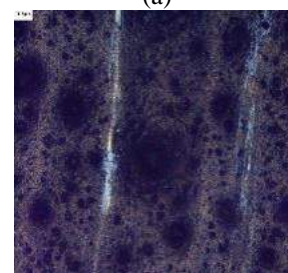
Filler (%)	Estimation Error (%)					
	Sample A			Sample B		
	1	2	3	1	2	3
60	7.06	21.16	32.23	6.41	17.46	16.23

### 3.2 Morphological study

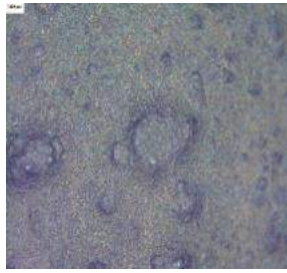
Figure 3.1 shows the morphological imaging for silver nanoparticles-filled epoxy conductive ink. The dark spot is presumed as silver nanoparticles while the bright area presumed filled by an epoxy. Overall, the silver nanoparticles was continued particle and finally gave the low resistivity.



(a)



(b)



(c)

Figure 3.1 Morphological imaging for silver nanoparticles-filled epoxy conductive ink at (a) 5x magnification, (b) 10x magnification and (c) 20x magnification.

#### 4. SUMMARY

This study was conducted to examine the sheet resistivity and the morphological effect on silver nanoparticles-filled epoxy conductive ink using TPU substrate. The 60 % filler loading was chosen as a baseline formulation due to resistivity level and economic criteria.

#### REFERENCES

- [1] Lee, S., Choi, D., Piao, H., & Son, Y. (2016). One step synthesis of Ag nano-filler for e-ink and its low temperature metallization. *Microelectronic Engineering*, 163, 98-104.
- [2] Cruz, S., Rocha, L. A., & Viana, J. C. (2016). Enhanced printability of thermoplastic polyurethane substrates by silica particles surface interactions. *Applied Surface Science*, 360, 198-206.
- [3] Mirkin, C. A., Letsinger, R. L., Mucic, R. C., & Storhoff, J. J. (1996). A DNA-based method for rationally assembling nanoparticles into macroscopic materials. *Nature*, 382(6592), 607-609.

# Modelling and simulation of assembled components of an integrated diffusion method

A.N. Yusoff<sup>1</sup> and M.A. Salim<sup>1,2,\*</sup>

<sup>1</sup> Faculty of Mechanical Engineering, Universiti Teknikal Malaysia Melaka, Hang Tuah Jaya, 76100 Durian Tunggal, Melaka, Malaysia

<sup>2</sup> Centre for Advanced Research on Energy, Universiti Teknikal Malaysia Melaka, Hang Tuah Jaya, 76100 Durian Tunggal, Melaka, Malaysia

\*Corresponding e-mail: azli@utem.edu.my

**Keywords:** Diffusion method; conductive ink; integrated system

**ABSTRACT** – This paper presents the modelling and simulation of modified microwave oven in order to improve the curing process of silver nanoparticles (AgNPs). The models of component are developed by using CATIA design part and finite element analysis is performed by using Analysis System (ANSYS). The force acting on the model is represented by ultrasonic transducer that is placed on top of microwave oven. Static structural analysis is used to show the equivalent stress and total deformation of the microwave oven structure. The results show bending effect on the microwave oven when the load is applied and require extra structural support.

## 1. INTRODUCTION

Microwave oven is known to speed up the process of heating the foods. Generally, microwaves are produced in a magnetron which it feeds by way of a waveguide into the cooking chamber. The strong interaction between electric fields of the waves and nearly free electrons of the metal causes microwave absorption become more effective. However, a few factors cause the heating temperatures inside the food become non uniform such as the location of microwave waveguide, composition of food, geometry and placement of food.

Ultrasonic is the sound wave that consists of frequencies bands above edible range of about 20,000 Hz. Basically, ultrasonic waves are produced by magneto-stiction generator or oscillator and piezoelectric generator or oscillator. Ultrasonic welding involves the joining process of metals together by using ultrasound which known as future-oriented process. The materials used such as metal is placed under low pressure and high-frequency mechanical vibrations. It creates excellent physical properties of a permanent, solid and metallurgical pure joint without thermally stressing the components.

Heating rod is a heating element which changes the electricity into heat via the resistive process. In this study, the problems of existing microwave oven are investigated to prove its capability in curing the conductive inks such as silver nanoparticles (AgNPs). The innovation of novel diffusion method involves microwave oven that combines with ultrasonic transducer and heating rod.

The purpose of this study is to develop a model of microwave oven and simulate the effects of design modification. The model is developed by using CATIA

part design and simulated by using computational software, ANSYS.

## 2. RESEARCH METHODOLOGY

### 2.1 Modelling of microwave

To produce the model of microwave oven, ultrasonic transducer, heating rod for this project, the parts were sketched in CATIA V5R20 by using part design. The dimension of each part was included in order to draw the model in accordance with the desired size. The sample of the dimension procedure is shown in Figure 2.1.

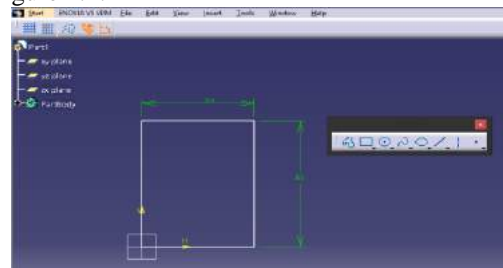


Figure 2.1 Dimension of the sample.

Firstly, the rectangular profile was sketched by considering the shape of microwave oven. Then, pad in sketch-based features was used to make it in 3-Dimensional form. Figure 2.2 below shows the sketch modelling of ultrasonic transducer, heating rod and microwave oven in CATIA part design.

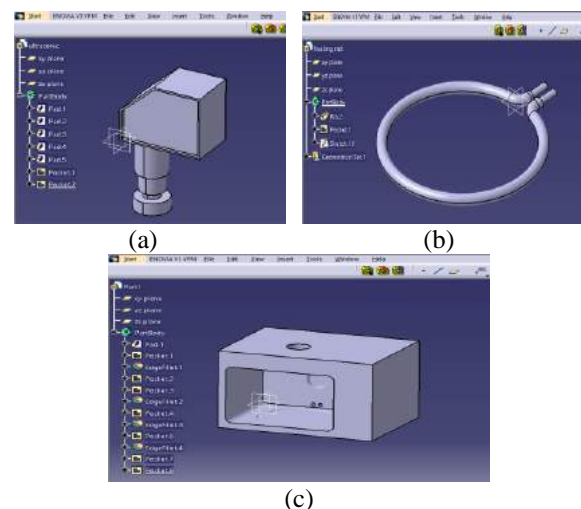


Figure 2.2 Integrated system (a) ultrasonic transducer, (b) heating rod and (c) microwave oven.

## 2.2 Simulation on microwave

To analyze the microwave oven, the computational software which known as Analysis System (ANSYS) version 18.2 was used in this project. The static structural analysis was conducted to simulate the force and stress on microwave oven when ultrasonic transducer and heating rod were inserted into it. Figure 2.3 shows the tetrahedral volume elements of mesh of microwave oven before constructing the static structural analysis.

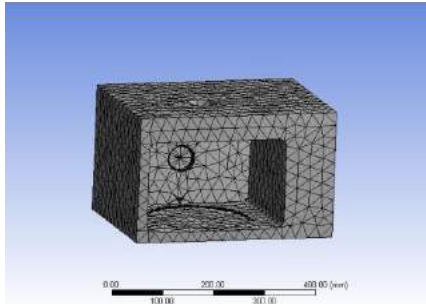


Figure 2.3 Finite element mesh for static structural of microwave oven with ultrasonic transducer and heating rod in ANSYS.

## 3. RESULTS AND DISCUSSION

In this section, results of modelling and simulation were discussed in detail. The separated parts of microwave oven, ultrasonic transducer and heating rod were assembled together to form one complete model. The process of assemble was done in 'Assembly Design' workbench. Ultrasonic transducer and heating rod were inserted into a microwave oven as shown in Figure 3.1.

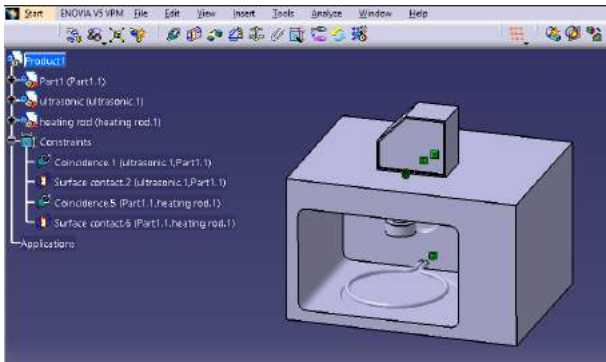


Figure 3.1 Assembly of microwave oven, ultrasonic transducer and heating rod in CATIA.

After assembly process was completed, it then simulated in ANSYS. Fixed support was set at the bottom of the microwave oven and the direction of force was facing downward. The force was represented as a load when the ultrasonic transducer was placed on top of microwave oven. Figure 3.2 shows the results of equivalent stress.

In addition, Figure 3.3 shows the results of total deformation when the distributed force of 45.5 N was applied on top of the microwave oven. There was a bending at the top center of the microwave oven which may lead to the failure of holding the load. Hence, an additional support was needed to support the top of the microwave oven from destruction due to excessive load.

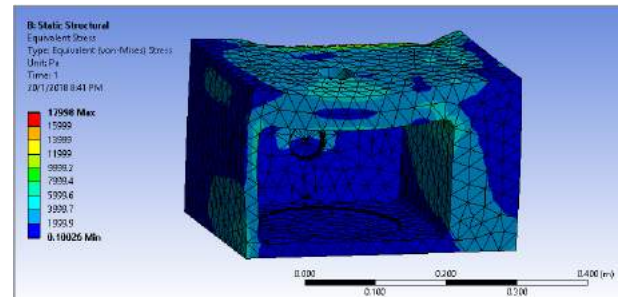


Figure 3.2 Equivalent stress on the microwave.

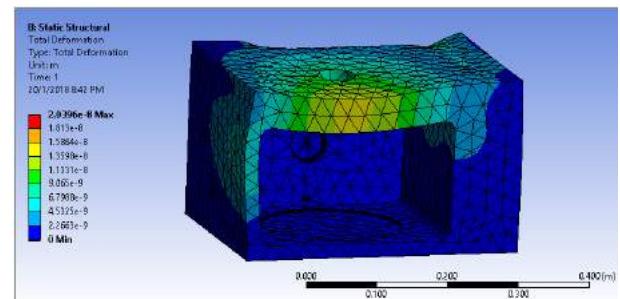


Figure 3.3 Total deformation on the microwave.

## 4. SUMMARY

This study was performed to create a model and analyse it by using simulation method of microwave oven equipped with ultrasonic transducer and heating rod. CATIA V5R20 was used to assemble these three parts by inserting ultrasonic transducer and heating rod into microwave oven. Then, the analysis was performed by using ANSYS version 18.2 to simulate the structural static strength of microwave oven with ultrasonic transducer and heating rod. Results showed the bending effect on the microwave oven when load was applied, thus required extra support to avoid the destruction of the microwave oven structure.

## REFERENCES

- [1] Vollmer, M. (2004). Physics of the microwave oven. *Physics Education*, 39(1), 74.
- [2] Geedipalli, S. S. R., Rakesh, V., & Datta, A. K. (2007). Modeling the heating uniformity contributed by a rotating turntable in microwave ovens. *Journal of Food Engineering*, 82(3), 359-368.



# Investigation of silver nanoparticles ink resistivity on polyethylene terephthalate

N.A. Abd Rahim<sup>1</sup>, M.A. Salim<sup>1,2,\*</sup>

<sup>1</sup> Faculty of Mechanical Engineering, Universiti Teknikal Malaysia Melaka, Hang Tuah Jaya, 76100 Durian Tunggal, Melaka, Malaysia

<sup>2</sup> Centre for Advanced Research on Energy, Universiti Teknikal Malaysia Melaka, Hang Tuah Jaya, 76100 Durian Tunggal, Melaka, Malaysia

\*Corresponding e-mail: azli@utem.edu.my

**Keywords:** Silver nanoparticles; polyethylene terephthalate

**ABSTRACT** – The aim of this study is to identify the effects of resistivity for silver nanoparticles conductive ink. The research was conducted by following several processes such as formulation process, curing process, and testing process. In the testing process 4-point probe is used to study the resistivity effect on the silver nanoparticles ink using a polyethylene terephthalate. The electrical properties of silver nanoparticles conductive ink can be indicated in the result show on 4-point probe.

## 1. INTRODUCTION

Conductive ink has been widely studying due to its popularity in printed electronic and the market. Conductive ink is the ink that can conduct electricity. Conductive ink is an innovation have been fabricated after research have been conducted in which able to reduce cost and faster to fabricate the electronic component [1]. There are many advantage of this technology such as its capability to print a controlled amount of ink, at high frequency and on almost any type of substrate, low cost, additive and efficient handling of expensive materials. The materials of conductive filler various in shapes and sizes which are consist of metal properties such as carbon (C), copper (C), gold (Au), and silver (Ag) particles.

There are many type of stretchable substrate that were used in conductive ink like glass slide substrate, polyethylene terephthalate (PET), thermoplastic poly urethanes (TPU), polyurethane (PUT), and poly dimethyl siloxane (PDMS). Basically, these substrate does not tend to be very smooth and have a very low glass transitions temperature (Tg). Therefore, in curing process the temperature generally under 150 °C . Another challenging is compatibility issue, this can cause to metal delamination under mechanical and thermal stress. These stretchable substrate is tending to be quite thin (1 mil to 5 mils thick), hence these substrates are easily stretch. Therefore, it is easily to get deformed when the printing process take place leading to distortion in the print image [2].

In this research, conductive ink consists of silver nanoparticles as a conductive filler, epoxy as a binder and hardener. A silver nanoparticle has been used in this due to its characteristic which are high electrical conductivity, high stability and low sintering temperature. Meanwhile, the binder was used in this study since binder provide adhesion to the substrate and cohesion to each other. The ink will print into PET

substrate. PET stands for “polyethylene terephthalate” is a type of plastic that available in many variations depending on specific applications. PET is a thermoplastic polymer and it is a naturally transparent. PET have a poor adhesion on silver nanoparticle ink, low cost substrate could be and used in many applications such as conductive ink. There are two ways to increase the adhesion PET between substrate and ink which are the wet of ink are increasing and control the composition of ink [2].

The objective for this study is to investigate the effect of resistivity study on silver nanoparticles ink using polyethylene terephthalate. The electrical properties will be studied by using a 4-point probe. The 4-point probe was used to investigate the presence of resistivity.

## 2. RESEARCH METHODOLOGY

### 2.1 Ink development

To develop the samples of conductive ink in this research, the material involved were silver nanoparticles (AgNPs) as a conductive filler, epoxy as a binder and hardener as a solvent. The total material used in this research is 2 g. All materials were weighed using a measuring cylinder. Ther percentage of silver nanoparticles used were 60% from the total weighed which are 1.2g and epoxy is 40% from the total material which are 0.8g. The quantity of hardener is 30% from the epoxy. Formulation is a material or mixture prepared according to a formula. The formulation in this stage is to mix the filler loading, binder and hardener to form a conductive ink. The stirring process is to mix the filler loading, binder and hardener until they completely dissolved. The three material which are silver nanoparticles, epoxy and hardener were stirred by using glass rod in the same direction and constant speed for 10 minutes.

### 2.2 Preparation of the ink

For the preparation of conductive nanoparticles ink, the synthesis AgNPs were deposited into a substrate this is PET by applying blade coating process. Subsequently, the synthesis AgNPs was cured using an oven at 160°C and 60 minutes in order to preserve the adhesion between ink and substrate. Finally, the last process, the sample were dry at the room temperature within one or two days until the ink fully dried and does not sticky.

### 2.3 Samples characterization

After the conductive ink form, the analysis process was conducted. The analysis process was to test the resistivity of the conductive ink by using a 4-point probe. Three reading of resistivity will be taken.

## 3. RESULTS AN DISCUSSION

In this part, results from 4-point probe will be discussed in detail. By following the required step in the previous, the conductive ink was testing the resistivity by using 4-point probe. The testing of the presence of resistivity of synthesis AgNPs were taken with three different point. Figure 3.1 shows the conductive ink printed on the substrate.



Figure 3.1 Conductive ink printed on the substrate

From the testing there is no resistivity presence on the conductive in. Even though, three difference point were testing, no resistivity presence. Thus, there are some error on this experiment. The error occurred may be caused from the curing temperature. The curing temperature for the PET must below than 150 °C or better 120 °C [2]. In this research the curing temperature used was 160 °C. Therefore, there is no resistivity presence on the conductive ink.

In this research, to obtain a good result resistivity a holistic approach needs to be considered because there are many parameter and that will be affecting the final result. The experiment should set up properly such as formulation process, printing process, curing process and analysis process, are all required for a successful process. The aspect that should be considered to obtain a successful process are proper squeegee, screen, ink substrate and the environment [3].

The factor effecting the quality of the ink such as viscosity, morphology, stability, binder system, particle distribution, size of particles, and compatibility with the substrate. Next the factor effecting the quality of the substrate are surface roughness, compatibility with ink, chemical resistance, cleanliness, mechanical strength and glass transition (T<sub>g</sub>). Besides, the factor effecting on the environment are temperature, humidity and contaminants. Therefore, the factor affecting of conductive ink should be consider getting a best result and resistivity in the experiment.

## 4. SUMMARY

This research was conducted to investigate the effect of resistivity on the silver nanoparticles using polyethylene terephthalate. The research was conducted by following several processes such as formulation process, curing process, and testing process. The 4- point probe was used to measure the resistivity of the sample in ohm-cm. From the result,

the resistivity of the sample does not present. This is because of the curing temperature is highest then the glass transition (T<sub>g</sub>) of the substrate. The properties of the electrical can be identified through the presence of resistivity from the 4 point-probe.

## REFERENCES

- [1] Rajan, K., Roppolo, I., Chiappone, A., Bocchini, S., Perrone, D., & Chiolerio, A. (2016). Silver nanoparticle ink technology: state of the art. *Nanotechnology, science and applications*, 9, 1.
- [2] Black, K., Singh, J., Mehta, D., Sung, S., Sutcliffe, C. J., & Chalker, P. R. (2016). Silver ink formulations for sinter-free printing of conductive films. *Scientific reports*, 6, 20814.
- [3] Mohammed, A. A. (2017). *Development of a New Stretchable and Screen Printable Conductive Ink* (Doctoral dissertation, University of Maryland, College Park).

# Design of experiment on energy conservation using solar energy

Choong Chee Guan<sup>1\*</sup>, Koh Foo Hin<sup>2</sup>, Saw Chun Lin<sup>3</sup>

<sup>1)</sup> Department of Mechanical Engineering, Politeknik Tuanku Syed Sirajuddin, Pauh Putra, 02600 Arau, Perlis, Malaysia

<sup>2)</sup> Department of Mechanical Engineering, Politeknik Tuanku Sultanah Bahiyah, 09000 Kulim, Kedah, Malaysia

<sup>3)</sup> Department of Mechanical Engineering, Politeknik Ungku Omar, Jalan Raja Musa Mahadi, 31400 Ipoh, Perak, Malaysia

\*Corresponding e-mail: dr.choong@ptss.edu.my

**Keywords:** Energy conservation, efficiency, magnet

**ABSTRACT** – Energy conservation is very important and efforts have been made to consume less energy, by increasing the efficiency of converted energy. In this paper, magnetic energy was used as power transmission method. A DC motor generator was used to test out the efficiency of this method. The recorded results were based on the output of DC motor generator. Different numbers of permanent magnets were used as the drive and driven disk (built to repulsive each other at 90 degrees). The results showed potential energy was needed to work the conversion continuously, thus solar energy was used as eco-energy starting potential.

## 1. INTRODUCTION

The design of experiment was to include solar panel as potential energy in order to supply the electrical energy to DC motor. This construction performed two ways of energy conversion, which was from solar energy to electrical energy and electrical energy to mechanical energy; while another energy conversion was from mechanical energy to mechanical energy which was using the magnetic energy as way of transmitting mechanical energy to electrical energy. The output of electrical energy was stored up in a super capacitor, which for future used (charging USB electronic devices).

Most people are still confused about the reality of perpetual machine concept [1]. In this experiment, the results have proved that the theory of perpetual machine cannot work. Thus, the solar panel was used to collect solar light and convert into electrical energy, while this energy was stored inside a battery for future used. To activate the system, the toggle switch can be selected to change either to store electrical energy from solar panel or to use the stored energy to run the motor.

Tools were installed inside the box. In this system, user can choose several Neodymium magnets to start with an experiment. The main part design was the two rotating disks. Each disk can be installed 1 to 12 magnet holes of Ø13mm or 1 to 3 magnet holes of Ø25mm Neodymium. Both disks were installed on the shaft of motor and generator respectively.

## 2. METHODOLOGY

Figure 2.1 shows the flow chart of the energy conversion in the system. DC generator converts mechanical energy to electrical energy. After the mechanical energy transmitted by magnetic drive from

motor to generator, the generator generates electrical energy that can be used to charge electronic devices. To smoothly activate the magnetic drive, the generator output should not connect to any electronic device before the disk rotate stably, or it will affect the torque of generator, and increase the difficulty of magnetic drive.

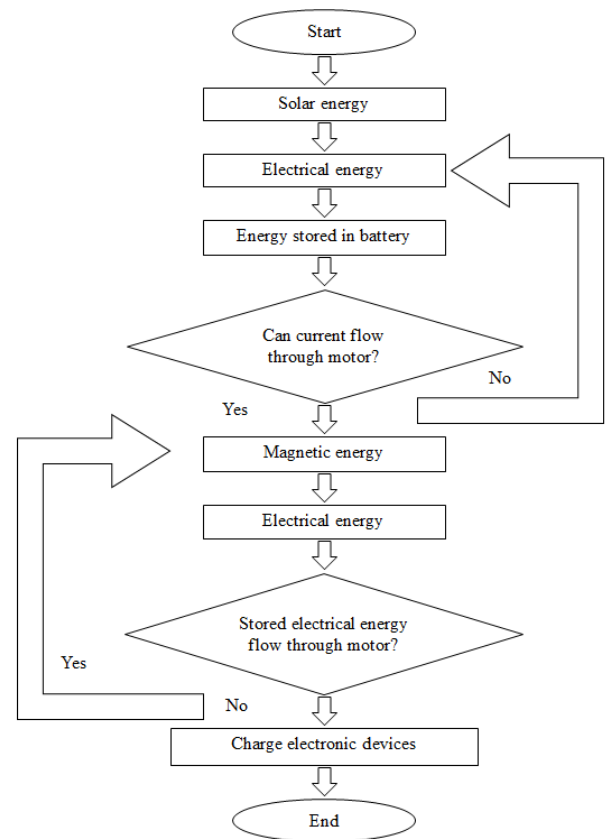


Figure 2.1 Flow chart of the energy conversion in design.

## 3. RESULTS AND DISCUSSION

The 3D printed disks were used due to more precise angle was done compared to man-work disk. The angles between each magnet holes were (12 small magnet holes) 30°. The used of different number of magnets can be calculate with the formula to estimate the distance between each magnet at a disk. To calculate the efficiency of the magnetic drive, use the theoretical output and actual output to estimate the

efficiency.

\*Important: Theory stated DC motor converted to DC generator must lost around 50% efficiency, so the maximum generated power of generator was half to the motor [2].

$$P_G = \frac{P_M}{2} \quad (1)$$

$$P_G = \frac{2W}{2}$$

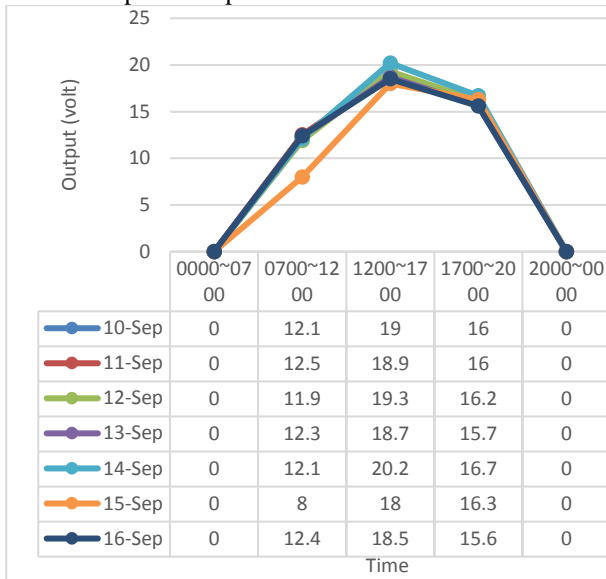
$$P_G = 1W$$

The efficiency of magnetic drive,

$$\text{Efficiency} = 2 * \frac{\text{Actual power}}{\text{Theoretical power}} * 100\% \quad (2)$$

$$\eta_G = 2 * \frac{P_A}{P_G} * 100\%$$

Table 3.1 Average solar panel output voltage at outdoor from 10 Sep ~ 16 Sep 2017.



From the Table 3.1, it showed the output of solar panel within 7 days from 10 to 16 September 2017. The table stated around 8.00pm to 7.00am is 0 volt, which was not suitable to charge the battery. The highest output of solar panel was 12.00pm to 5.00pm, which generate around 18.94 volt. After 5.00pm, the output of solar panel decreased gradually, but still acceptable for charging battery.

Assume solar panel worked with 10W, and maximum operating voltage is 21.67 volt,

Given:

$$P = 10W$$

$$V_{max} = 21.67V$$

The average voltage from 1200~1700 was 18.94V, calculate the current of solar panel within the time range.

Efficiency of voltage,

$$\eta_v = \frac{V_{actual}}{V_{max}} * 100\% \quad (3)$$

$$\eta_v = \frac{18.94}{21.67} * 100\%$$

$$\eta_v = 87.4\%$$

Efficiency of wattage,

$$P_{output} = P_{max} * \eta_v \quad (4)$$

$$P_{output} = 10W * 87.4\%$$

$$P_{output} = 8.74W$$

Output current,

$$A_{output} = \frac{P_{output}}{V_{actual}} \quad (5)$$

$$A_{output} = \frac{8.74}{18.94}$$

$$A_{output} = 0.46A$$

With the estimated output 18.94 volt and 0.46 ampere, the IC7812 was used to maintain the battery charging input to 12V. Assume there's no energy loss, calculate the estimated time to fully charge a 12V 1200mAh battery.

Estimated time,

$$t_{chrg} = \frac{mAh}{mA} \quad (6)$$

$$t_{chrg} = \frac{1200}{46}$$

$$t_{chrg} = 26.08 \text{ hours}$$

With fully charged battery 1200mAh, the motor consumed 12V, 0.3A. Estimated the motor life by using the fully charged battery,

$$t_{motor} = \frac{mAh}{mA}$$

$$t_{motor} = \frac{1200}{30}$$

$$t_{motor} = 40 \text{ hours}$$

The time of motor life equaled to time of system work. As long as the motor was activated, the output from generator can be used to charge electronic devices. When the variable resistor set to minimum resistance, the meters reading stated generator generate 2.5V, 0.6A. The output was step-up by booster to 20V.

#### 4. SUMMARY

At the end of this experiment, it is recommended that magnetic energy can be used as a type of mechanical energy transmission. This transmission method provides a very good advantage, with zero friction between two disks. Permanent magnets have its own strength, which replaced the role of teeth on the sprocket, and can increase the efficiency during energy transmission.

#### REFERENCES

- [1] Tsaousis, D. (2008). Perpetual Motion Machine. *Journal of Engineering Science and Technology Review*, pp. 53-57. (ISSN: 1791-2377)
- [2] Hambley, Allan R. (2005). *Electrical Engineering: Principles and Applications*. Pearson Education, Inc.

## Product development of a fertilizer dispensing machine

Choong Chee Guan<sup>1\*</sup>, Robert @ Kerk Swee Tian<sup>2</sup>, Saw Chun Lin<sup>3</sup>, Salvinder Singh Karam Singh<sup>4</sup>

<sup>1</sup>) Department of Mechanical Engineering, Politeknik Tuanku Syed Sirajuddin,  
Pauh Putra, 02600 Arau, Perlis, Malaysia

<sup>2</sup>) Kolej Komuniti Kota Marudu,  
Sabah, Malaysia

<sup>3</sup>) Department of Mechanical Engineering, Politeknik Ungku Omar,  
Jalan Raja Musa Mahadi, 31400 Ipoh, Perak, Malaysia

<sup>4</sup>) Faculty of Engineering and Built Environment, Universiti Kebangsaan Malaysia,  
43600 UKM Bangi, Selangor, Malaysia

\*Corresponding e-mail: dr.choong@ptss.edu.my

**Keywords:** Dispensing machine, pineapple plantation, pallet

**ABSTRACT** – The concept of this machine design is based on the current phenomenal of fertilization methods used in today's agricultural field. The amount of fertilizer required to fertilize the plants is the key element for the plant to grow healthy. Such equipment for the exact amount of fertilizer pallets to be dispensed is needed. The new machine dispenser design consists of a cup which can contain 20 grams of fertilizer pallets. The cup is attached to a mechanism below the storage tank, which a trigger is fabricated to perform the dispensing action of the fertilizer pallets. Hence, fertilizer pallets which had been dispensed travel through a flexible hose and into a metal pipe that is made to pierce the soil with ease so the fertilizer pallets can be dispensed easily into the soil. The end of the metal pipe consists of a cone like sharp pointy edge which helps agricultural workers to pierce the soil with ease. With the aid of this equipment, a single worker is able to fertilized 1 plot of pineapple plants within 8.3 hours only, hence minimizing the time required to perform fertilizing of the plants in the agricultural ecosystem and industry. Lightweight materials such as aluminum and plastic were used to construct the fertilizer storage compartment and the injector to minimize effort.

### 1. INTRODUCTION

The concept of fertilizer dispensing machine is actually based on the current phenomenal in plantation system. Workers require a lot of forcing exerting during fertilizing plants and at the same moment a lot of time is being wasted. Due to that, workers at the plantation prefer force and time saving mechanism that can eventually improve the output of plantation products solid fertilizer dispensing machine can play a big difference in the whole fertilizing process. This machine is a dispenser that can dispense pallets fertilizer which the aid of a mechanical dispensing mechanism. It is designed for commercial use therefore it is very durable, versatile and easy to use and operate. This machine is a portable fertilizer dispenser which can be carried around in the agricultural field with ease. In addition, this mechanism can also save time of employees/workers in the agricultural field in analogy to the manual method that takes prolonged amount of time to complete the fertilizing task.

### 2. METHODOLOGY

The machine is used for fertilizing pineapple plants. The tank is placed as a backpack for the user and can be adjusted for comfort ability. The lever is designed upon the reach of palms to trigger the openings at the injector while below the tank there is an isolating mechanism to isolate 20g from 16kg of contained fertilizers. This designed trigger mechanism only needed around 10N of force to dispense the fertilizer. The 10N of force is sufficient to activate the spring and cord tensions that are used to support the injector (dispensing mechanism). For a perfect fertilizing process for the plant, it is recommended that the metal rod and injector should be bent slightly as 15° angle to inject the fertilizers into the soil. This is because the injector will pierce the soil in ease [1]. There is also a support (static pedal) provided to help the injector to pierce the soil [2]. The basic steps of fertilizing processes are explained in Figure 2.1.

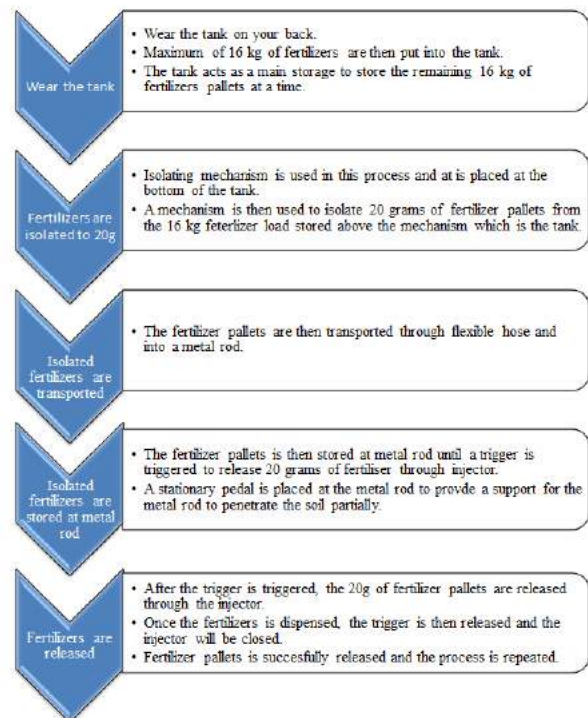


Figure 2.1 Basic steps of fertilizing processes.

### 3. RESULTS AND DISCUSSION

Manual fertilizing method consumes more time and energy compared to solid fertilizer dispensing machine as more manpower is needed. This is because there will be 2 separate methods done by 2 people. The first man will be poking the crop making a small compartment for the fertilizers followed by another man spreading fertilizers into the compartment. This method is done for many acres fertilizing more than  $\pm 10,000$  pineapple plants. The storage for this machine will be 16kg and dispenses 20g every time fertilizing.

#### 3.1 How many plants can 16 kg of fertilizers cover?

$$1 \text{ acre} = 43560 \text{ft}^2,$$

$$1 \text{ plot} = 0.5 \text{ acre} (21,780 \text{ft}^2)$$

$$1 \text{ acre} = 10,000 \text{ plants}$$

$$\therefore 0.5 \text{ acre} = 5,000 \text{ plants}$$

$$20 \text{ g fertilizes 1 plant}$$

$$16,000 \text{ g fertilizes 800 plants}$$

#### 3.2 Approximately, how long does it take to fertilize 1 acre of plantation?

Require 6 seconds to fertilize each plant using this method.

$$\text{For 1 acre (10,000 plants)} = 60,000 \text{ seconds} = 1000 \text{ minutes} = 16.7 \text{ hours}$$

$$\text{For 0.5 acre (5,000 plants)} = 30,000 \text{ seconds} = 500 \text{ minutes} = 8.3 \text{ hours}$$

$$800 \text{ plants} = 4,800 \text{ seconds} = 80 \text{ minutes} = 1.3 \text{ hours}$$

16,000 g of fertilizers can fertilize 800 plants in 1.3 hours. 1 acre (10,000 plants) will be fertilized in 16.7 hours whereas 0.5 acre (5,000 plants) can be fertilized in 8.3 hours.

#### 3.3 What is the amount of fertilizers needed?

$$16000 \text{ g fertilizes 800 plants}$$

$$1 \text{ acre} = 10,000 \text{ plants}$$

$$200,000 \text{ g fertilizers} = 10,000 \text{ plants}$$

$$200,000 \text{ g} = 200 \text{ kg of fertilizers needed to cover 1 acre of plantation}$$

#### 3.4 How many times the worker has to refill the tank to cover 1 acre of pineapple plants?

$$16,000 \text{ g fertilizers needed to fertilize 800 plants}$$

$$1 \text{ acre} = 10,000 \text{ plants}$$

$$10,000 \div 800 = 12.5 \text{ times} = 13 \text{ times}$$

The tank should be refilled with fertilizers for 13 times to fertilize 1 acre of pineapple plants.

$$\text{The worker will be working 8 hours a day,}$$

$$16.7 \text{ hours} = 2 \text{ days and 7 hours}$$

The worker needs around 2 days and 7 hours only to fertilize 1 acre of pineapple plants.

$$8.3 \text{ hours} = 1 \text{ day and 3 hours}$$

The worker needs around 1 day and 3 hours only to fertilize 1 plot of pineapple plants.

### 4. SUMMARY

The agricultural industry has developed many kinds of agricultural products and evaluation process to fulfil objectives used with all kinds of energy sources, mechanical tools and equipment design, construction development, distribution, marketing, publishing, education, operation and user-related issues.

The fertilizing dispenser is a machine that requires minimal effort to fertilize the plants in agricultural fields. Different levels of mechanization and application development had been implemented. The proposed design is able to fertilized 1 plot of pineapple plants within 8.3 hours by a single worker with dispensing rate of 20g per time, and has a storage capacity of 16kg.

Other advantages of the proposed fertilizer dispensing machine discovered in this project were:-

- (i) Minimize human labor
- (ii) Time saving
- (iii) Mobility
- (iv) Detachable
- (v) Reduce cost of hiring labours

### REFERENCES

- [1] Baker, C.J., Saxton, K.E., Ritchie, W.R., Chamen, W.C.T., Reicosky, D.C., Ribeiro, F., Justice, S.E., and Hobbs, P.R. (2007). No-tillage Seeding in Conservation Agriculture (2<sup>nd</sup> Edition). Food and Agriculture Organization of the United Nations. Cabi, USA. (ISBN: 1-84593-116-5, 978-1-84593-116-2)
- [2] Krishna, K.R. (2013). Precision Farming: Soil Fertility and Productivity Aspects. CRC Press. London. (ISBN: 78-1-4665-7829-6 (eBook - PDF))

# Design of an eco-charger using wind turbine concept

C.C. Guan<sup>1\*</sup>, R. Yusof<sup>2</sup>, S.W. Lin<sup>2</sup>

<sup>1</sup>) Department of Mechanical Engineering, Politeknik Tuanku Syed Sirajuddin, Pauh Putra, 02600 Arau, Perlis, Malaysia

<sup>2</sup>) Department of Mechanical Engineering, Politeknik Ungku Omar, Jalan Raja Musa Mahadi, 31400 Ipoh, Perak, Malaysia

\*Corresponding e-mail: dr.choong@ptss.edu.my

**Keywords:** Renewable energy; electrical energy; rotor design

**ABSTRACT** – The increasing cost and deprivation of sources for fossil fuels sparks the needs for alternative source of energy. Thus, Eco-Charger is a type of charger that uses the concept of renewable energy, in the form of wind energy. Most of the current researches mainly focusing on large scale wind turbine. In this conceptual design, a small scale wind turbine is designed specifically to produce electrical power at low speeds. Kinetic energy obtained from a moving vehicle will generate electrical power and will be used to recharge portable device. Eco-Charger is designed by using the concept of wind turbine with specified blades. The shape of the blades is designed with three blades of horizontal axis wind turbine, so it can rotate continuously at any direction of the wind. This will ease the portable-device user to recharge their device when travelling as no electrical socket is needed to be plugged in. This renewable energy source charger can reduce problems regarding environmental pollution compare to the non-renewable energy. The designs review complete picture of wind turbine blades and shows the dominance wind turbine using horizontal axis rotors. The aerodynamic principles of the modern wind turbine blade design are detailed, including blade shape, quantity, aerofoil selection and optimal attack angles.

## 1. INTRODUCTION

In the era of the future, renewable energy will be the fundamental sources to replace the non-renewable energy [1]. Renewable energy is the energy that came from the surrounding and from natural sources that will not polluting the environment. Wind energy is an example of renewable energy, where it is usually used in industry to generate electricity by using wind turbines. The designs and efficiencies have been improved from time to time to increase the power generation as the population increases. In this modern generation, portability of the necessities is important. A portable-device user sure needs a power source to recharge their device such as laptop or smartphone. Eco-Charger is designed to ease the portable-device user as it will use wind energy to recharge their devices, which mean portable-device user can recharge their device without having to plug in into any electrical socket and can use their device while travelling.

The wind system is influenced by regional and local effects, and depends on seasonal and short-time

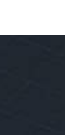


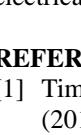
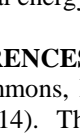
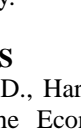
variations [2]. Modern wind turbines are mostly constructed as fast running machine with horizontal shaft, upwind arrangement and preferably three, five or seven rotor blades. In this design, to erect a wind energy system, a realistic expertise to predict the wind velocity distribution and its average at the relevant place is of foremost importance. Eco-Charger is applied at a moving vehicle, so that the turbine will rotate when there is a presence of wind. DC generator is used to convert kinetic energy of the wind turbine blade into electrical energy. DC generator of 3000 rpm is used with maximum voltage of 12 Volts. As the speed of the vehicle increases voltage generation also increases [3].

Table 2.1 Speed of vehicle and voltage generated.

Speed of vehicle	Voltage generated
10 km/h	1.2 volts
30 km/h	3.8 volts
40 km/h	5.3 volts
50 km/h	6.4 volts
60 km/h	7.5 volts
70 km/h	8.4 volts

Over the centuries many types of design have emerged, and are listed in Table 2.1. The Persian windmills, utilizing drag by means of sails made from wood and cloth, were principally similar to their modern counterpart the Savonius rotor which can be seen in use today in ventilation cowls and rotating advertising signs. Similar in principle is the cup type differential drag rotor, utilizing today by anemometers for calculating airspeed due to their ease of calibration and multidirectional operation. The American farm windmill is an early example of a high torque lift driven rotor with a high degree of solidity, still in use today for water pumping applications. The Dutch windmill is an early lift type device utilizing for grinding corn which has now disappeared from mainstream use. The Darrieus Vertical Axis Wind Turbine (VAWT) is a modern aerodynamic aerofoil blade design which despite extensive research and development has so far been unable to compete with the modern Horizontal Axis Wind Turbine (HAWT) design, although recent developments could see a resurgence of this rotor type. Due to its efficiency and ease of control, the aerofoil three bladed HAWT has become the wind turbine industry benchmark, with a fully established international supply chain securing its dominance for the foreseeable future.

Table 2.2 Examples of rotor designs [4].

Design	Orientation	Uses	Propulsion	Peak Efficiency	Diagram
Savonius rotor	VAWT	Historic Persian windmill to modern day ventilation	Drag	16%	
Cup	VAWT	Modern day cup anemometer	Drag	8%	
American farm windmill	HAWT	Farm use for pumping water, grinding wheat, generating electricity	Lift	31%	
Dutch windmill	HAWT	Use for grinding wheat	Lift	27%	
Dameus rotor	VAWT	Electricity generation	Lift	40%	
Modern wind turbine	HAWT	Electricity generation	Lift	50%	

## 2. RESEARCH METHODOLOGY

Three conceptual designs of the prototype were proposed using AutoCAD.

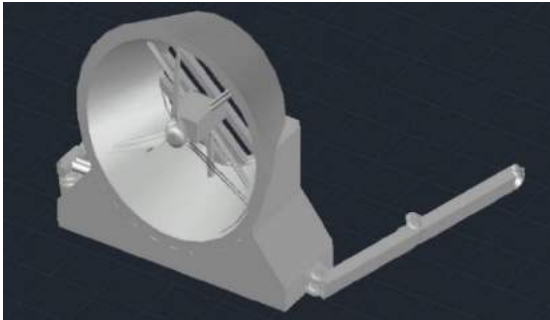


Figure 3.1 First conceptual design.

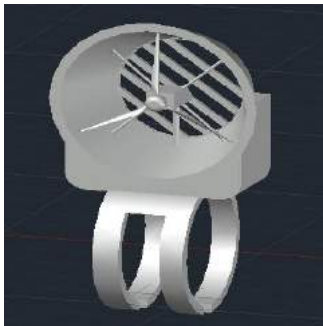


Figure 3.2 Second conceptual design.

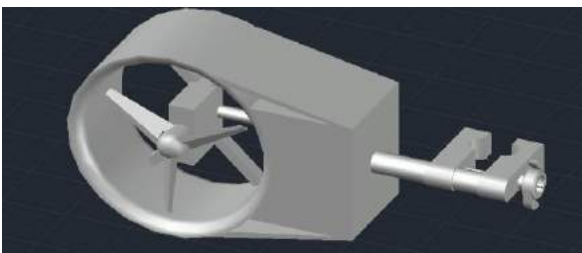


Figure 3.3 Third conceptual design.

## 3. RESULTS AND DISCUSSION

It is known that power has been extracted from wind over hundreds of years with historic designs, known as windmills and constructed from wood. The idea of Eco-Charger has been studied to use the difference angle, dimension and number of blades to increase the efficiency. The conceptual designs of the Eco-Charger can enable a larger amount of wind to be captured. This prototype is expected to generate more electricity within an average speed of a vehicle. It is expected that when the DC generator of the wind turbine will obtain a speed at around 70 km/h and is able to generate voltage up to 5 Volts.

## 4. SUMMARY

As years goes by, the non-renewable energy sources kept on decreasing to the level. Hence, initiatives are taken to preserve the world for the future generation, which is by using renewable energy sources. By using renewable energy sources, problems such as environmental pollution can be reduced. Eco-Charger is designed using the concept of wind energy, where it is much easier to capture wind, when there is a moving vehicle and from kinetic energy, can be changed into electrical energy.

## REFERENCES

- [1] Timmons, D., Harris, Jonathan M. and Roach, B. (2014). The Economics of Renewable Energy. Global Development And Environment Institute, Tufts University.
- [2] Manwell, J.F., McGowan, J.G. and Rogers, A.L. (2009). Wind Energy Explained: Theory, Design and Application. *John Wiley and Sons Ltd.* (ISBN: 978-0-470-01500-1)
- [3] N Raghu Ram Reddy, Yeshala Sreekanth, and .M. Narayana. (2013). Mechanical and Electrical Mobile Charger. *International Journal of Engineering Research and Applications, Vol. 3 Issue 6, pp. 1705-1708.* (ISSN: 2248-9622)
- [4] Schubel, Peter J. and Crossley, Richard J. (2012). Wind Turbine Blade Design. *Energies, 5, 3425-3449, doi:10.3390/en5093425.* (ISSN: 1996-1073)



# Data extraction from impulsive muscle under preplanned gesture

A.Y. Bani Hashim<sup>1</sup>, Z. Fu<sup>1</sup>, Z. Jamaludin<sup>1</sup> and I.S. Mohamad<sup>2</sup>

<sup>1</sup>Faculty of Manufacturing Engineering, Universiti Teknikal Malaysia Melaka, Hang Tuah Jaya, 76100 Durian Tunggal, Melaka, Malaysia

<sup>2</sup>Faculty of Mechanical Engineering, Universiti Teknikal Malaysia Melaka, Hang Tuah Jaya, 76100 Durian Tunggal, Melaka, Malaysia

\*Corresponding e-mail: yusairi@utem.edu.my

**Keywords:** Electromyography; raw EMG; muscle contraction; forearm

**ABSTRACT** – Electromyography signals are obtainable from the contraction of the human muscles, based on the human movements. The human forearm muscles consist of Brachioradialis muscle, Pronator Teres muscle, Flexor Carpi Radialis muscle, Palmaris Longus muscle, Flexor Carpi Ulnaris muscle and Extensor Carpi Ulnaris muscle. All those muscles are responsible for the movement of the human forearm. By performing specific hand gestures, the contraction of the muscles was captured through the raw electromyography signals. The study aimed to learn from the raw signals by looking at how each burst was unique from another about a muscle that was producing the signal. The Myonator—an in-house developed device that collects and reads the signals, was used to record the muscle contraction from hand gestures of four subjects. The plots from the recorded data were obtained through LabVIEW. The results show that specific burst patterns distinctively identify specific muscles contraction. Therefore, mapping the burst patterns to some muscles is proven viable.

## 1. INTRODUCTION

The data extraction of electromyography (EMG) signal is obtainable from the movement of the forearm which results in the contraction of the muscles. The human-machine interface will be satisfied when the signals are attainable where the signals are used as an input means to control a particular machine, for example, a robot arm.

The method is required to obtain the electromyography signals is by placing the electrodes on the experimental subject's forearm to extract the surface electromyography (sEMG) signals. Whenever the forearm moves, some EMG signals will be captured.

The affecting factors in this study is that a person has a different type of skin type and muscle composition that affect the reading of the EMG. Therefore, this study sought to learn from the raw EMG signals that how each burst was unique from another about a muscle that was producing the signal. It was hypothesized that mapping the burst patterns to some muscles is possible.

The classification and extraction of individual motor unit action potentials from intramuscular electromyographic signals show that EMG raw signals are needed to be extracted first to proceed to the classification of the signals [1]. In fact, the accuracy of EMG classification could be improved further by the inclusion of an accelerometer to monitor wrist movement [2].

A low-cost testing system was developed to perform the pattern-recognition-based control strategies, which can be used in the real-time operation [3]. There is a mutual relationship between electroencephalogram and electromyogram signals due to the time delay of information flow [4]. It shows that a shorter time delay was obtained when subjects were performing the active exercise with movement intention rather than performing the passive activity without movement intention.

The integration between electroencephalogram and electromyogram could benefit the patients with a nerve disorder. Electromyography signals have long been used for the benefits of sports science [5]. It is stated that electromyographic fatigue threshold is a correlation of critical power and torque or force limits. It establishes general exercise intensities below which neuromuscular fatigability is negligible and unpredictable. Moreover, usage of EMG signals are found in the medical field where the signals were used as the examined signals in EMG-EMG coherence function analyses and EMG-EMG transfer function. In some other study [6], while chewing gum, the physiological features of the rhythmically coordinated jaw and neck muscle EMG activities were studied using EMG-EMG transfer function and EMG-EMG coherence function analyses in 20 healthy subjects.

On the other hand, investigation done by [7] supports the sports field. During the golf swing, it explores the relationship between the patterns of EMG signals recorded from eight muscle regions of forearms and shoulders, and the patterns of peak rotational speed of thorax, pelvis, and arm, and. By doing so, golfer's injuries could be minimized by learning the EMG signal patterns. In [8], the extraction of the motor unit profile which is the representation of the trajectories of negative and positive turns of a scanning-EMG signal was studied. With the success of motor unit profile extraction, an algorithm was developed that has been able to detect turns of the scanning-EMG signal and would then link them by using point tracking techniques. Also, analyzing the algorithm's behavior and the influence of the algorithm's parameters and determining which parameter values provide the real scanning-EMG signals did the best performance.

The current pattern recognition and machine learning using EMG signals have several inherent problems regarding the gait subphase detection [9]. It is shown that electromyogram with a signal graph matching algorithm has good timing characteristics of

EMG signals as compared to the algorithm for time-domain feature extraction.

Human body gestures play an important role in determining the EMG signals as gestures such as wrist flexion, double wrist flexion, hand closing and hand opening. All of these gestures are found to be important and can be used to control a prosthetic terminal based on the hand gestures [10]. In [11], a combination of surface and intramuscular recordings are used so that investigation could be done to compare the action potentials from gastrocnemius and soleus which are represented in sEMG with various inter-electrode distances. The results stated that by reducing inter-electrode gap could result in the detection of sEMG to be insensitive to gastrocnemius activity without substantial attenuation of soleus crosstalk.

In [12], a regression model which relates the multichannel surface EMG signals to human lower limb flexion/extension joint angles was constructed. They have proved that their proposed model can form human-machine interaction interface which will then lead to continuous bioelectric control and not to mention further improve human and machine motion stability such as for lower limb wearable, intelligent equipment.

## 2. RESEARCH METHODOLOGY

The first step of analyzing the electromyography signals is to obtain and record the signals before examining them. Different hand gestures are required so that experiment could be done to secure the electromyography signals. The order of performed hand gestures throughout the test was, starting from the flex, extend, abduct, adduct, open and close finger, an 'OK,' and a thumb up. The approach to get the EMG signal is by using a named Myonator which will be connected to the electrodes that are placed on the skin of the experimental subjects.

The experiments were conducted by using gel electrodes attached to Myonator (an in-house developed EMG measurement tool, see Fig. 1(a)), which was connected to Ni-DAQ LabVIEW (see Fig. 1(b)). There were more subjects participated but for simplicity, this study reported the results obtained from four subjects, two of whom were female.

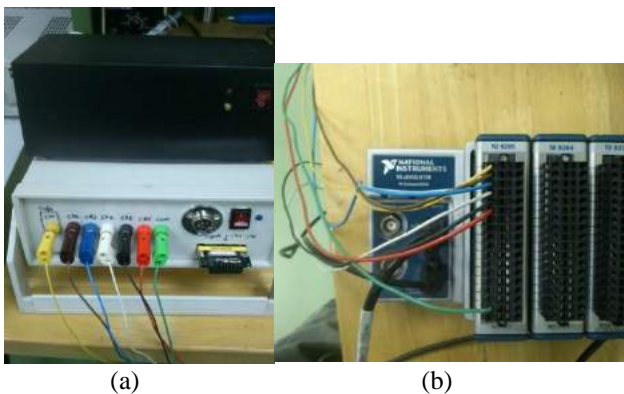


Figure 1 (a) The Myonator has six channels where each channel is connected to a set of three electrodes, (b) Ni-DAQ LabVIEW is a data acquisition device that allows smooth data transmission between hardware and

dynamic signal analyses using its computational tools.

The subjects were taught on the preplanned gestures. They would act the gestures upon instructed. They were prepared for the electrodes installation on their forearm where their skin of the essential areas would be clean before the arrangement took place. The electrodes (six sets) were placed at the selected locations encasing the forearm.

## 3. RESULTS AND DISCUSSION

Results showed that there were nine bursts of EMG signals following the order of hand gestures. Figures 2(a), 2(b), and 3(a) exhibited somewhat similar patterns, whereas Fig. 3(b) showed distorted signals.

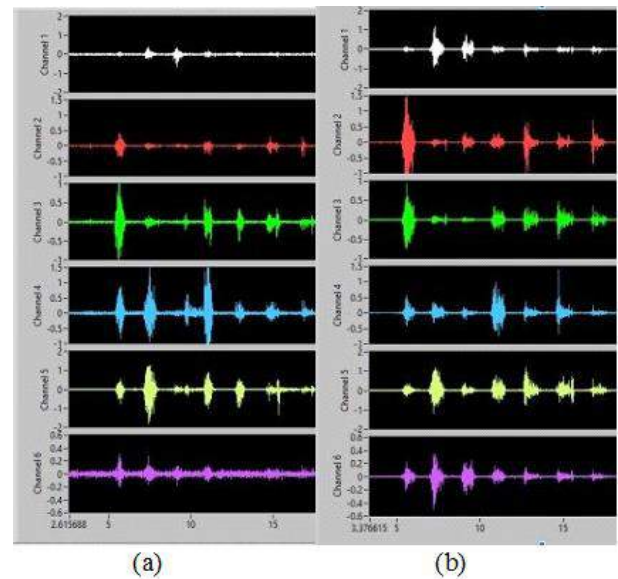


Figure 2 (a) Raw EMG recorded from subject-1 (male), (b) subject-2 (male). It is noticed that although both subjects acted the same preplanned gestures, the data showed that each subject produced a unique set of burst, especially the spikes.

The apparent cause of EMG signal from Fig. 3(b) was due to subject-4 herself. It was suspected that the subject who is a female did not apply enough energy when performing the hand gestures. Because the subject has thin arms, the electrodes were placed very close to one another. Signal chattering could have had happened resulted in the strange bursts at channel 4 (see Fig. 3(b)). The apparent burst of signals seen in Fig. 3(a), Fig. 2(b), and Fig. 3(a) was from the flexing hand gesture, which contracted the Flexor Carpi Radialis and Palmaris Longus muscles. The burst train (successive bursts) of the digital-analog code of 011000 was noticed in Fig. 2(a), Fig. 2(b), Fig. 3(a).

The second noticeable burst train was the extending hand gesture that contracted the Brachioradialis muscle yielded the digital-analog code of 100111 for Fig. 2(a), Fig. 2(b), Fig. 3(a), which was opposite of flexing hand gesture. It was believed that the reverse digital-analog code was the effect of the particular muscles that are situated at the different end of the forearm. The muscles contract oppositely from one other.

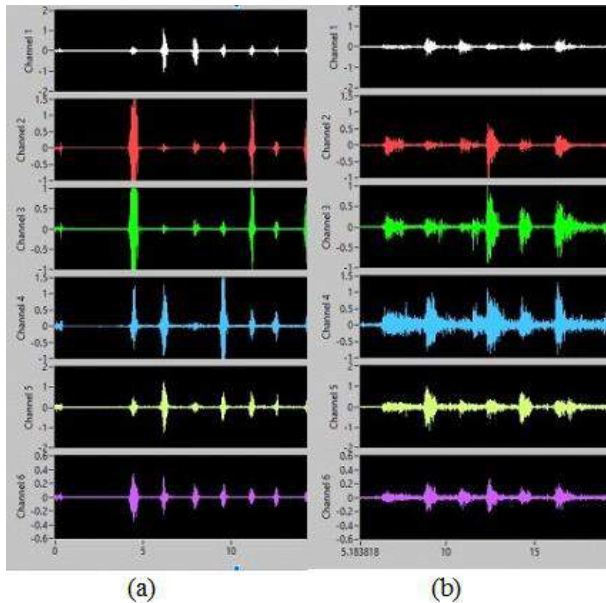


Figure 3 (a) Raw EMG recorded from subject-1 (male), (b) subject-2 (male). It is noticed that although both subjects acted the same preplanned gestures, the data showed that each subject produced a unique set of burst, especially the spikes.

#### 4. SUMMARY

The EMG signals were successfully collected using the Myonator. The results showed that on different body gestures would produce unique EMG signals where specific burst patterns distinctively identify particular muscle contraction. Therefore, mapping the burst patterns to some muscles was proven viable.

#### ACKNOWLEDGMENT

This work was supported in part by the Universiti Teknikal Malaysia Melaka under Grant FRGS/2/2013/SG02/FKP/02/2/F00176.

#### REFERENCES

- [1] Katsis, C. D. (2006). A novel method for automated EMG decomposition and MUAP classification. *Artificial Intelligence in Medicine*, 37(1).
- [2] Khushaba, R.N., Al-Timemy, A., Kodagoda, S., & Nazarpour, K. (2016). Combined influence of forearm orientation and muscular contraction on EMG pattern recognition. *Expert Systems with Applications*, vol. 61, pp. 154-161.
- [3] Akhmadeev, K., Rampone, E., Yu, T., Aoustin, Y. (2017). A testing system for a real-time gesture classification using surface EMG. *IFAC-PapersOnLine*. 50(1), pp. 11498–11503
- [4] Kim, B., Kim, L., & Kim, Y.H. (2017) Cross-association analysis of EEG and EMG signals according to movement intention state. *Cognitive Systems Research*. 44, pp. 1–9.
- [5] McCrary, J.M., & Ackermann, B.J. (2017). EMG amplitude, fatigue threshold, and time to task failure: A meta-analysis. *Journal of Science and*

*Medicine in Sport*. In press.

- [6] Ishii, T., Narita, N., & Endo, H. (2016). Evaluation of jaw and neck muscle activities while chewing using EMG-EMG transfer function and EMG-EMG coherence function analyses in healthy subjects. *Physiology & Behavior*, vol. 160, pp. 35-42.
- [7] Verikas, A., Parker, J., & Bacauskiene, M. (2017). Exploring relations between EMG and biomechanical data recorded during a golf swing. *Expert Systems with Applications*. 88, pp. 109–117.
- [8] Corera, I., Malanda, A., Rodriguez-Falces, J., & Porta, S. (2017). Motor unit profile: A new way to describe the scanning-EMG potential. *Biomedical Signal Processing and Control*. 34, pp. 64–73.
- [9] Ryu, J. (2017). Real-time gait subphase detection using an EMG signal graph matching (ESGM) algorithm based on EMG signals. *Expert Systems with Applications*. Pergamon, 85, pp. 357–365.
- [10] Tavakoli, M., Benussi, C., & Lourenco, J.L. (2017). Single channel surface EMG control of advanced prosthetic hands: A simple, low cost and efficient approach. *Expert Systems with Applications*, vol. 79, pp. 322-332.
- [11] Vieira, T. M., Wakeling, J.M., & Hodson-Tole, E. (2016). Is there sufficient evidence to claim muscle units are not localised and functionally grouped within the human gastrocnemius? *J Physiol*, 594: pp. 1953-1954.
- [12] Chena, J., Zhanga, X., & Cheng, Y. (2017). Surface EMG based continuous estimation of human lower limb joint angles by using deep belief networks. *Biomedical Signal Processing and Control*. 40, pp. 335–342.

# Electrically tested nanofluids on printed mini channels

A.Y. Bani Hashim<sup>1</sup>, I.S. Mohamad<sup>2</sup>, Z.A. Syazwani<sup>2</sup>, A. Abdullah<sup>2</sup>

<sup>1</sup>Faculty of Manufacturing Engineering, Universiti Teknikal Malaysia Melaka, Hang Tuah Jaya, 76100 Durian Tunggal, Melaka, Malaysia

<sup>2</sup>Faculty of Mechanical Engineering, Universiti Teknikal Malaysia Melaka, Hang Tuah Jaya, 76100 Durian Tunggal, Melaka, Malaysia

\*Corresponding e-mail: yusairi@utem.edu.my

**Keywords:** Mini channel; hydraulic diameter; carbon nanotube; carbon nanofiber

**ABSTRACT** – The behavior of nanofluids bathed in constricted channels was observed by exciting these fluids with a low electrical potential. It was hypothesized that currents should flow through them because carbon is naturally a semiconductor. The results showed little currents were flowing in the circuit as the fluids recorded high resistances. However, the real nature of the fluids exposed to electrical potentials for a longer duration was still unknown.

## 1. INTRODUCTION

### 1.1 Experimental channel

Experimental channels (ECs) are canals that deliver chemical samples or analytes. The channels can be fabricated in polymers, silicon, glass, and metals. As such, the corresponding dimensions of the channel should be exceedingly small. There are various processes used to fabricate an EC that include surface micromachining, molding, bulk micromachining, embossing and micro cutting.

In general, there are two types of ECs. One is a channel for fluid control, and the other one is for heat transfer. The ECs have important applications in microdevices. It is due to their high surface-to-volume ratio and their small volumes [1]. The fluid flow and heat transfer in ECs have various applications in electronics, bioengineering, advanced fuel cells, and micro heat exchangers.

Channels are human-made systems. The transport processes occur across the channel walls. Meanwhile, the bulk flow takes place through the cross-sectional area of the channel. Thus, the channel cross-section acts as a duct to transport fluid to or away from the channel walls.

A channel aims to fulfill two objectives; First is to bring fluid into close contact with the channel walls and second is to bring fluid to the walls and remove fluid away from the walls as the transport process is achieved.

The rate of the transport process of the fluids depends on the surface area. For a circular tube, the surface area is varied with the diameter. Meanwhile, the flow rate depends on the cross-sectional area. Thus, this varies linearly with the square diameter, which means the tube surface area to volume ratio changes as the reciprocal of the diameter. When the diameter is decreased, surface area to volume ratio is increased. The diameter that affects the channel is called the hydraulic diameter [2].

The channel classification is based on the

hydraulic diameter. A smaller channel size has different effects on different processes. Table 1 lists the classification with their respective hydraulic diameters range. Equation (1) defines the hydraulic diameter of a rectangular channel where B is the width and C is the depth of the channel.

$$D_H = \frac{2BC}{B+C} \quad (1)$$

Table 1 The channel classification scheme [2]

No	Channel type	Hydraulic diameter, $D_H$
1	Conventional	$D_H > 3mm$
2	Mini	$200\mu m < D_H \leq 3mm$
3	Micro-	$10\mu m < D_H \leq 200\mu m$
4	Transitional micro-	$1D_H < D_H \leq 10D_H$
5	Transitional nano-	$0.1\mu m \leq D_H \leq 1\mu m$
6	Nano-	$D_H \leq 0.1\mu m$

### 1.2 Nanoparticles

Among nanoparticles, carbon nanotubes (CNT) has the highest thermal conductivity. Macroscopic assemblies of CNTs seem to be advantageous as lightweight and highly conductive wires can be obtained. Nanofluids are considered as a passive technique, but also a promising way for advanced thermal fluid science. Any efforts to deploy them as heat transfer fluids by dispersing them into any kinds of base fluids called CNT nanofluids [3].

In preparing for the CNF-based nanofluid, the CNF powder was mixed with the base fluids containing ethylene glycol and deionized water to synthesize the CNF-based electrode. The reason for using ethylene glycol (EG) and deionized water (DW) as the base fluid was because they are the primary liquid base for convective heat transfer [4].

This work sought to observe how the nanofluids respond to electricity on constricted channels by exciting these fluids with a low electrical potential.

## 2. RESEARCH METHODOLOGY

### 2.1 Channel development

The channels were fabricated using the Vagler 3D printer. Before the channel was printed, their shape must be drawn. The outline of the channels is of an S-shape. SolidWorks was utilized to construct the channels in the 3D model. The model was later being sliced into a large number of horizontal layers. The file would be uploaded to the 3D printer.

Table 2 lists the channels' dimensions. Channel-2

is much smaller than channel-1, regarding, the hydraulic diameter. Both of the channels are categorized as mini channels as their hydraulic diameter falls with the range shown in Table 1. Figure 1 shows the printed mini-channels.

Table 2 The channel's basic dimensions. Based on the values of the hydraulic diameter, we categorize our channels as mini channels, according to the listing of Table 1.

Channel №	Length (mm)	Width (mm)	Depth (mm)	Hydraulic diameter (mm)
1	284	2	5	2.86
2	284	1	5	1.67

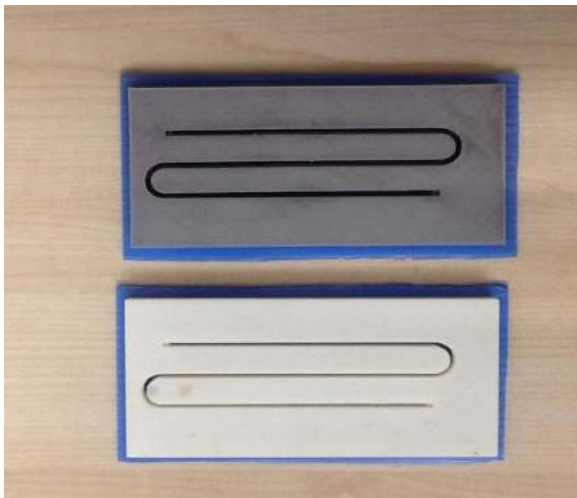


Figure 1 The mini-channels that were produced by 3D-printing using ABS filament. Channel-1 (above, gray) hydraulic diameter is 2.86 mm while channel-2 (below, white) hydraulic diameter is 1.67 mm.

**2.2 Nanoparticle preparation**

Figure 2 shows nanofluid samples with respective percent weight used in this work. There are three CNT-based and another three CNF-based liquids. The bottles labeled with green stickers that mark the respective liquids according to the percent weight. The samples have different values of concentration. From left the concentration in %wt for each sample fluid are: CNF\0.3, CNF\0.6, CNF\0.9, CNT\0.3, CNT\0.6, CNT\0.7.

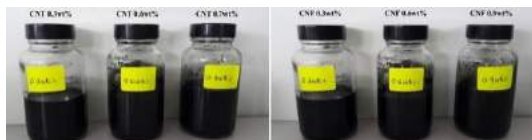


Figure 2 The samples of CNT and CNF used in the experiment.

**2.3 Experimental setups**

A direct current power supply of low voltage was used to provide the potential across the circuit depicted in Figure 4. The schematic is showing the power supply, the standard resistor (R1), the channel that holds the

fluid resistant (R2), and how the electrical behavior would be evaluated. The supply voltage was a fixed 5V.

The equipment used in assessing the samples electrical response was the Digilent Analog Discovery (DAD), the AMPROBE PM51A multimeter, a generic digital multimeter, and general model analog and digital multimeters. The DAD provides a USB Oscilloscope and power supplies. So, the power supply came from the DAD while the measurement from the DAD and also the multimeter. The generic multimeter was used to check for circuit continuity.

A low voltage supply would induce stress to the bathed channel (R2) so that how the fluid would respond to the electrical potential across it may be observed. There is a standard resistor (R1) connected in series with the channel. It works as a transducer that would confirm the existence of current flow in the circuit by measuring the voltage across it.

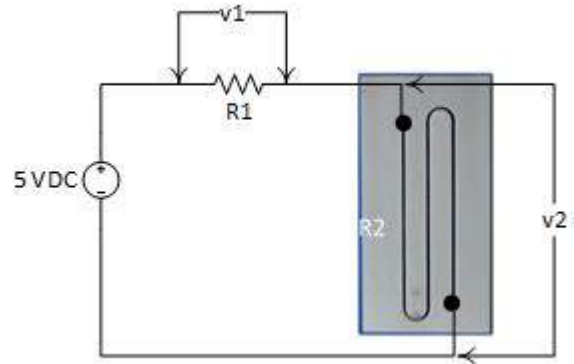


Figure 3 The schematic used to run the tests.

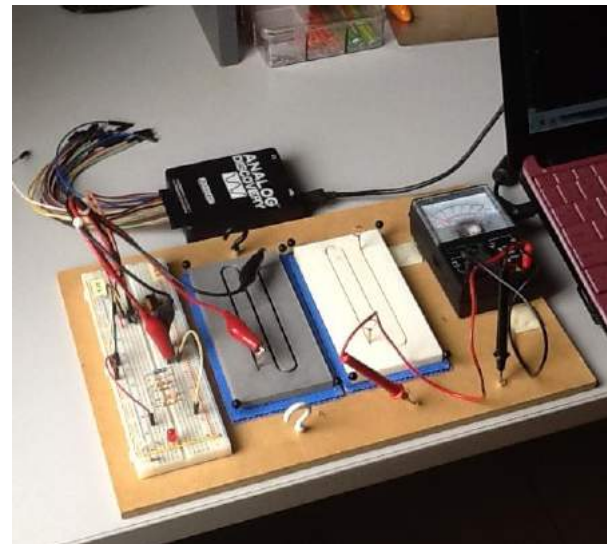


Figure 4 The resistances obtained by direct measurement on the channels bathed with the samples.

**3. RESULTS AND DISCUSSION**

Table 3 lists the results for CNT of 0.3% wt. Since the sample has high resistance, the voltage drop across it was high enough comparable to the supply voltage. The only observable potential was found across R1 because of very small resistance relative to R2. The

results showed that as the resistance of R1 increased the voltage drop across it also showed the same symptom. At the same time, the potential across R2 slowly decreased. The current, however, did not exhibit drastic change. Throughout all the tests, the current was reaching saturation.

The results in Table 3 to Table 8 summarize the behavior of the nanofluids of different concentration when excited by a low voltage power source. Tiny currents were recorded flowing in the circuit. The phenomenon was apparently due to a low potential and a very high overall circuit resistance.

The voltage drops were obtained by direct measurement using a multimeter on the simple network that consists of a power supply and an assortment of resistors in series with the bathed mini-channels. The channels act as a resistor module, R2. When tested on channel-1, the sample of CNTs exhibit increased in the current flow as the liquid concentration decreased. Also, CNFs exhibit increased in the current flow as the liquid concentration decreased.

Table 3 CNT of 0.3% wt.

Actual Resistance $R_1$ ( $\Omega$ )	In series with Channel 1			In series with Channel 2		
	$v_1$ (mV)	$v_2$ (V)	$i$ ( $\mu A$ )	$v_1$ (mV)	$v_2$ (V)	$i$ ( $\mu A$ )
40.90	0.30	5.00	7.33	0.10	5.00	2.44
56.50	0.40	5.00	7.08	0.20	5.00	3.54
217.20	2.40	4.99	11.05	1.40	4.99	6.45
466.00	5.60	4.99	12.02	3.20	4.99	6.87
994.00	12.30	4.98	12.37	10.60	4.98	10.66

Table 4 CNT of 0.6% wt.

Actual Resistance $R_1$ ( $\Omega$ )	In series with Channel 1			In series with Channel 2		
	$v_1$ (mV)	$v_2$ (V)	$i$ ( $\mu A$ )	$v_1$ (mV)	$v_2$ (V)	$i$ ( $\mu A$ )
40.90	0.1	5.00	2.44	0	5.00	0.00
56.50	0.4	5.00	7.08	0.3	5.00	5.31
217.20	2.1	5.00	9.67	1.4	5.00	6.45
466.00	4.9	4.99	10.52	3.3	4.99	7.08
994.00	10.6	4.98	10.66	7.4	4.99	7.44

Table 5 CNT of 0.7% wt

Actual Resistance $R_1$ ( $\Omega$ )	In series with Channel 1			In series with Channel 2		
	$v_1$ (mV)	$v_2$ (V)	$i$ ( $\mu A$ )	$v_1$ (mV)	$v_2$ (V)	$i$ ( $\mu A$ )
40.90	0.2	5.00	4.89	0.1	5.00	2.44
56.50	0.3	5.00	5.31	0.3	5.00	5.31
217.20	1.7	4.99	7.83	1.5	4.99	6.91
466.00	3.9	4.99	8.37	3.3	4.99	7.08
994.00	8.9	4.99	8.95	7.4	4.99	7.44

Similarly, when tested on channel-2, the sample of all CNTs and CNFs allowed some current to flow in the circuit, except CNT of 0.3%wt allowed the largest current. It was evident that minute current was flowing in the circuit proving that the nanofluids were naturally electrolytic of high resistant.

Table 6 CNF of 0.3% wt

Actual Resistance $R_1$ ( $\Omega$ )	In series with Channel 1			In series with Channel 2		
	$v_1$ (mV)	$v_2$ (V)	$i$ ( $\mu A$ )	$v_1$ (mV)	$v_2$ (V)	$i$ ( $\mu A$ )
40.90	0.1	5.00	2.44	0.3	5.00	7.33
56.50	0.3	5.00	5.31	0.2	5.00	3.54
217.20	1.8	4.99	8.29	1.5	4.99	6.91
466.00	4.1	4.99	8.80	3.5	4.99	7.51
994.00	9.0	4.98	9.05	7.8	4.98	7.85

Table 7 CNF of 0.6% wt

Actual Resistance $R_1$ ( $\Omega$ )	In series with Channel 1			In series with Channel 2		
	$v_1$ (mV)	$v_2$ (V)	$i$ ( $\mu A$ )	$v_1$ (mV)	$v_2$ (V)	$i$ ( $\mu A$ )
40.90	0.2	5.00	4.89	0.1	5.00	2.44
56.50	0.3	5.00	5.31	0.2	5.00	3.54
217.20	1.9	4.99	8.75	1.3	4.99	5.99
466.00	4.3	4.99	9.23	3.0	4.99	6.44
994.00	9.4	4.98	9.46	6.7	4.99	6.74

Table 8 CNF of 0.9% wt

Actual Resistance $R_1$ ( $\Omega$ )	In series with Channel 1			In series with Channel 2		
	$v_1$ (mV)	$v_2$ (V)	$i$ ( $\mu A$ )	$v_1$ (mV)	$v_2$ (V)	$i$ ( $\mu A$ )
40.90	0.1	5.00	2.44	0.1	5.00	2.44
56.50	0.3	5.00	5.31	0.2	5.00	3.54
217.20	2.1	4.99	9.67	1.5	4.99	6.91
466.00	4.8	4.99	10.30	3.4	4.99	7.30
994.00	10.4	4.98	10.46	7.5	4.98	7.55

#### 4. SUMMARY

Two mini channels were constructed using additive manufacturing approach. The nanofluids filled up the channels where they were subjected to electricity to see their response to a small voltage. Minute currents were recorded flowing through the fluids for a short period. The fluids themselves were found to have high resistances. However, the real nature of the fluids exposed to electrical potentials for a longer duration is unknown.

#### ACKNOWLEDGMENT

This work was supported in part by the Universiti Teknikal Malaysia Melaka under Grant FRGS/2/2013/SG02/ FKP/02/2/F00176.

#### REFERENCES

- [1] Sharp, K. V., Adrian, R. J., Santiago, J. G. & Molho, J. I. (2002). The MEMS Handbook, CRC, New York, pp. 1-33.
- [2] Kandlikar, S. G., Kuan, W. K., Willistein, D. A. & Borrelli, J. (2006). Stabilization of flow boiling in microchannels using pressure drop elements and fabricated nucleation sites. *Journal of Heat Transfer*, vol. 128, pp. 389-396.
- [3] Sarafraz, M., Hormozi, F., & Peyghambarzadeh, S. (2015). Role of nanofluid fouling on thermal performance of a thermosyphon: Are nanofluids

reliable working fluid? *Applied Thermal Engineering*, vol. 82, pp. 212-224.

- [4] Ryglowski, B. K. (2009). Characterization of Carbon Nanotube-Enhanced water as a phase change material for thermal energy storage systems. Monterey, California. Naval Postgraduate School.
- [5] Selvam, C., Irshad, E. M., Lal, D. M. & Harish, S. (2016). Convective heat transfer characteristics of water–ethylene glycol mixture with silver nanoparticles. *Experimental Thermal and Fluid Science*, vol. 77, pp. 188-196.

# Conversion of plastic waste to fuel oil using pyrolysis process

S. Ahmad<sup>1\*</sup> and M. Shafie<sup>2</sup>

<sup>1</sup>) Department of Mechanical Engineering, Politeknik Tuanku Syed Sirajuddin,  
Pauh Putra, 02600 Arau, Perlis, Malaysia

<sup>2</sup>) Sekolah Menengah Sains Tuanku Syed Putra,  
01000 Kangar, Perlis, Malaysia

\*Corresponding e-mail: suhairi.ahmad@gmail.com

**Keywords:** Plastic waste; plastic waste oil

**ABSTRACT** – The development of this project is based on the purpose of converting plastic waste into fuel oil. The study is focusing on the design and fabrication of a plastic waste oil converter as an effort in finding environment-friendly means of waste recycling. It is an alternative solution to increasing problem of waste disposal by converting waste plastics into a resource. Pyrolysis process was the basis in the design and fabrication of the equipment. The conversions of Polypropylene (PP), Low Density Polyethylene (LDPE) and High Density Polyethylene (HDPE) into Plastic Waste Oil (PWO) are the key element of this design and development project. The converter consists of a filler tube, stove, working table, condensing rod, beaker, stop valve, condensing chamber, cooling outlet and intake. The filler tube attached to a mechanism of condensing unit, which collect the amount of PWO in a beaker. The stop valves functioned to allow the cooling medium entering the condensing system. Hence, plastic waste which evaporated travel through a condensing chamber, which made to turn the vapour into PWO. The filler tube is made of stainless steel with holding capacity of 500g/batch of plastic waste. The equipment tested for five trials using 500g of Polypropylene (PP), Low Density Polyethylene (LDPE) and High Density Polyethylene (HDPE) plastics per trial. With the aid of this equipment, it can optimize the amount of PWO produced due to its arrangement. Recommendations also discussed in order to increase the performance of plastic waste converter.

## 1. INTRODUCTION

The development of this project is based on the purpose of converting plastic waste into fuel oil. Plastic is the general common term for a wide range of synthetic or semi synthetic organic amorphous solid materials used in the manufacture of industrial products. Plastics are typically polymers of high molecular mass, and may contain other substances to improve performance and reduce costs. Plastics are dominantly contributed 70% of domestic waste. The effect of plastics waste was seen in water and land pollutions. The study focused on the design and fabrication of a plastic waste oil converter as an effort in finding environment-friendly means of waste recycling. It is an alternative solution to increasing problem of waste

disposal by converting waste plastics into a resource.

Pyrolysis process was the basis in the design and fabrication of the equipment. It is a prototype model that will serve as baseline in developing technology for energy recovery from plastics waste [1]. The conversions of Polypropylene (PP), Low Density Polyethylene (LDPE) and High Density Polyethylene (HDPE) into Plastic Waste Oil (PWO) are the key element of this design and development project.

## 2. RESEARCH METHODOLOGY

The equipment used for converting plastic waste into fuel oil. 500g of plastic waste of Polypropylene (PP), Low Density Polyethylene (LDPE) and High Density Polyethylene (HDPE) were collected into filler tube. The stove is then heated the plastic waste to become liquid. Plastic waste was later evaporated travel through a condensing chamber, which is made to turn the vapour into PWO. The stop valves functioned to allow the cooling medium entering the condensing system. The duration of heating is set for 1 hour. The amount of PWO produced is then measured. The basic steps of plastic waste pyrolysis processes explained in Figure 2.1.

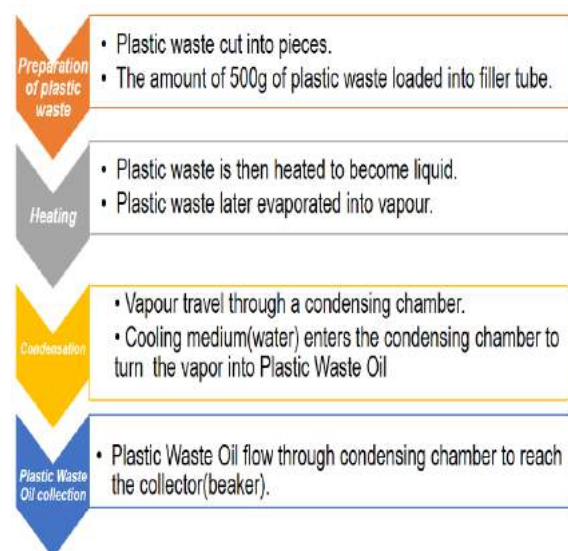


Figure 2.1 Basic steps of plastic waste pyrolysis processes.

## 3. RESULTS AND DISCUSSION

For the performance evaluation of the equipment, only Polypropylene (PP), Low Density Polyethylene



(LDPE) and High Density Polyethylene (HDPE) were used as feedstock. Two thousand and five hundred grams of each plastic waste were prepared, cut into small pieces and divided into five sample weighing 500g each. Five trials conducted for each type of plastic. The performance of the equipment measured in terms of volume of oil recovery [2]. The observations of PWO colours and time for melting were also taken into consideration. The data gathered during plastic waste pyrolysis processes shown in Table 3.1.

Table 3.1 Data gathered during plastic waste pyrolysis processes.

Parameters	TRIAL					Total	Average	Observation
	1	2	3	4	5			
Weight of PP/ LDPE/ HDPE plastic (g)	500	500	500	500	500	2,500	500 g	
Duration of Operation (1 hr)	1	1	1	1	1	5	1 hr	Duration for plastic to melt: 1.PP-20 minutes 2.LDPE-20 minutes 3.HDPE-50 minutes
Volume of oil recovered PP (ml)	381	385	383	384	383	1,916	382.2 ml	Colour of oil observed-yellow
Volume of oil recovered LDPE (ml)	379	378	376	371	373	1,877	375.4 ml	Colour of oil observed-light brown
Volume of oil recovered HDPE (ml)	489	492	493	488	495	2,457	491.4 ml	Colour of oil observed-dark brown

### 3.1 Average Volume per Mass Produced

- (i) Polypropylene (PP) produced 382.2 ml for 500 g, therefore the average volume capacity of PP is 0.765 ml /g
- (ii) Low Density Polyethylene (LDPE) produced 375.4 ml for 500 g, therefore the average volume capacity of LDPE is 0.751 ml /g
- (iii) High Density Polyethylene (HDPE) produced 491.4 ml for 500 g, therefore the average volume capacity of HDPE is 0.983 ml /g

### 3.2 Physical Observations

- (i) Polypropylene (PP) produced a Yellow PWO
- (ii) Low Density Polyethylene (LDPE) produced a Light Brown PWO
- (iii) High Density Polyethylene (HDPE) produced a Dark Brown PWO

## 4. SUMMARY

The process was successful in converting Polypropylene (PP), Low Density Polyethylene (LDPE) and High Density Polyethylene (HDPE) plastics into oil without using catalyst. It is able to convert PWO at an average volume capacity of 0.765 ml /g, 0.751 ml /g and 0.983 ml /g respectively. Although it is a laboratory scale model, it can be used to address the demanding problem of waste disposal in the country. Further study on other factors that affects the performance of the plastic waste oil converter could be also conducted. Factors such as temperature,

pressure and duration can be taken into consideration. Further study should also consider using other types of plastic waste. Oil recovered must be analyzed to determine its physical and chemical properties. Studies should be conducted on the applications and benefits that can be drawn from Plastic Waste Oil.

## REFERENCES

- [1] Elmo C. Rapsing, Jr. (2016). Design and Fabrication of Waste Plastic Oil Converter. *International Journal of Interdisciplinary Research and Innovations*, Vol. 4, Issue 2, pp. 69-77.  
[ISSN: 2348-1218, ISSN 2348-1226]  
Available at: [www.researchpublish.com](http://www.researchpublish.com)
- [2] Elmo C. Rapsing, Jr. (2017). Performance Evaluation of Waste Plastic Oil Converter. *Asia Pacific Journal of Multidisciplinary Research*, Vol. 5, No. 2, pp. 58-63.  
[P-ISSN: 2350-7756, E-ISSN: 2350-8442]  
Available at: [www.apjmr.com](http://www.apjmr.com)

# Effective maintenance engineering and management in welding industry

C.G. Choong<sup>1\*</sup> and L.F. Zakaria<sup>2</sup>

<sup>1</sup>) Department of Mechanical Engineering, Politeknik Tuanku Syed Sirajuddin,  
Pauh Putra, 02600 Arau, Perlis, Malaysia

<sup>2</sup>) Department of Mechanical Engineering, Politeknik Kota Kinabalu,  
No. 4, Jalan Politeknik, KKIP Barat, Kota Kinabalu Industrial Park, 88460 Kota Kinabalu, Sabah, Malaysia

\*Corresponding e-mail: dr.choong@ptss.edu.my

**Keywords:** Maintenance management system; welding industry

**ABSTRACT** – The purpose of this paper is to investigate the maintenance needed for machine in welding industry and giving suggestion to overcome the breakdown time and prevent for any major losses. Therefore, the paper contains maintenance organization, strategy, system approach, planning, scheduling and the computerized maintenance management system suitable for welding industry. Basically, the first thing need to be consider is the organization to simulate the company and organize the maintenance well. Then, task is brought to next step which is choosing the right strategy to implement into the company and with the strategy, comes the system approach to maintenance which will be needed the organize/secure planning and scheduling. Computer system is when everything kept in place and secure and in that particular application one's company can be more organized toward a better maintenance.

## 1. INTRODUCTION

Welding today is applied to a wide variety of materials and products, using such advanced technologies as lasers and plasma arcs. The future of welding holds even greater promise as methods are devised for joining dissimilar and non-metallic materials, and for creating products of innovative shapes and designs. Chosen industry for this study is Welding Industries (M) Sdn. Bhd. which is located at Pusing, Perak. Welding Industries (M) Sdn. Bhd. has become the only local company in Malaysia that manufactures welding machines for use by industries.

Effective maintenance engineering and management is an orderly and systematic approach of administrative, financial, and technical framework for assessing, planning, organizing, monitoring and evaluating maintenance and operation activities and their costs on a continual basis. A good maintenance management system coupled with knowledgeable and capable maintenance and operation staff can prevent health and safety problems and environmental damage; yield longer asset life with lower breakdowns and downtime; and result in lower operating costs, higher productivity and profitability and a higher quality of life.

In Figure 1.1, the Facility Manager (FM) function has been gaining increasing recognition for the important role it can play to create cost savings and efficiency of the workplace. The primary task of FM is to manage support services to meet the needs of the organization, its core operations and employees. It

deals with the maintenance management of the physical assets and incorporates controlling services necessary for successful business [1].

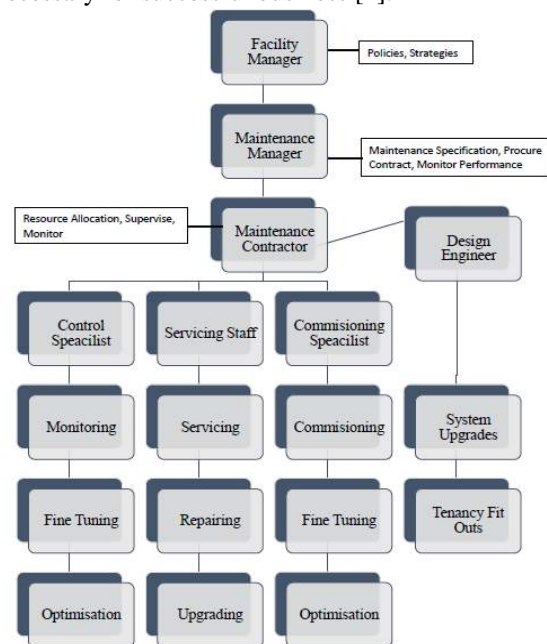


Figure 1.1 A maintenance management structure proposed for welding industry.

A maintenance system can be viewed as a simple input/output system. The inputs to the system are manpower, failed equipment, material and spare parts, tools, information, policies and procedures, and spares. The output is equipment that is up, reliable and well configured to achieve the planned operation of the plant. The system has a set of activities that make it functional. The activities include planning, scheduling, execution and control. The control is achieved in reference to the objectives of the maintenance system. The objectives are usually aligned with the organization objectives and include equipment availability, costs and quality. The feedback and control is an important function in this system that can be used to improve the system performance.

## 2. MAINTENANCE STRATEGY USED IN WELDING INDUSTRY

A good preventive maintenance program anticipates and prevents equipment failures such as doing periodic inspections, parts replacement and equipment cleaning. Automated equipment, such as a robotic welding cell, for example, requires a targeted,

routine preventive maintenance program to ensure proper operation and provide maximum in-service lifespan. An effective program involves a routine systematic inspection, adjustment, lubrication, and replacement of components, as well as software upgrades and performance testing and analysis.

In order to extend the life of welding equipment, Total Productive Maintenance (TPM) can be implemented to improve the productivity and reduce the operating costs [2]. TPM enables a company to:-

- (i) Increase output/productivity without increasing the size of its welding fleet.
- (ii) Meet deadlines easier and avoid outsourcing welding.
- (iii) Conserve capital or free it for other uses.
- (iv) Increase profit margins (which in turn can enable pricing flexibility if necessary).
- (v) Improve cross-functional teamwork and communication.
- (vi) Empower associates to not just solve welding equipment problems, but also to eliminate the source of the problem.

### 3. IMPLEMENTATION OF SYSTEM APPROACH TO MAINTENANCE IN WELDING INDUSTRY

Operators are exposed to fume and gases when welding and exposures vary depending upon the process and specific working conditions. Fabricators are under continual pressure to reduce worker exposure to potentially harmful substances in the workplace, including welding fume.

There are many ways to reduce exposure to welding fume. Each solution addresses part of the welding system. Approaches to controlling welding fume actually fall into two broad categories:-

#### (i) Reducing fume generation

Limiting the generation of welding fume begins at the design stage. All other things being equal, a properly sized weld will result in the lowest amount of welding fume for a given process and set of procedures. Over welding, on the other hand, unnecessarily increases welding fume. As the amount of weld metal increases, the amount of fume also increases. The welding engineer should be aware of the role that weld size plays in the creation of fume.

#### (ii) Limiting operator exposure to fume

The most direct approach to limiting personnel exposure is simply to limit the amount of time an operator spends welding. This can often be accomplished via job sharing, automated welding systems, fume extraction technology, wall mounted low vacuum/high volume system and portable high vacuum/low volume extraction unit.

The limits for fume exposure set by OSHA and others are measured in milligrams of particulate per cubic meter of air (mg/m<sup>3</sup>).

OSHA proposed an 8-hour Time-weighted average of 5 mg/m<sup>3</sup> for these fumes; this limit is established in the final rule. This limit applies to the total fume concentration generated during the welding

of iron, mild steel, or aluminum; the fumes generated by the welding of stainless steel, cadmium, or lead-coated steel, or other metals such as copper, nickel, or chrome [3].

### 4. EFFECTIVE MAINTENANCE PLANNING AND SCHEDULING SYSTEM

An effective maintenance scheduling system will decrease a considerable amount of non-productive time and provide a schedule of work orders with job descriptions, material requirements, necessary documentation, asset location, etc., enables the maintenance technicians to spend more time accomplishing the work. At the same time, certain repairs and/or modifications may require the equipment to be inactive, so it is extremely important that there is coordination with operations to plan and schedule the jobs in order to minimize downtime. Advanced planning and scheduling will also help avoid unnecessary overtime costs, and scheduling equipment and personnel will lead to an increase in production and a decrease in downtime. Maintenance scheduling is level of maintenance that requires planning, allocation of significant amount of time, and high degree of coordination between different departments, and is typically initiated through a work order. Scheduling deals with the specific time and phasing of planned jobs together with the orders to perform the work, monitoring the work, controlling it, and reporting on job progress.

### 5. CMMS SOFTWARE IN WELDING INDUSTRY

A Computerized Maintenance Management System (CMMS) is a software program designed specifically to help maintenance teams carry out their jobs more efficiently. The software is designed to assign maintenance tasks to the staff within a company in a more organized manner. Software such as WELDSPEC, Welding Coordinator and Welding Estimator can be used in welding industry to:-

- (i) Track and manage welding procedures;
- (ii) Trace fabrication information; and
- (iii) Project cost estimation.

### 6. SUMMARY

This paper covered knowledge regarding maintenance of facilities and machine/equipment activities in good working condition and develops good maintenance management knowledge in the welding industry.

### REFERENCES

- [1] De Marco, A. & Mangano, G. (2012). A Review of the Role of Maintenance and Facility Management in Logistics. *Proceedings of the World Congress on Engineering 2012, Vol III, July 4 - 6, , London, U.K.*
- [2] Ahuja, I.P.S. & Khamba, J.S. (2008). Total productive maintenance: Literature review and directions. *International Journal of Quality &*

*Reliability Management, Vol. 25 Issue: 7, pp.709-756.*

- [3] Hutter, G.M. (1991). Airborne contaminants in the machine tool industry. *Safety Brief*, Vol. 7, No. 1. [ISSN: 1041-9489]

# Development of an oil trap system for wastewater handling

Zulkifli Sulaiman<sup>1\*</sup>, Sahrijan Ahmad<sup>1</sup>, Mohd Fadhli Ahmad<sup>1</sup>

<sup>1</sup>) Department of Mechanical Engineering, Politeknik Tuanku Syed Sirajuddin, Pauh Putra, 02600 Arau, Perlis, Malaysia

\*Corresponding e-mail: zulkifliptss@gmail.com

**Keywords:** Wastewater; oil trap system; grease

**ABSTRACT** – Removal of oil and fat waste into the sewerage system at the cafeteria of Politeknik Tuanku Syed Sirajuddin (PTSS) has been a major cause of water pollution to the environment. Among the identified sources were the released of solid food waste, oil, and grease from the food premises into the drainage systems. To address the problem of water pollution, a new modified oil trap system was developed and installed at the cafeteria sewage system. By installing the oil trap system, results obtained showed that wastewater quality was improved while the solid waste and oil residuals were filtered into a dedicated storage compartment and prevented from entering the sewerage system.

## 1. INTRODUCTION

Reduction or prevention of pollution at the source is a key element in any pollution control strategy [1]. Effluents produced by the restaurant trade, the dairy industry and food processing are a small sample of those that present potential problems in terms of wastewater management [2].

Improper act by the cafeteria owner to drain the waste of food, oil, and grease has been a major problem, especially at the cafeteria of Politeknik Tuanku Syed Sirajuddin (PTSS) Perlis. Based on the observations carried out, the oily food wastage will be drained into the outlet and indirectly will emit a type of stinky odor, causing bad environmental image to the PTSS cafeteria wastewater handling performance. Hence, this project was initiated with the objective to filter and channel the sewage wastes at PTSS cafeteria and improve the wastewater quality before being discharged into the drainage system. An innovative and simple oil trap system was designed and installed to the current cafeteria sink system. Performance evaluation was conducted to assess the oil trap system performance through visual observation on the wastewater quality and amount of trapped solid waste and oil residues.

## 2. METHODOLOGY

As shown in Figure 2.1, the new oil trap system developed in this project was installed at the end of the residual wastewater from the sink before the sewage water was discharged into the drain. The waste water from the sink flows into the inlet and pass through the filtering process where the food waste is segregated from the water by using filter. The segregation method is based on the simple principle whereby low density oil and fat will “float” at the surface of the mixture, leaving clean water at the bottom of the mixture and be

discharged out from the holding tank. The samplings of drainage wastewater were also performed to assess the performance of the oil trap system installed.



Figure 2.1 The modified oil trap system design.

Based on Figure 2.2, the working mechanism for the oil trap system are explained as follows:-

- (i) The dregs were trapped first inside compartment A, while the oil and wastewater mixture will flow to compartment B and C.
- (ii) Oil will float and be on top of the mixture region. The rest of oil floating on the surface of compartment B will overflow into the oil storage tank.
- (iii) The wastewater remained after oil is filtered from the mixture is channeled to the sewage system.



Figure 3.1 Oil trap system configuration with three storage compartments of A, B and C.

## 3. RESULTS AND DISCUSSION

Table 3.1 summarized the visual observation on the wastewater quality before and after the installation of the oil trap system. In addition, Figure 3.1 shows the results on the wastewater samples taken with and

without the implementation of the oil trap system.

Table 3.1 The differences before and after the installation of oil trap system.

Before the installation of oil trap system	After the installation of oil trap system
Food waste residue in the wastewater is taken in large quantities.	After installation, it can be seen that the food waste residue is reduced.
The color of the wastewater is yellowish.	The change in color of the wastewater can also be seen in more brighter and less yellowish.
Oil and grease flow into the sewage system with sewage wastewater.	Oil and grease are trapped and stored in oil and grease storage tanks, where the discharged wastewater is free from oils and grease.
Wastes contain residual oils and grease can be seen on the surface of the water.	No oil on the surface of the water.



Figure 3.1 Wastewater quality (a) before, and (b) after installation of the oil trap system.

Based on results shown in Table 3.1, it was identified the root cause of the stinky odor problem faced is caused by the oil and grease wastes flowing from the existing oil trap in the cafeteria. The wastewater from the cafeteria contains relatively high fat and oil quantities emanated from cooking.

In addition, the color of the wastewater becomes yellowish and glazed as there were mixtures of waste oil and grease. The oil layer on the surface will disrupt the microorganisms in the water because the layer blocks oxygen from air into the water. The size of the existing oil trap system was not capable of accommodating the waste oil discharge. Furthermore, it was found that the existing pipe system cannot flow smoothly due to mixed wastewater with oil and grease residues. The less efficient of the existing oil trap filtering has resulted in wastewater draining out mixed oil and grease. It has also caused unpleasant odor problem arising from the oil and grease which were mixed with the wastewater.

After the installation of modified oil trap system

(with the addition of oil storage tanks), it was found that wastewater from the system outlet was cleaner than before. In addition, the color of the wastewater was also cleaner, caused there was no food waste mix and no oil layer on the surface (Figure 3.1). In addition, with the modified oil trap system, it can accommodate the great quantity of oils due to the smooth flow of the flushing system. The efficient refinement of the new oil trap system was able to isolate wastewater from drain outlet which was not mixed with the rest of oil and grease. Furthermore, there was no unpleasant smell behind at the cafeteria because the wastewater has been isolated from the oil and grease.

Other notable improvements obtained by using the oil trap system as compared to the existing system are summarized in Table 3.2 below.

Table 3.2 Comparison of performance between existing and modified oil trap system.

Existing System	Modified System
It stinks if it is not maintained properly	Smooth waste disposal system
Oils and fats residual can cause damage to the sludge fan of the ventilation system.	All waste and oil residuals can be stored in a single compartment.
If the trap outlet is clogged and not well maintained, wastewater will overflow.	Able to accommodate more than the existing tank.

#### 4. SUMMARY

A new oil trap system for wastewater improvement was successfully designed and implemented in this project. The modified oil trap system was able to prevent the blockage pipeline caused by the formation of solid fats in the drainage piping system. In addition, it also made it easy to do maintenance work, as well as able to contain large quantity of oils and wastewater during operation. The additional oil storage tank can also isolate waste oil and grease from wastewater more effectively to obtain better wastewater quality and cleaner oil trap system.

#### REFERENCES

- [1] Willey, R. (2001). Fats, Oils, and Greases: The Minimization and Treatment of Wastewaters Generated from Oil Refining and Margarine Production. *Ecotoxicology and Environmental Safety*, 50, pp. 127-133.
- [2] Cammarota, M.C., Teixeira, G.A., Freire, D.M.G. (2001). Enzymatic pre-hydrolysis and anaerobic degradation of wastewaters with high fat contents. *Biotechnology Letters*, 23, pp. 1591-1595.

# Enriched laboratory experiments with interactive simulation

N. I. Haris<sup>1\*</sup> and A. Talip<sup>2</sup>

<sup>1)</sup>Department of Mechanical Engineering, Politeknik Tuanku Syed Sirajuddin,  
Pauh Putra, 02600 Arau, Perlis, Malaysia

<sup>2)</sup>Centre of Diploma Studies, Universiti Malaysia Perlis,  
UniCITI, 02100 Padang Besar, Perlis, Malaysia

\*Corresponding e-mail: nurlyena@gmail.com

**Keywords:** Laboratory experiment, computational experiment, interactive simulation

**ABSTRACT** – Mechanical engineering syllabus contain compulsory laboratory experiments because the development and application of theories used to rest only on real experiments. The three pillars of science maps state that students need to validate the theory through real experiments and then do the verification by using computational experiments. In this paper, PhET interactive simulation which is stand for “Physics Education Technology” was used to help students to verify the lab experiment. The simulation can be used as post practical to enhance student understanding after real experiment.

## 1. INTRODUCTION

Engineering education emphasizes on practices in laboratory and is incomplete without laboratory practice. The overall goal of engineering education is to prepare students to practice engineering and in particular to deal with the nature of problems faced by the society [1]. And laboratory experiences also provide opportunities for students to interact directly with the material world (or with data drawn from the material world), using the tools, data collection techniques, models, and theories of science [2].

Even there are lot of benefit that students can gain from laboratory experiment, there still lacking because of limited time, limited apparatuses or the damage of the apparatuses. Sometimes these experiments are too hard, too dangerous and too expensive to carry out.

To overcome this situation, the distribution of student learning time was designed to fulfil this lacking. The time allocated for independent learning are 7 hours for student to enrich their practical ability.

Figure 2.1 shows the three pillars of science maps that have been used in this study. This paper recommends on how to improve students understanding from the theory they have learned in class and what they have practiced on real experiments at the laboratory.

Literature shown that there are three types of educational laboratories in engineering education [3, 4]:

- (i) Hands-on laboratory with real instruments;
- (ii) Simulation or virtual laboratory;
- (iii) Remote or distributed learning laboratory

This paper has proposed to use interactive simulation to help student understanding after laboratory experiment session.

## 2. METHODOLOGY

Figure 2.1 shows the three pillars of science maps that have been used in this study [5].

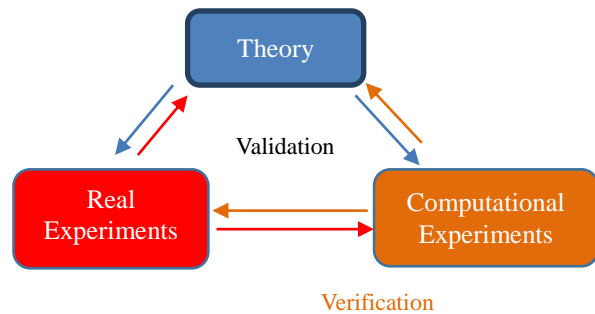


Figure 2.1 Three pillars of science maps. [5]

Friction is one of the topics that must be studied by the Mechanical Engineering program students. Students need to do the laboratory experiments to validate what they have learned before. They then need to do calculation by referring to the theory taught earlier.

For verification purposes, students need to conduct computational experiments by using interactive simulation, for example by PhET interactive simulation developed by the University of Colorado [6].

## 3. RESULTS AND DISCUSSION

### 3.1 Theory Validation

Given example:-

Material = Steel

Mass of object = 200 kg

Coefficient of friction,  $\mu = 0.3$

Hence;

$$\text{Normal force, } N = mg \quad (1)$$

$$\text{Normal force, } N = (200 * 9.8) \\ = \mathbf{1960 \text{ N}}$$

$$\text{Friction force, } F_f = \mu N \quad (2)$$

$$\text{Friction force, } F_f = (0.3 * 1960) \\ = \mathbf{588 \text{ N}}$$

### 3.2 Computational Experiments Verification

After the laboratory experiments, students can enhance their knowledge of frictional force with verification using interactive simulation. Figure 3.1

shows the object applied force have the same value with frictional force, **588N**. Thus, the object is still on static condition.

Meanwhile Figure 3.2 shows the object start moving because the applied force showed more than the frictional force, **588.1 N**.

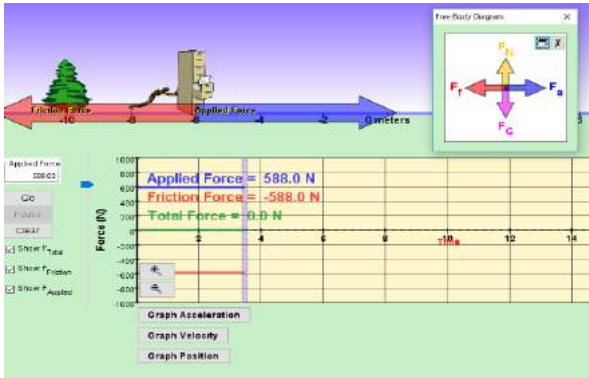


Figure 3.1 Applied Force same value with frictional force, 588N.

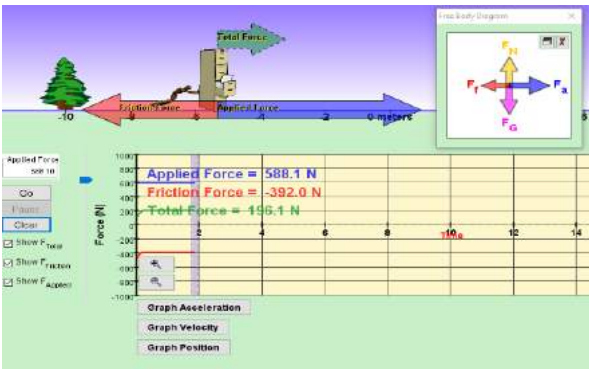


Figure 3.2 Applied Force more than frictional force, 588.1N.

#### 4. SUMMARY

Laboratory experiments are compulsory which enable students to develop their experimental skills, ability to work in teams, responsible for their own results and collected data, and also to anticipate the findings that already described in theory. However, not all of the students can grab the experience and enhance their knowledge about what they had practice at the laboratory.

It is recommended that the computational experiments can be used to do the verification. Students can spend their independent learning time by doing the simulation to enrich their understanding of the experiment.

#### REFERENCES

- [1] S. K. Tomar (2016). Role of Laboratory Practice in Engineering Education. Retrieved from *Role of Laboratory Practice in Engineering Education*: <http://jklu.edu.in/blog/role-of-laboratory-practice-in-engineering-education/>
- [2] Susan R. Singer, Margaret L. Hilton, and Heidi A. Schweingruber (2006). Introduction, History, and

Definition of Laboratories. *America's Lab Report: Investigations in High School Science* (p. 13). Washington, DC: National Academies Press .

- [3] University, Q. (2018). *Centre for Teaching and Learning*. Retrieved from Queen's University: <http://www.queensu.ca/ctl/what-we-do/teaching-and-assessment-strategies/lab-based-learning>
- [4] Alam, F. (2014). Using Technology Tools to Innovate Assessment, Reporting, and Teaching Practices in Engineering Education. Australia: IGI Global.
- [5] Lee, D. (2014). *Numerical Algorithms for Scientific Computation*. Retrieved from Numerical Algorithms for Scientific Computation: [https://users.soe.ucsc.edu/~dongwook/wp-content/uploads/2014/10/DongwookLee\\_AMS280B.pdf](https://users.soe.ucsc.edu/~dongwook/wp-content/uploads/2014/10/DongwookLee_AMS280B.pdf). Retrieved from University of Colorado: <https://phet.colorado.edu>



# Effects of engine sizing on battery state-of-charge for hybrid electric vehicle

A.Md Saad<sup>1,2\*</sup>, M.A. Salim<sup>1,2</sup>, M.R. Mansor<sup>1,2</sup> and M.Z. Akop<sup>1,2</sup>

<sup>1)</sup> Faculty of Mechanical Engineering, Universiti Teknikal Malaysia Melaka, Hang Tuah Jaya, 76100 Durian Tunggal, Melaka, Malaysia

<sup>2)</sup> Centre for Advanced Research on Energy, Universiti Teknikal Malaysia Melaka, Hang Tuah Jaya, 76100 Durian Tunggal, Melaka, Malaysia

\*Corresponding e-mail: adzni@utem.edu.my

**Keywords:** Engine sizing; battery SOC; hybrid electric vehicle

**ABSTRACT** – The purpose of this study is to investigate the effects of engine sizing on battery state of charge (SOC) for hybrid electric vehicle (HEV). It is carried out by using ADVISOR software, in which the vehicle system is simulated based on US06 driving cycle to represent both highway and city driving. The battery parameters are kept constant and 3 different sizes of engine are used. The optimum engine size obtained from the simulation is 36 kW. The engine manages to charge the battery at considerable rate and the battery SOC is 0.46 at the end of the simulation. All the engine sizes manage to propel the vehicle following the US06 driving cycle. But, smaller engine size causes the battery to deplete excessively below 15 % of SOC and larger engine size causes the battery to overcharge.

## 1. INTRODUCTION

Automotive industry is moving towards producing vehicles equipped with powertrain system that able deliver the best fuel consumption. The ideal approach is by having powertrain system that is totally independent of fossil fuel source, which is the electric vehicle. The immaturity of battery technology forces industrial players to come out with mid-term solution. Currently, hybrid electric vehicle is the best approach of having better fuel consumption vehicle.

Hybrid electric vehicle consists of several major components such as internal combustion engine (ICE), battery, generator and electric motor. Each of these components needs to be sized properly to ensure the vehicle meets the required performance characteristics. The size of two power sources of the vehicle, which are the ICE and battery needs to be determined in the initial stage of vehicle development. It is because, both of these power sources are inter-dependent in propelling the vehicle. ICE is the main source of energy to charge the battery other than by utilizing the regenerative braking.

The objective of this study is to investigate the effects engine sizing in battery SOC. Improper size of engine causes the battery to deplete excessively during used or overcharge. Both conditions are not good to preserve the battery life and also decrease the optimum performance of the battery.

## 2. RESEARCH METHODOLOGY

### 2.1 Vehicle parameters

This study is conducted by using simulation approach. ADVISOR software is used to investigate

the battery performance of the vehicle. The type of vehicle chosen for this study 5-door passenger car, which is the typical type of HEV currently in the market. The required vehicle performance is shown in Table 2.1. For the purpose of this study, Li-ion battery is used and the battery parameters are set to be constant. The details of battery are shown in Table 2.2.

Table 2.1 Desire vehicle performance.

Acceleration (0-60 mph)	Top Speed	All-electric range	Gasoline-only fuel economy
8 sec	95 mph	40 miles	50 mpg

Table 2.2 Battery Specifications.

Type	Cylindrical
Capacity (Ahr)	89.8
Voltage (V)	362
Energy (kWhr)	32.5
Weight (kg)	157.8
Volume (dm <sup>3</sup> )	122.4
No of cells	4000
No of modules	200

The investigation is carried out by using 3 different engine sizes which are 25 kW, 36 kW and 40 kW. All these engine specifications are obtained from ADVISOR software.

### 2.2 Simulation

The simulation is carried by using US06 driving cycle. This driving cycle is chosen because it is able to represent both highway and city driving. It is run for a total of 12 cycles for each engine size. The initial battery SOC is at 0.3 or 30 %.

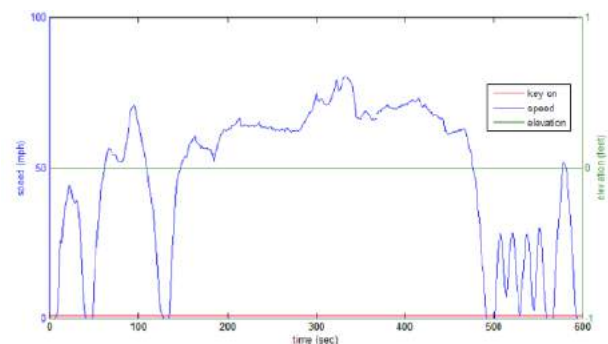


Figure 2.1 US06 Driving Cycle.

### 3. RESULTS AND DISCUSSION

In this section, the behavior of battery SOC due to engine sizing is discussed in detail. Firstly, the simulation was run by using 25 kW engine. The results of simulation are shown in Figure 3.1 below. The simulated vehicle could meet the required speed by following the US06 driving cycle. It indicated that, both power sources of the vehicle, engine and battery could provide enough power to propel the vehicle. But, battery SOC was continuously depleting. The engine did not have the capability to charge the battery during the simulation process. Battery SOC went below 15 % at the end of simulation. When the engine size of 40 kW was used, it overcharged the battery to be over 80 %.

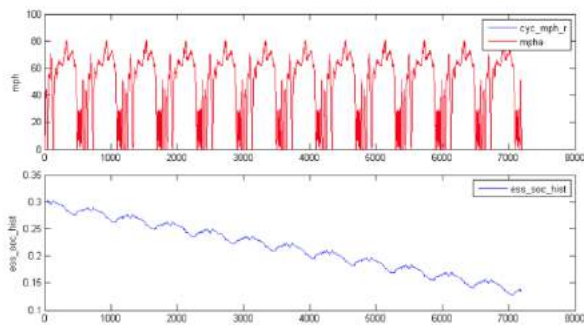


Figure 3.1 US06 Driving Cycle and Battery SOC for engine 25 kW.

The optimum engine size obtained from the simulation is 36 kW and the simulation results are shown in Figure 3.2. It was achieved by having lower limit of engine size of 20 kW and upper limit of 40 kW based on previous simulation results. The results showed that both power sources of the vehicle, engine and battery were able to deliver enough power to propel the vehicle by following the US06 driving cycle. The battery SOC was not depleting and the engine was able to charge the battery at considerable rate. By the end of simulation, battery SOC is at 0.47 or 47 %.

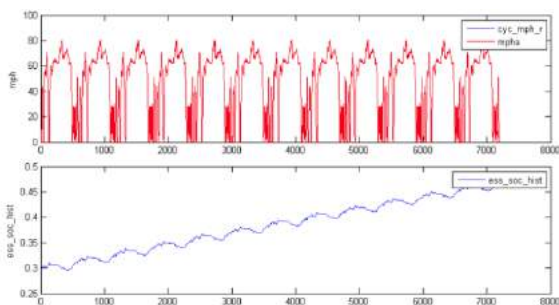


Figure 3.2 US06 Driving Cycle and Battery SOC for Engine 36 kW.

Even though the charging process of battery can be controlled by implementing proper control strategies, but engine sizing is very important particularly in the early design stage of HEV. For this simulation, it showed that the vehicle powertrain system could provide enough power in fulfilling the vehicle performance requirements. The vehicle could meet the required speed of US06 driving cycle but improper

engine sizes could not charge the battery effectively. The small engine size was not able to charge the battery and when the vehicle was travelling at longer distance, the battery was going to be totally depleted. This vehicle was depended only on engine to propel the vehicle and the electric drive system became useless. Vehicle fuel consumption was going to suffer if this condition occurred. On the other hand, bigger engine size was overcharging the battery. Furthermore, the excessive energy from the engine was going to be wasted and not fully utilized for this vehicle system. Bigger engine size was more expensive and it increased the total cost of the vehicle.

It is also important to note that battery charging process is very critical in preserving the battery life. For HEV, there are lower and upper SOC limits that have been set to avoid undercharge and overcharge. If the battery is depleting and charging exceeding these limits, it will tremendously shorten the battery life.

### 4. SUMMARY

This study was performed to investigate the effects of engine sizing on battery SOC for HEV. ADVISOR software was used to determine the behavior of battery SOC on various engine sizes. Simulation was run by using US06 driving cycle to represent both highway and city driving. All the engine sizes were able to meet the change of required speed by following US06 driving cycle. The results also showed that the optimum engine size for this vehicle is 36 kW. By having lower engine power such as 20 kW as in the simulation caused the battery SOC to drop below 15%. Engine power of 40 kW caused the battery to overcharge exceeding the upper limit. Both conditions can jeopardize the battery life. Because of that, optimum engine size is very important for HEV. It has to satisfy both vehicle performance requirements and also charging the battery within the allowable limits.

### REFERENCES

- [1] Fang, W.F., Kwon, O.J. & Wang, C.Y. (2009), Modelling of Li-ion Battery Performance in Hybrid Electric Vehicles. *SAE Technical Paper* No 2009-01-1388.
- [2] Li, Z., Onar, O., Khaligh, A. & Schaltz, E. (2009). Design, Control and Power Management of a Battery/Ultra Capacitor Hybrid System for Small Electric Vehicles. *SAE Technical Paper* No 2009-01-1387
- [3] Kelly, K.J., Zolot, M., Glinsky, G. & Hieronymus, A. (2001). Test Results and Modelling of the Honda Insight using ADVISOR. *SAE Technical Paper* No 2001-01-2537.
- [4] Syed, F.U., Yamazaki, M., Nallapa, V.R. & Kuang, M.L. (2009). Energy Management in a Dual-Drive Hybrid Powertrain. *SAE Technical Paper* No 2009-01-1329
- [5] Konev, A., Lezhnev, L. & Kolmanovsky, I. (2006). Control Strategy Optimization for a Series Hybrid Vehicle. *SAE Technical Paper* No 2006-01-0663

# Effect of coconut shell powder in brake friction materials

M.A.M. Daud<sup>1,2,\*</sup>, N. F. Bayanuddin<sup>1,2</sup>, M. Z. Selamat<sup>1,2</sup> and  
D.M. Sivakumar<sup>1,2</sup>

<sup>1</sup>) Faculty of Mechanical Engineering, Universiti Teknikal Malaysia Melaka,  
Hang Tuah Jaya, 76100 Durian Tunggal, Melaka, Malaysia.

<sup>2</sup>) Centre for Advanced Research on Energy, Universiti Teknikal Malaysia Melaka,  
Hang Tuah Jaya, 76100 Durian Tunggal, Melaka, Malaysia.

\*Corresponding e-mail: ahadlin@utem.edu.my

**Keywords:** Coconut shell; brake pad; hardness; porosity; density

**ABSTRACT** - The purpose of this study is to investigate the effects of coconut shell powder in brake friction materials. The specimens are made from four different compositions of aluminum oxide, maleic anhydride, epoxy resin and coconut shell powder. The shore hardness is measured using ASTM D 2240. The density and porosity of a specimen with 25 mm diameter by 14 mm high is estimated using ASTM C 380-79. The applied pressure is 100 kN/cm<sup>2</sup> for 5 minutes at temperature of 80 °C and cooling time of 15 minutes. Five different sets of specimen are produced with different composition of ingredients. The best result is for specimen C with the Shore hardness, 69.7, porosity of 0.27 % and density of 1.858 g/cm<sup>3</sup>.

## 1. INTRODUCTION

Brake pad plays an important role in safety and performance as it is the most important component in any types of vehicles [1]. Lining materials is the crucial major component in the brake pad and it can be categorized as organic materials, metallic materials and semi materials. Friction materials are composites that consists of binders, fillers, friction modifier and reinforcing fibres. The friction materials can contain asbestos or non-asbestos friction material. However, asbestos has been recognized to be hazardous and the effect of asbestos to human can cause serious diseases [2].

Coconut shell is a wasted product and does not contribute any good value to human except as alternative fuel. Previously, the coconut shell was burnt as a solid water disposal which contributed to CO<sub>2</sub> and methane emissions to environment [3]. Furthermore, the coconut shell waste is renewable, cheap, completely or partially recyclable and biodegradable [4] From the previous study, the coconut shell has better physical properties as well as high compressive strength which depends on the coconut shell composition [5]. From these properties, coconut shell has a potential as an alternative to fibre reinforcement material of friction material non-asbestos brake pad on light weight automobile such as motorcycle.

The objective of this study is to determine the effect of coconut shell powder content as reinforcement materials in brake pad and to study the characteristics of coconut shell powder in brake pad including mechanical properties and physical properties.

## 2. METHODOLOGY

The specimens were made of four different

percentage composition of aluminum oxide, maleic anhydride, epoxy resin and coconut shell powder. Table 2.1 shows the composition of raw materials. This study consisted of shore hardness test, density and porosity percentage and surface structure. The shore hardness was estimated using the Shore Hardness Type D (ASTM D 2240). The apparent density and porosity of a specimen measuring 25 mm in diameter and 14 mm in high was estimated using the Archimedes method (ASTM C 380-79). Figure 2.1 shows the coconut shell powder and Figure 2.2 shows the process of samples. The applied pressure is 100 kN/cm<sup>2</sup>, time pressure is 5 minutes, temperature is 80°C and cooling time is 15 minutes.

Table 2.1 Table of composition for the raw materials.

Sample	Epoxy resins (%)	Coconut shell powder (%)	Aluminum oxide (%)	Maleic anhydride (%)
A	45	2	53	3
B	45	4	51	3
C	45	6	49	3
D	45	8	47	3
E	45	10	45	3



Figure 2.1 Coconut shell powder.

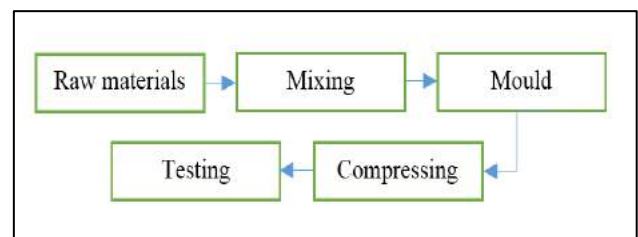


Figure 2.2 Fabrication process of samples.

### 3. RESULTS AND DISCUSSION

#### 3.1 Density and Porosity of Brake Pad Materials

Figure 3.1 shows that when the coconut shell powder is increasing, the density is decreasing with the increasing of porosity. In selecting an optimal friction material, the density of the material should be reasonable and the porosity should have certain amount to reduce the effect of oil and water on the friction coefficient [5]. Lower porosity will result in higher coefficient and low wear rate due to higher contact areas between the mating surfaces. The aluminum oxide is added to improve the friction coefficient.

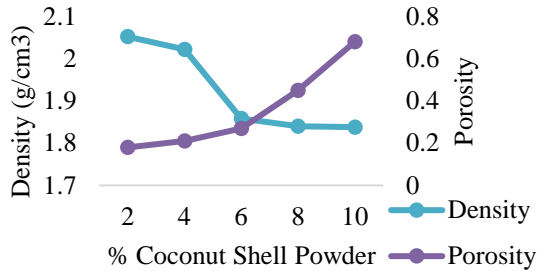


Figure 3.1 Graph of density and porosity vs % of coconut shell powder.

#### 3.2 Hardness of Brake Pad Materials

Figure 3.2 shows the hardness is decreasing when the porosity is increasing when content of coconut shell powder is increased. This is due to the high porosity in the sample where it has low content of aluminum oxide. Figure 3.3 shows that the hardness is decreasing when the density is decreased when content of coconut shell powder is increased. In selecting an optimal friction material, the hardness should be average because if the friction material has too high of hardness, it indicates the brittleness. If the friction material has too soft hardness it indicates higher wear and porosity with lower density.

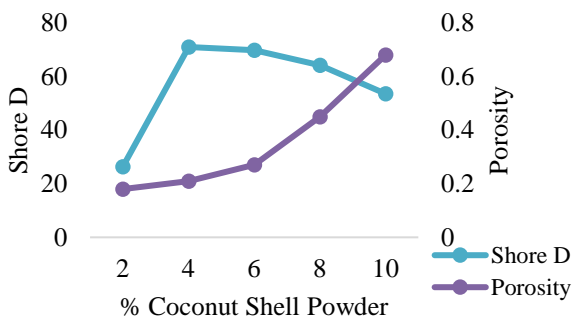


Figure 3.2 Graph of shore 'D' and porosity vs % of coconut shell powder.

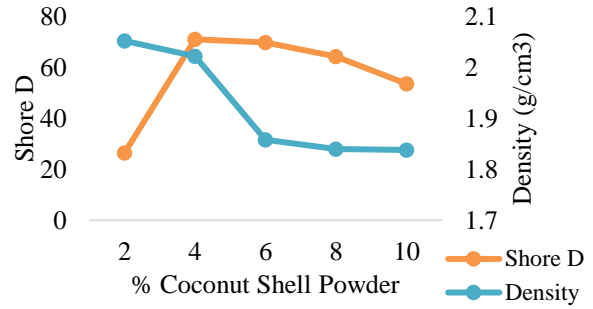


Figure 3.3 Graph of Shore 'D' and density vs % of coconut shell powder.

#### 4. SUMMARY

In conclusion, an optimum formulation was achieved for specimen C with an overall content of 49% aluminum oxide, 45% epoxy resin, and 6% coconut shell powder with 3 % of maleic anhydride. The hardness of this specimen is 69.7 Shore D, porosity of 0.27 % and the density 1.858 g/cm<sup>3</sup>. With these properties, it can give high friction coefficient and low wear rate of friction material. The coconut shell powder can be effectively used as a replacement of asbestos in brake pad manufacture.

#### ACKNOWLEDGEMENT

The author would like to thank to the Centre for Advanced Research on Energy (CARE), Faculty of Mechanical Engineering, Universiti Teknikal Malaysia Melaka for providing financial, infrastructure and supporting for this research.

#### REFERENCES

- [1] Ruzaidi, C. M., Kamaruddin, H., Shamsul, J. B. & Abdullah M. M. A. (2012). Mechanical Properties and Wear Behavior of Brake Pads Produced from Palm Slag, 341-342, 26-30.
- [2] Blau P. J. (2001). Composition, functions and testing of friction brake materials and their additives.
- [3] Madakson, P. B., Yawas, D.S., Apasi, A. (2012). Characterization of Coconut Shell Ash or Potential Utilization in Metal Matrix Composites for Automobile Applications. 4 (3), 1190-1198.
- [4] Singh, A., Singh, S. & Kumar A. (2013). Study of Mechanical Properties and Absorption Behaviour of Coconut Shell Powder-Epoxy Composites. 2 (5), 157-161.
- [5] Maleque, M.A., Atiqah, A., Talib, R.J. & Zahurin, H. (2012). New Natural Fibre Reinforced Aluminium Composite for Automotive Brake Pad, 7 (2), 166-170.

# Effect of temperature on reliability performance of electrically conductive nano – composites

M.A. Othman<sup>1</sup>, S.H.S.M. Fadzullah<sup>1,2,\*</sup>, M.M.Nasaruddin<sup>1</sup>, G. Omar<sup>1,2</sup> and M.Z.Akop<sup>1,2</sup>

<sup>1</sup>) Faculty of Mechanical Engineering, Universiti Teknikal Malaysia Melaka, Hang Tuah Jaya, 76100 Durian Tunggal, Melaka, Malaysia

<sup>2</sup>) Centre for Advanced Research on Energy, Universiti Teknikal Malaysia Melaka, Hang Tuah Jaya, 76100 Durian Tunggal, Melaka, Malaysia

\*Corresponding e-mail: hajar@utem.edu.my

**Keywords:** Multi – walled carbon nano tube; electrically conductive adhesives; thermal aging; moisture absorption

**ABSTRACT** – This research investigates the effect of temperature and humidity on the reliability performance of electrically conductive nanocomposites made from solution mixing process using epoxy matrix and multi-walled carbon nano tube (MWCNT). The test specimens were subjected to 168 hours of thermal aging and specified test specimens were characterized at normal condition as controlled specimens. The reliability performance were tested in terms of its electrical conductivity and lap shear strength using the 4 point probe and universal testing machine respectively. With the presence of moisture attack, the electrical conductivity of the ECA increase with thermal aging period while the shear strength revealed contradicting trend which results in a decrease in the shear strength of the ECA.

## 1. INTRODUCTION

Electrically conductive adhesives (ECA) is known to be the replacements for the use of lead-bearing solders. The characteristic of the ECA is that it conducts electricity as well as heat. The electrical conductivity in the ECA is important since the adhesive must be able to create an electric connection between components as well as providing electromagnetic interface (EMI) or radio frequency interference functions [1].

The ECA consists of conductive metallic properties and polymer matrix. The most typically used conductive metal in the ECA is silver in an epoxy resin. This is due to the environment friendly properties that silver has, rather than using lead which is harmful towards humans.

It is reported that ECA is greatly affected when the ambient temperature and humidity are changed. The water gain in the polymer matrices causes an internal hydrolysis of colloids which can results in an increase in the electrical resistance and reduces the bonding strength which may lead to failure.

This study aims to study reliability performance of the ECA when being subjected to thermal aging process in terms of electrical conductivity and mechanical properties of the ECA using varying MWCNT filler loading.

## 2. RESEARCH METHODOLOGY

### 2.1 ECA preparation

The ECA is being made up of three raw materials, polymer matrix, curing agent and conductive filler. All these materials were mixed by using solution mixing

method. The process starts by mixing polymer matrix and hardener then stirred for 1 minutes and lastly MWCNT conductive filler was inserted with the mixture of polymer matrix and hardener and stirred for 5 minutes to produce an ECA. Three filler loadings are prepared, which is 5 wt%, 6 wt% and 7 wt%.

### 2.2 Test sample preparation

There are two types of sample that is needed to be prepared for electrical conductivity test and lap shear test. For the electrical conductivity test, the sample is prepared on an insulator substrate in which the six strip of ECA were printed in accordance with ASTM F390. As for mechanical test, the samples are prepared in accordance with the ASTM D – 1002 – 05 standard for lap shear test. There are about 4 test specimens per filler loading which consists of 1 test specimen for electrical test and 3 for lap shear test.

The thermal aging process are conducted prior to electrical and the lap shear test except for 0 hours test specimens, since the test specimens are used as the controlled data for this research. Test specimens are inserted into the humidity chamber. The humidity chamber is set at 85°C temperature and 85% RH.

### 2.3 Experiment setup

The reliability performance of the ECA is studied in terms of electrical characterization by measuring the electrical conductivity on each strip by using 4-point probe. As for the mechanical characterization, the lap shear test is conducted by using the universal testing machine. The electrical and mechanical characterization were tested in accordance to ASTM F390 and ASTM D – 1002 – 05 respectively.

## 3. RESULTS AND DISCUSSION

In this section, results from the electrical and mechanical characterization are discussed in terms of electrical conductivity and shear strength.

### 3.1 Electrical characterization

The experimental results following electrical conductivity test for the controlled specimens suggest that the sheet resistance of the ECA decreases with increasing filler loadings. From the result obtained, during the electrical conductivity test, it is found that the resistance for each filler loading decreases from 5 wt.%, 6 wt.% and 7 wt.% due to the amount of which the conductive filler and the non-conductive polymer, differs in each filler loadings. For the 5 wt.% filler

loading, the ECA does not reach the percolation threshold. The transition from insulator to conductor is still not enough since the amount of the polymer matrix is still higher than the conductive filler [2]. However, there is a slight decrease in the sheet resistance for 6 wt.% and 7 wt.% filler loadings. Such decrease is due to the moisture absorption during the thermal aging which either breaks or constructs the conductive path of the conductive filler. Meanwhile, the ECA with filler loading of 5 wt.% decreases significantly. This shows that the thermal aging process on the 5 wt.% ECA absorbs more moisture compared to 6 wt.% and 7 wt.% ECA. The mass of the ECA also increases following the thermal aging process for each of the filler loadings.

Table 3.1: Electrical characterization data

Filler loadings	Sheet resistance, R/sq	
	0 week, 0 hr	1 week, 168 hr
5 wt. %	64.96 ±	39.17 ±
6 wt. %	5.61 ±	5.55 ±
7 wt. %	1.75 ±	1.34 ±

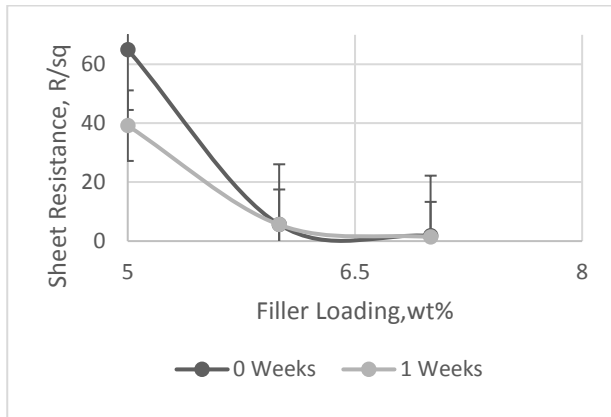


Figure 3.1 Electrical characterization results following 0 week and 1 week of thermal aging.

### 3.2 Mechanical characterization

For the mechanical characterization results, Figure 3.2 shows the controlled and the 1 week thermal aged specimen results. The decrease in shear stress with each filler loading is due to the amount of polymer resin which acts as the adhesive decreases in each filler loading. Both of the 5 wt.% filler loading has the highest average shear stress because it has the most polymer matrix inside the ECA. The ECA with filler loading of 6 wt.% and 7 wt.% is poor in load transfer, possibly because of the agglomeration of the MWCNT that is formed at the conductive filler. This makes the movements in the ECA easier to be initiated [3]. The result from the 1 week thermal aged specimen, the ECA with varying filler loadings exhibit a significant decrease in the shear stress. This is possibly due to the moisture absorption, which disturbs the conductive filler in the ECA and results in formation of voids and fracture [4].

Table 3.2: Mechanical characterization data.

Filler loadings	Average Shear Stress (N/mm <sup>2</sup> )	
	0 week, 0 hr	1 week, 168 hr
5 wt%	9.55 ±	3.67 ±
6 wt%	7.22 ±	3.47 ±
7 wt%	6.34 ±	2.97 ±

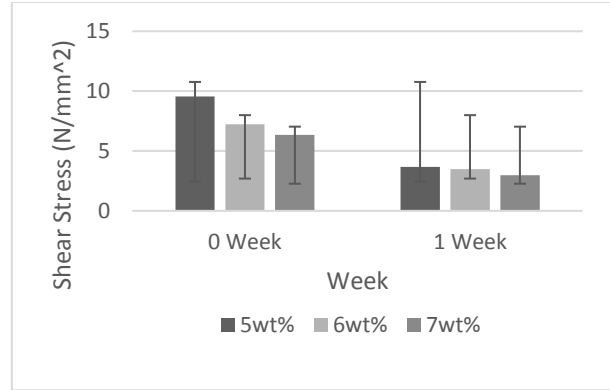


Figure 3.2 Mechanical characterization results

## 4. SUMMARY

The reliability performance of the ECA is based on the electrical conductivity and shear stress following the thermal aging process. With the presence of moisture, lower contact resistance between the ECA and the substrates are observed, possibly due to the act of the moisture absorption, which aid in developing a conductive path which allows current to flow through which reduces the sheet resistance of the ECA. Regardless of the amount of MWCNT filler loading (5-7 wt.%), due to moisture attack, voids are created in the epoxy matrix of the ECA, which results in a decrease in the shear strength of the ECA, when the samples were subjected to thermal aging up to 1 week (168 hours) at 85°C and 85% RH.

## ACKNOWLEDGEMENTS

This work is funded by PJP/2016/FKM/HI1 /S01464 and GLUAR/JABIL/2016/FKM-CARE /I00016 grants from Faculty of Mechanical Engineering, Universiti Teknikal Malaysia Melaka (UTeM) and JABIL Circuit Sdn. Bhd. Penang.

## REFERENCES

- [1] Li, Y., Lu, D. & Wong, C. P. (2010). Electrical conductive adhesives with nanotechnologies.
- [2] Ma, P. C., Siddiqui, N. A., Marom, G. & Kim, J. K. (2010). Dispersion and functionalization of carbon nanotubes for polymer-based nanocomposites: A review. *Compos. Part A Appl. Sci. Manuf.*, vol. 41, no. 10, pp. 1345–1367.
- [3] Chew, C. S. (2015) The effect of nano fillers in electrical and mechanical properties of isotropic conductive adhesive. *Proc. IEEE/CPMT Int. Electron. Manuf. Technol. Symp.*, vol. 2015–June.
- [4] Ahmad Mir, I. & Kumar, D. (2012). Carbon nanotube-filled conductive adhesives for electronic applications. *Nanosci. Methods*, vol. 1, no. 1, pp. 183–193.

# Effects of carbon nanotube aspect ratio on the functional properties of electrically conductive adhesive

A.M. A Raheem<sup>1</sup>, S.H.S.M. Fadzullah<sup>1,2\*</sup>, M.M. Nasaruddin<sup>1</sup>, G. Omar<sup>1,2</sup> and M.Z. Akop<sup>1,2</sup>

<sup>1</sup>) Faculty of Mechanical Engineering, Universiti Teknikal Malaysia Melaka, Hang Tuah Jaya, 76100 Durian Tunggal, Melaka, Malaysia

<sup>2</sup>) Centre for Advanced Research on Energy, Universiti Teknikal Malaysia Melaka, Hang Tuah Jaya, 76100 Durian Tunggal, Melaka, Malaysia

\*Corresponding e-mail: hajar@utem.edu.my

**Keywords:** Conductive ink; multi-wall carbon nanotube; electrically conductive adhesive

**ABSTRACT** – This project investigates the effect of carbon nanotubes aspect ratio on the functional properties of electrically conductive adhesive (ECA). Two types of multi walled carbon nanotubes (MWCNT) conductive filler are considered, with the same outer diameter but different length which have aspect ratios of 1750, termed high aspect ratio and 112.5, termed low aspect ratio and manually mixed with epoxy to produce the ECA. Results on the ECA using MWCNT of low aspect ratio on the electrical conductivity suggest that percolation threshold is reached at relatively high filler loading while the percolation threshold for high aspect ratio MWCNT is reached at lower filler loading. The results suggest that higher aspect ratio MWCNT has better conductivity as compared to low aspect ratio MWCNT.

## 1. INTRODUCTION

The effort to eliminate lead in solder have driven the electrical industries to two alternatives, that is lead-free metal solder alloys and polymer-based electrically conductive adhesive (ECA). There are two components in ECA which consists of resin or polymer matrix which can be either thermoplastic or thermosetting and a conductive filler typically based on metallic materials. The polymer matrix in electrically conductive adhesive (ECA) provides the mechanical properties such as mechanical strength, adhesion, and impact strength while the conductive filler provides the electrical properties.

In this study, the functional properties of MWCNT-ECA is studied with the aim to achieve good electrical conductivity, depending on the aspect ratio of MWCNT, by varying the length as well as using filler loading between 5 to 7 wt.%. A four-point probe test unit is used to determine the electrical conductivity of the MWCNT-filled ECA in terms of the sheet resistance value.

## 2. RESEARCH METHODOLOGY

### 2.1 Samples preparation

Three main substance is needed to formulate ECA which is, epoxy, hardener and conductive filler. Epoxy resin Araldite 506 is used as the polymer matrix and Polyetheramine Jeffamine D-230 is the hardener used which is thermoset hardener. MWCNT is used as the conductive filler with 2 different aspect ratio and different filler loading.

All the samples were prepared first by blending the

epoxy Araldite 506 with Jeffamine D-230 Polyether amine which is the hardener. Before blending, the amount of epoxy used need to be measured using a weight balance. The MWCNT filler loading that are chosen for this research are 5 wt.%, 6 wt.%, and 7 wt.%. The rule of mixture formula is used to calculate the mixture amount needed. Table 2.1 below show the weight of each material used to formulate 5 g of ECA according to each filler loading.

Table 2.1 Formulation of 5g ECA

Filler loading (WT%)	5	6	7
Epoxy (g)	4.75	4.7	4.65
Hardener (g)	1.425	1.41	1.395
MWCNT (g)	0.25	0.3	0.35

Once the hardener is added to the epoxy, it was stirred for 1 minute with constant speed and rotation direction. Then, the required amount of MWCNT is added. The sample was then stirred for another 5 minutes to blend the mixture and MWCNT. The formulated ECA is then cured in a Memmert oven for 30 minutes with temperature of 100°C for curing.

### 2.2 Samples characterization

Six strips of the ECA was applied onto a 3-mm thick acrylic with dimensions of 45 mm (wide) and 88.9 mm (length) by using printing technique. Figure 2.2.1 shows the drawing illustration of the sample. The strip is 12.7 mm in length and 2 mm wide and were subjected to electrical test using a four-point probe test unit, with reference to ASTM F390-1.

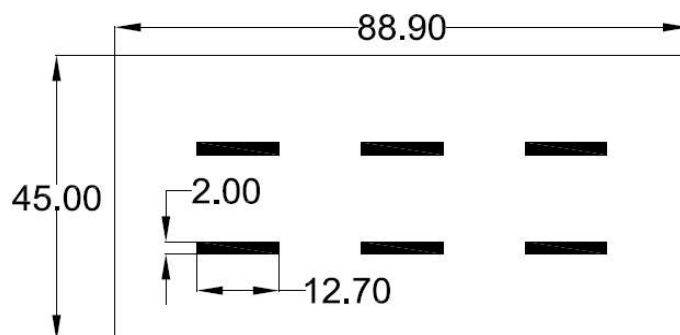


Figure 2.2.1 Drawing of electrical specimen.

## 3. RESULTS AND DISCUSSION

The results from the electrical test and scanning electron microscope (SEM) image MWCNT distribution

in the ECA is discussed in this section. As the aspect ratio of filler increase, the conductivity generally increases. Excluded volume concept is used to describe this trend in which the volume around an object as the overlapping of two similar object is to be avoided when the center of the object is not allowed to enter. As the two MWCNT excluded volume overlapped, a conducting link may be formed. The percolation threshold decreases with decreasing excluded volume. This indicates that at lower filler loadings, better conductivity is achieved.

Table 3.1 Sheet resistance of high and low aspect ratio MWCNT ECA with respect to their filler loading.

Filler Loading	Sheet Resistance (k $\Omega$ /sq.)	
	High aspect ratio	Low aspect ratio
5	10.66 $\pm$ 3.19	180.87 $\pm$ 48.70
6	3.79 $\pm$ 1.89	143.40 $\pm$ 45.84
7	1.367 $\pm$ 0.49	77.33 $\pm$ 51.15

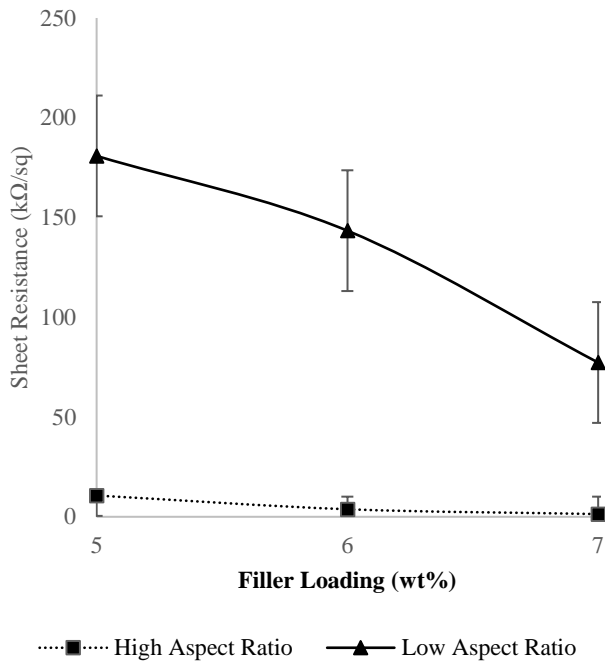


Figure 3.1 Sheet Resistance of different aspect ratio and filler loading of MWCNT ECA.

Figure 3.1 shows the sheet resistance of the MWCNT of different aspect ratio and filler loading. The high aspect ratio MWCNT filled ECA has a lower sheet resistance as compared to low aspect ratio MWCNT filled ECA with respect to the filler loading used in this research. Thus, the percolation threshold of high aspect ratio MWCNT filled ECA occurred at lower filler loading compared to low aspect ratio MWCNT filled ECA. This may due to the agglomeration of the MWCNT and the conductive path created by the MWCNT in the ECA. Figure 3.2 (a) and (b) show the distribution of high aspect ratio MWCNT in the ECA for 5 wt.% and 7 wt.% where for 7 wt.% the agglomeration of MWCNT is observe in Figure 3.2 (b) due to the non-uniformity of the MWCNT filler.

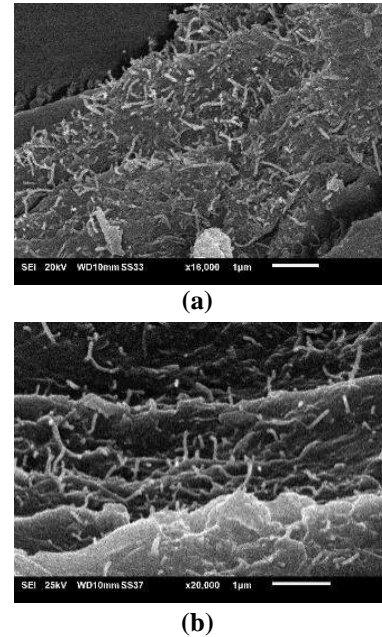


Figure 3.2 SEM image of high aspect ratio MWCNT distribution with (a) 5 wt.% (b) 7 wt.%.

#### 4. SUMMARY

MWCNT with different aspect ratio is used to formulate the ECA and characterized in terms of electrical performance with respect to different filler loading. From the result obtained, high aspect ratio MWCNT-filled ECA yield in better conductivity as compared to the ECA with low aspect ratio MWCNT filler. Moreover, the electrical conductivity suggests that percolation threshold of ECA mixed with MWCNT is achieved at relatively low filler loading due to the continuity of conductive path created by the MWCNT in the ECA.

#### ACKNOWLEDGEMENTS

This work is funded by PJP/2016/FKM/ HII/S01464 and GLUAR/JABIL/2016/FKM-CARE/ 100016 grants from Faculty of Mechanical Engineering, Universiti Teknikal Malaysia Melaka (UTeM) and JABIL Circuit Sdn. Bhd. Penang.

#### REFERENCES

- [1] Nash, C., Spiesschaert, Y., Amarandei, G., Stoeva, Z., Tomov, R. I., Tonchev, D., & Glowacki, B. A. (2015). A Comparative Study on the Conductive Properties of Coated and Printed Silver Layers on a Paper Substrate. *Journal of Electronic Materials*, 44(1), 497.
- [2] Kazani, I. (2012). Study of screen-printed electroconductive textile materials (Doctoral dissertation, Ghent University).
- [3] Kim, D., & Moon, J. (2005). Highly conductive ink jet printed films of nanosilver particles for printable electronics. *Electrochemical and Solid-State Letters*, 8(11), J30-J33.
- [4] Kamyshny, A., Steinke, J., & Magdassi, S. (2011). Metal-based inkjet inks for printed electronics. *The Open Applied Physics Journal*, 4(1).



# Fabrication of hybrid oil palm empty fruit bunch and kenaf reinforced epoxy composite panels at varying fiber layering sequence

M.R. Mansor<sup>1,2\*</sup>, M.A.A. Hadi<sup>1,2</sup>, M.J. Taufiq<sup>1,2</sup>, M.A. Salim<sup>1,2</sup> and A. Md. Saad<sup>1,2</sup>

<sup>1</sup>) Faculty of Mechanical Engineering, Universiti Teknikal Malaysia Melaka, Hang Tuah Jaya, 76100 Durian Tunggal, Melaka, Malaysia

<sup>2</sup>) Centre for Advanced Research on Energy, Universiti Teknikal Malaysia Melaka, Hang Tuah Jaya, 76100 Durian Tunggal, Melaka, Malaysia

\*Corresponding e-mail: muhd.ridzuan@utem.edu.my

**Keywords:** Hybrid natural fiber composite panels, oil palm empty fruit bunch fiber, kenaf fibers, epoxy matrix, fiber layering sequence, porosity

**ABSTRACT** – Hybrid natural fiber composites offer many advantages especially in achieving balance between mechanical performance and cost as compared to single natural fiber-matrix composites. In this paper, the fabrication process of preparing novel hybrid oil palm empty fruit bunch (OPEFB) and kenaf fibers reinforced epoxy composite panels is explained. Four varying fiber stacking sequences were applied to prepare the hybrid composites panels, at thermoset epoxy matrix between 58.1 wt% until 68.6 wt%. Three types of fibers were used in the composites fabrication, which are short fiber (sf) OPEFB, short fiber (sf) kenaf and woven kenaf mat. The hybrid composites fabrication involved fiber crushing (to form short fibers at fiber length between 1 mm to 3 mm), and compression moulding (at 25 psi and room temperature). All panels were fabrication based on steel mould with fix length x width x height of 200 mm x 200 mm x 3 mm. End of fabrication process showed that high quality compressed hybrid composites panels with very low porosity were successfully obtained for fiber layering sequence of kenaf\_sf/OPEFB\_sf/kenaf\_sf and kenaf\_mat/OPEFB\_sf/kenaf\_mat. In the other hand, the final hybrid composite panels which consist of fiber layering sequence OPEFB\_sf/Kenaf\_sf/OPEFB\_sf and OPEFB\_sf/Kenaf\_mat/OPEFB\_sf yielded high porosity at the end of the fabrication process. The results obtained showed that hybrid composite panels which are fabrication using higher kenaf fiber weightage were able to yield good quality panels with very low porosity compared to panels fabricated using higher OPEFB fiber weightage, which indicated good wettability between the epoxy matrix and the kenaf fibers.

## 1. INTRODUCTION

Hybridization technique is one of the solutions to improve single fiber-matrix system in natural fiber composite product development [1]. The prominent advantage of the hybridization technique is the ability to achieve a balance between performance and cost between the two combined fibers, which are usually made from fiber with low mechanical properties but low cost and fiber with high mechanical properties but high cost [2].

Up to date, there are several studies on the effect of layering sequence on the hybrid natural fiber reinforced thermoset composites performance such as

by Jawaid et al [3] using hybrid oil palm empty fruit bunch (OPEFB)/jute reinforced epoxy composites and by Yahaya [4] using kenaf/Kevlar reinforced epoxy composites. Their studies showed that varying layering or stacking sequence between the plies affected the final composites mechanical properties.

In this project, a novel hybrid natural fiber reinforced thermoset epoxy composites was developed, using the combination of locally and abundantly available OPEFB fibers, and kenaf fibers. The objective of the project was to determine the final hybrid composites quality in term of porosity, by varying the layering sequences between the OPEFB fibers and kenaf fibers. Compression moulding process was utilized for the hybrid composites sample preparation, and all hybrid composites formulation were pressed up to 25 psi of pressure into 3 mm thick window-framed panels.

## 2. RESEARCH METHODOLOGY

### 2.1 Raw Materials

Kenaf bast fiber (short fiber and mat) was obtained from Lembaga Kenaf dan Tembakau Negara (LKTN) Malaysia, while the OPEFB fiber was obtained from Kilang Kelapa Sawit Kempas, Melaka. Neat epoxy resin (CP360 Part A) and amine hardener (CP360 Part B) with resin to hardener ratio of 2:1 was used as matrix for the hybrid composites.

### 2.2 Sample Preparation

Four varying fiber stacking sequences were applied to prepare the hybrid composites panels, at thermoset epoxy matrix between 58.1 wt% until 68.6 wt%, as shown in Table 2.1. Three types of fibers were used in the composites fabrication, which are short fiber (sf) OPEFB, short fiber (sf) kenaf and woven kenaf mat. The hybrid composites fabrication involved fiber crushing (to form short fibers at fiber length between 1 mm to 3 mm), and compression moulding (at 25 psi and room temperature). All panels were fabrication based on steel mould with fix length x width x height of 200 mm x 200 mm x 3 mm. The compressed panels were left to cure at room temperature for 24 hours.

Table 2.1 Summary of hybrid OPEFB/kenaf reinforced epoxy composite panels layering sequence.

Layering Sequence	Composition (wt%)		
	OPEFB	Kenaf	Epoxy
OPEFB_sf/Kenaf_sf/ OPEFB_sf	28.9	13	58.1
OPEFB_sf/Kenaf_mat/ OPEFB_sf	34.5	4	61.5
Kenaf_sf/OPEFB_sf/ kenaf_sf	14.9	26	59.1
Kenaf_mat/OPEFB_sf/ kenaf_mat	21.6	9.8	68.6

### 3. RESULTS AND DISCUSSION

Figure 2.1 shows the final hybrid composite panels fabrication at the end of the project, while Table 2.2 summarized the final results obtained through visual inspection on the compressed panels. It can be observed that that high quality compressed hybrid composites panels with very low porosity were successfully obtained for fiber layering sequence of kenaf\_sf/OPEFB\_sf/ kenaf\_sf and kenaf\_mat/OPEFB\_sf/kenaf\_mat. In the other hand, the final hybrid composite panels which consist of fiber layering sequence OPEFB\_sf/Kenaf\_sf/ OPEFB\_sf and OPEFB\_sf/Kenaf\_mat/OPEFB\_sf yielded high porosity at the end of the fabrication process.



Figure 2.1 Compressed hybrid composites panels

The results obtained showed that hybrid composite panels which are fabrication using higher kenaf fiber weightage were able to yield good quality panels with very low porosity compared to panels fabricated using higher OPEFB fiber weightage, which indicated good wettability between the epoxy matrix and the kenaf fibers. In addition, the compression methodology applied to fabricate all samples was also able to produce good panels without any fiber distortion. This allowed

even fiber distribution across the panel surface hence creating high strength properties for all samples.

Table 2.2 Final observation on the compressed hybrid OPEFB/kenaf reinforced epoxy composite panels.

Layering Sequence	Visual Observation	
	Porosity	Fiber Distortion
OPEFB_sf/Kenaf_sf/ OPEFB_sf	High	No
OPEFB_sf/Kenaf_mat/ OPEFB_sf	High	No
Kenaf_sf/OPEFB_sf/ Kenaf_sf	Low	No
Kenaf_mat/OPEFB_sf/ Kenaf_mat	Low	No

### 4. SUMMARY

In conclusion, the results obtained showed that hybrid composite panels which are fabrication using higher kenaf fiber weightage were able to yield good quality panels with very low porosity compared to panel fabricated using higher OPEFB fiber weightage. This indicated good wettability property between the epoxy matrix and the kenaf fibers compared to epoxy and OPEFB fibers. Further research shall be carried out to reduce the porosity on panels with high OPEFB fiber contents such as through modifying the compression moulding pressure scheme and applying fiber treatment process using sodium hydroxide (NaOH) on both kenaf and OPEFB fibers.

### REFERENCES

- [1] Mastura, M.T., Sapuan, S.M., Nuraini, A.A. and Mansor, M.R. (2017). Environmentally Conscious Hybrid Bio-Composite Material Selection for Automotive Anti-Roll Bar. *The International Journal of Advanced Manufacturing Technology*, Vol. 89, No. 5-8, pp. 2203-2219.
- [2] Mansor, R., Sapuan, S.M., Zainudin, E.S., Nuraini, A.A. and Hambali, A. (2013). Stiffness Prediction of Hybrid Kenaf/Glass Fiber Reinforced Polypropylene Composites using Rule of Mixtures (ROM) and Rule of Hybrid Mixtures (RoHM). *Journal of Polymer Materials*, Vol. 30, No. 3, pp. 321-334.
- [3] Jawaid, M. and Abdul Khalil, H.P.S. (2011). Effect of Layering Pattern on the Dynamic Mechanical Properties and Thermal Degradation of Oil Palm-Jute Fibers Reinforced Epoxy Hybrid Composite, *Bioresources*, Vol 6, No. 3, pp.2309-2322.
- [4] Yahaya, R., Sapuan, S. M., Jawaid, M., Leman, Z., & Zainudin, E. S. (2015). Effect of layering sequence and chemical treatment on the Mechanical Properties of Woven Kenaf-Aramid Hybrid Laminated Composites. *Materials & Design*, Vol. 67, pp. 173-179.

# Effect of line thickness cross-sectional geometry to stretchable printed circuit

M.A. Suhaimi<sup>1</sup>, M.Z. Azmi<sup>1</sup>, N.S. Rozali<sup>1</sup>, N.H. Sobri<sup>1</sup> and M.Z. Akop<sup>1,2,\*</sup>

<sup>1</sup>Faculty of Mechanical Engineering, Universiti Teknikal Malaysia Melaka, Hang Tuah Jaya, 76100 Durian Tunggal, Melaka, Malaysia.

<sup>2</sup>Centre for Advanced Research on Energy, Universiti Teknikal Malaysia Melaka, Hang Tuah Jaya, 76100 Durian Tunggal, Melaka Malaysia.

\*Corresponding e-mail : [zaid@utem.edu.my](mailto:zaid@utem.edu.my)

**Keywords** : Carbon black; thermoplastic-polyurethane; ink thickness; screen printing; four point prob

**ABSTRACT** – The effect of thickness of the ink on the resistivity. There are five samples with different thicknesses (2, 4, 6, 8 and 10 layers). The layers was made using cellophane tape and each layer represent 0.04 mm. The printing method used was screen printing method and the samples was measured using four point probe in the unit of  $\Omega/\text{sq}$ . In this paper the conductive ink used is carbon black and the substrate used are glass and thermoplastic-polyurethane (TPU). The result of the study shows that when the thickness of the ink increase, the resistivity will decreased.

## 1. INTRODUCTION

Stretchable printed circuit board (SPCB) have similar function as printed circuit board (PCB) which is to connecting electrical component together and actually make the device working and functioning correctly. The existence of the SPCB really improve our technologies to another level. The characteristic of the SPCB making it is widely used not only in industry but also in fashion, health and sport [1]. The component of the SPCB can divided into two main components which are the conductive ink and substrate, where the conductive ink replacing the traces that being used in the PCB and the substrate as the medium to place the conductive ink. The function of the traces and the conductive ink is to making the path for the electric to flow in the circuit.

There are several kind of conductive ink such as silver, copper and carbon. Silver ink is widely used because of high conductivity but the cost is high. Meanwhile carbon black is cheaper but less conductivity compared to silver [2].

The objective of this study is to investigate the effect of thickness of the ink against the resistivity. The resistivity will be measured using the four point probe and the graph of sheet resistance against the thickness of the ink will be tabulated.

## 2. RESEARCH METHODOLOGY

### 2.1 Samples Preparation

There are 3 main processes to preparing the samples which are preparing the material and apparatus needed for printing process, the printing of the ink to the substrate and the curing of the samples process.

The material and apparatus needed for printing process are the razor blade that is used for spreading the ink paste, the cellophane tape to change the thickness of the ink, the conductive ink and the substrate. In this study the conductive ink used was carbon conductive

ink made by Bare Conductive and the substrate used were glass slide and TPU. The printing method used to print the ink to the substrate was screen printing method [1]. Before start printing the ink, the substrate will be tape using cellophane tape where the thickness of the tape is 0.04 mm, in order to create different thickness when the ink printed to the substrate. The tape will be stack together to create layers, the layers used for this study are 2, 4, 6, 8 and 10 layers.

Then the conductive ink will be place on the sample and spread using the razor blade. The method used to print the samples are following the standard of razor straight line printing method referred to standard ASTM D2739 [3]. After the printing process complete, the samples was cured in the room temperature for 15 minutes as mentioned in the technical datasheet of Bare carbon conductive ink [4].

### 2.2 Experiment Setup

The electrical test will be tested using the four point probe to measure the resistivity of each samples in the unit of  $\Omega/\text{sq}$ . The test conducted in the room temperature.

## 3. RESULTS AND DISCUSSION

In this section the result of the measurement will be discussed in detail on the effect of thickness on ink resistivity. There will be two result since there are two types of substrate being used which are glass slide and TPU.

### 3.1 Glass Slide

The glass slide physical characteristic is a rigid body non-flexible and non-stretchable substrate. The purpose printing the conductive ink on the glass slides are to focus the result only on the effect of the different thickness of the conductive ink to the resistivity of the conductive ink measured by the four point probe. So this are the result obtain from five samples of glass slides by the four point probe.

Table 3.1 : Glass slide data.

Sample	Num. Layer	Total Average Rs ( $\Omega/\text{sq}$ )
1	2	494.93
2	4	289.33
3	6	313.35
4	8	350.48
5	10	201.98

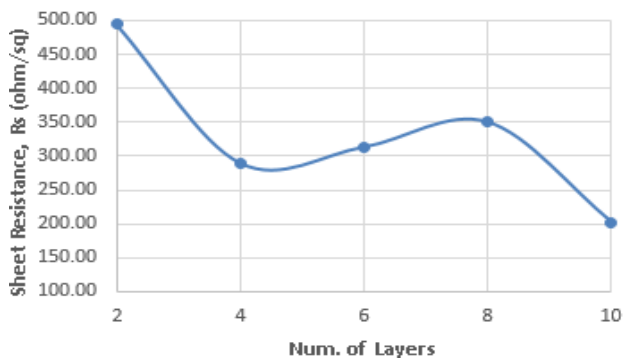


Figure 3.1 : Glass slide data.

As can be seen the lowest and the highest sheet resistance are 201.98 Ω/sq (10 layers) and 494.93 Ω/sq (2 layers) respectively. So basically as the number of the layers or the thickness of the ink increasing, the sheet resistance will be decreasing. The result is same as expected and based on other founding [5].

But there are sudden increasing in the graph on sample 3 and 4. This phenomenon can be due to the inexperience of printing technique which the samples are not printed smoothly and unevenly. It also can be due to void on the ink, the probability of the void become higher if the thickness of the ink is too thin which making the electrical flow not smooth and affecting the measurement of the data. The last reason is due to the cellophane tape not perfectly stack together while making the layers which causing the thickness of the ink not consistent after printing.

### 3.2 Thermoplastic-Polyurethane (TPU)

Thermoplastic-polyurethane physical characteristic is opposite from glass slide because it is stretchable and flexible. The result of the experiment as below.

Table 3.2 : TPU data.

Sample	Num. Layer	Total Average Rs (ohm/sq)
6	2	465.92
7	4	392.94
8	6	297.55
9	8	119.89
10	10	136.47

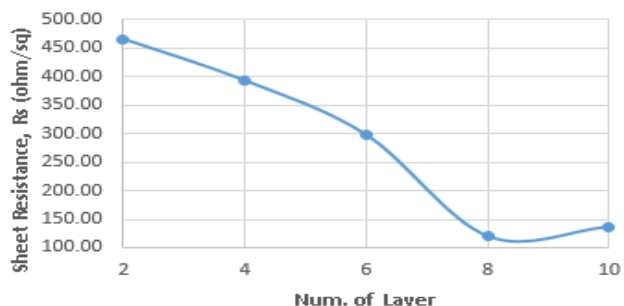


Figure 3.2 : TPU data.

The pattern of the data of TPU is quite similar as glass slide which as the thicker the ink, the lower the resistivity reading. As can be seen the lowest sheet resistance is 119.89 Ω/sq (8 layers) and the highest is

465.92 Ω/sq (2 layers).

The pattern of the graph is constantly decreasing until sample 9 and sudden increasing on sample 10. The increase in resistivity of sample 10 is due to same reason as the problem occur in the glass slide.

### 4. SUMMARY

The purpose of the study is to investigate the effects of thickness cross-sectional geometry of the ink against the resistivity by measuring the samples using the four point probe. The result from this study can be conclude that when the thickness of the ink increasing will decrease the resistivity of the samples or in other word the conductivity will be increasing.

### REFERENCES

- [1] J. Suikkola, "Printed Stretchable Interconnects for Wearable Health and Wellbeing Applications," no. June, p. 59, 2015.
- [2] S. S. Bhore, "Formulation and Evaluation of Resistive Inks for Applications in Printed Electronics," pp. 1–94, 2013.
- [3] ASTM, "Standard Test Method for Volume Resistivity of Conductive Adhesives 1," *Astm*, vol. 97, no. 4306, pp. 2010–2012, 2015.
- [4] BareConductive, "Bare Carbon Conductive Ink-Technical Sheet," pp. 1–3, 2015.
- [5] R. K. Khirotdin, T. S. Cheng, and K. A. Mokhtar, "Printing of conductive INK tracks on textiles using silkscreen printing," *ARPJ. Eng. Appl. Sci.*, vol. 11, no. 10, p. 6619–6624g, 2016.

# The effect of substrate surface conditions on mechanical performance of electrically conductive adhesive

W.A.W.A. Rahman<sup>1</sup>, S.H.S.M.Fadzullah<sup>1,2,\*</sup>, M.M.Nasaruddin<sup>1</sup>, G.Omar<sup>1,2</sup> and M.B.Ramli<sup>1,2</sup>

<sup>1</sup>) Faculty of Mechanical Engineering, Universiti Teknikal Malaysia Melaka, Hang Tuah Jaya, 76100 Durian Tunggal, Melaka, Malaysia

<sup>2</sup>) Centre for Advanced Research on Energy, Universiti Teknikal Malaysia Melaka, Hang Tuah Jaya, 76100 Durian Tunggal, Melaka, Malaysia

\*Corresponding e-mail: hajar@utem.edu.my

**Keywords:** Electrically conductive adhesive (ECA); surface treatment; lap shear strength

**ABSTRACT** – This project investigates the effect of surface treatment towards the surface roughness and surface wettability which contributed to the lap shear strength of electrically conductive adhesive (ECA) bonded to aluminum-aluminum substrate. Several surface treatment methods were applied on the aluminum substrate which involved chemical etching process with the utilization of NaOH solution and HCl solution, and mechanical abrasion process by SiC abrasive paper G180 and G1200. Four-point probe test on ECA sheet resistance shows that the increase of multi-walled carbon nanotube (MWCNT) filler loading decreased the ECA electrical resistivity. As chemically etched substrate provides highest surface roughness and the lowest contact angle, the ECA bonded to the substrate exhibit the highest shear strength when subjected to lap shear test.

## 1. INTRODUCTION

Nowadays, with increasing the awareness to protect the environment, the use of lead-based solder for electronic components interconnection in printed circuit board (PCB) are gradually replaced by the lead-free electrically conductive adhesive (ECA) in microelectronic industry [1]. As interconnect materials, the mechanical strength of ECA is another aspect to be improvised in addition to the electrical conductive performance. The adhesion performance is influenced by the surface wetting properties which play an important role to improve ECA bonded joint mechanical strength. The strong bonded joint requires adequate intimate contact with the substrate for generating strong physical and chemical bonds.

ECA being a type of polymer based composite materials exhibit poor surface properties to attain good adhesion as the material is inherently inert in nature. The surface properties of substrate shall be enhanced by increasing the surface roughness or by modifying the surface chemistry of the substrate via surface treatment methods [2].

The aim of this research is to study the effect of substrate surface conditions on mechanical strength of ECA bonded joint since there is only limited research found in the literature.

## 2. RESEARCH METHODOLOGY

In this study, ECA with MWCNT filler loading of 5 wt.%, 6 wt.% and 7 wt.% were prepared and characterized in terms of their conductivity performance

by determining the ECA sheet resistance using JANDEL In-Line Four Point Probes. The test was conducted with referring to ASTM F390. Different surface treatment methods were applied on aluminum substrate which are grinding with SiC abrasive paper G180, polishing with SiC abrasive paper G1200 and chemical etching. The surface roughness, Ra, of as-received and treated surface of aluminum substrate were determined by using stylus profilometer brand Mitutoyo SJ-410. The contact angle measurement on as-received and treated surface of aluminum substrate were carried out to determine the wettability of liquid toward the different substrate surface conditions, with reference to the ASTM D5725. Lap shear test were applied on ECA with varying MWCNT filler loading and different substrate surface conditions, in accordance with ASTM D1002. Morphological study using a Scanning Electron Microscopy (SEM) was carried out to understand the failure behavior of ECA following lap shear test.

## 3. RESULTS AND DISCUSSION

### 3.1 Sheet resistance

Figure 3.1 depicts that the sheet resistance decreased with an increase in the MWCNT filler loading from 5 wt.% to 7 wt.%, due to an increase the contact between MWCNT particles and enhancement formation of three-dimensional network [3].

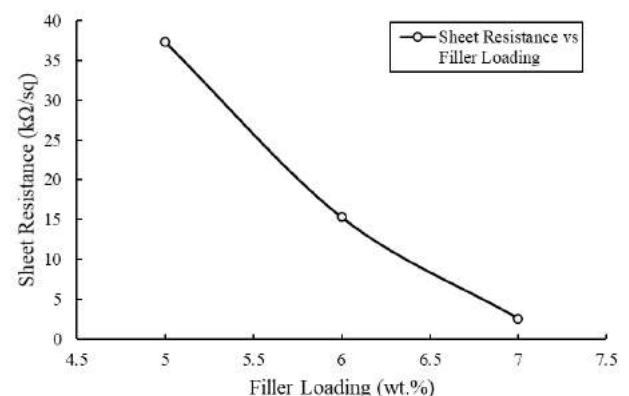


Figure 3.1 Graph of sheet resistance per unit area against percentage of MWCNT filler loading.

### 3.2 Surface roughness

Surface roughness measurement on as-received and surface-treated aluminum substrates as given in Table 3.1 show that the chemically etched substrate exhibits the highest surface roughness while polishing with SiC

abrasive paper G1200 yield in the lowest surface roughness.





Table 3.1 Surface roughness of different substrate surface conditions.

Surface Treatment	Surface Roughness, Ra ( $\mu\text{m}$ )
As-Received	$0.36 \pm 0.02$
Chemical Etching	$2.60 \pm 0.30$
Grinding with SiC Abrasive Paper G180	$0.52 \pm 0.05$
Polishing with SiC Abrasive Paper G1200	$0.10 \pm 0.01$

### 3.3 Contact angle

Based on the results from contact angle measurement in Table 3.2, the chemically etched substrate has the lowest contact angle, which indicates an excellent surface wettability since higher surface roughness promote better spreading of liquid to the substrate surface [4]. Besides, the grinded substrate with SiC abrasive paper G180 yield in the highest contact angle, an indication of poor surface wettability.

Table 3.2 Water droplet contact angle on different substrate surface conditions.

Surface Treatment	Water Droplet Behavior	Contact Angle ( $^\circ$ ) ( $\theta$ )
As-Received		$74.47 \pm 5.29$
Chemical Etching		$16.78 \pm 4.40$
Grinding with SiC Abrasive Paper G180		$85.66 \pm 6.42$
Polishing with SiC Abrasive Paper G1200		$68.52 \pm 3.17$

### 3.4 Lap shear test

Based on Figure 3.2, the highest shear strength is found for ECA with filler loading of 6 wt.% bonded to chemically etched substrate, which provide the highest surface roughness therefore enhancing the mechanical interlocking of the bonded joint. Meanwhile, ECA with 7 wt.% filler loading exhibit the lowest shear strength as compared to ECA with 5 wt.% and 6 wt.% filler loading when bonded to all surface conditions, possibly due to agglomeration of MWCNT in the composites, which results in poorer mechanical properties [5].

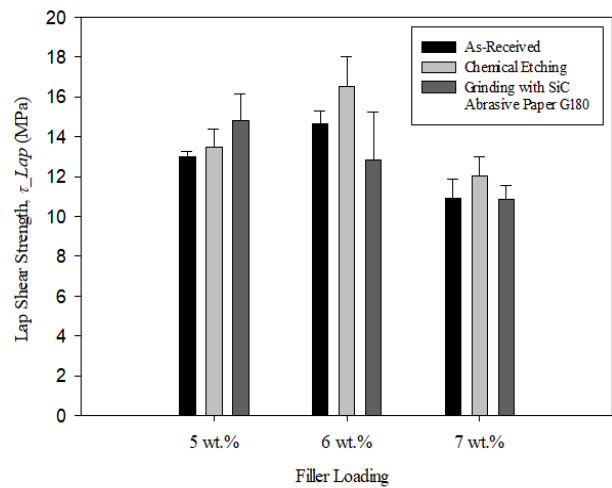


Figure 3.2 Graph of lap shear strength of ECA against MWCNT filler loading.

## 4. SUMMARY

The ECA with 7 wt.% filler loading exhibit an excellent electrical conductivity performance. In addition, shear strength of ECA is strongest when bonded to the chemically etched substrate, as the substrate has the lowest contact angle and highest surface roughness.

## ACKNOWLEDGEMENTS

This work is funded by PJP/2016/FKM/HI1/ S01464 and GLUAR/JABIL/2016/FKM-CARE/I00016 grants from Faculty of Mechanical Engineering, Universiti Teknikal Malaysia Melaka (UTeM) and JABIL Circuit Sdn. Bhd. Penang.

## REFERENCES

- [1] C. C. Sean, S. Pamornpol, O. H. Keat, and R. Durairaj, "Mechanical and Electrical Properties of Carbon Nanotubes Based Isotropic Conductive Adhesives," vol. 857, pp. 93–97, 2016.
- [2] H. M. S. Iqbal, S. Bhowmik, and R. Benedictus, "Study on the effect of surface morphology on adhesion properties of polybenzimidazole adhesive bonded composite joints," *Int. J. Adhes. Adhes.*, vol. 72, no. October 2016, pp. 43–50, 2017.
- [3] L. Yi, L. Daniel, and W. C.P., *Electrical Conductive Adhesives with Nanotechnologies*. New York: Springer Science+Business Media, 2010.
- [4] K. Leena, K. K. Athira, S. Bhuvanewari, S. Suraj, and V. L. Rao, "Effect of surface pre-treatment on surface characteristics and adhesive bond strength of aluminium alloy," *Int. J. Adhes. Adhes.*, vol. 70, pp. 265–270, 2016.
- [5] J. Trinidad, L. Chen, A. Lian, and B. Zhao, "Solvent presence and its impact on the lap-shear strength of SDS-decorated graphene hybrid electrically conductive adhesives," *Int. J. Adhes. Adhes.*, vol. 78, no. May, pp. 102–110, 2017.

# Thermal conductivity and heat transfer of MWCNT-OH ethylene glycol based nanofluids

A. Abdullah<sup>1\*</sup>, I.S. Mohamad<sup>1,2</sup>, A.Y. Bani Hashim<sup>3</sup>, M.H. Mohd Husin<sup>1</sup> and S. Zainal Abidin<sup>1</sup>

<sup>1</sup>) Faculty of Mechanical Engineering, Universiti Teknikal Malaysia Melaka, Hang Tuah Jaya, 76100 Durian Tunggal, Melaka, Malaysia

<sup>2</sup>) Centre for Advanced Research on Energy, Universiti Teknikal Malaysia Melaka, Hang Tuah Jaya, 76100 Durian Tunggal, Melaka, Malaysia

<sup>3</sup>) Faculty of Manufacturing Engineering, Universiti Teknikal Malaysia Melaka, Hang Tuah Jaya, 76100 Durian Tunggal, Melaka, Malaysia

\*Corresponding e-mail: amirahabdullah92@yahoo.com.my

**Keywords:** Thermal conductivity; heat transfer; nanofluids

**ABSTRACT** – The purpose of this study to investigate the thermal conductivity and heat transfer coefficient of MWCNT-OH ethylene glycol based nanofluids at 6°C, 25°C and 40°C. This research used two-step method in preparing the nanofluids. The results following the thermal performance test reveals that these nanofluids gained thermal conductivity enhancement by 2.232% to 20.10%. Meanwhile, the heat transfer coefficient shows an enhancement with the increase in weight loading and temperature. Factors that affects these results are surfactant, stability, dispersion process, nanoparticle size and surface area of MWCNT-OH nanoparticles. These results proved that the seeding of MWCNT-OH nanoparticles have enhanced the thermal performances of the nanofluids.

## 1. INTRODUCTION

Low thermal performance is a characteristic of conventional fluid such as ethylene glycol, deionized water and oil. This characteristic results in a limitation for thermal performance enhancements. Hence, nanotechnology related to nanofluids is used as an initiative to solve this problem. Nanofluids is defined as a suspension of nanometer sized particles in base fluids. In addition, higher thermal conductivity of nanoparticles within ranges 1800 W/m.K to 2000W/m.K results in the enhancing of the thermal performance of base fluids. Past literatures reported that the base fluids' thermal conductivity and heat transfer coefficient are improved with the inclusion of nanoparticles [1]. The enhancement of thermal conductivity is about 23% and 3.2% to 10% for ethylene glycol and deionized water based nanofluids with inclusion of multiwalled carbon nanotube (MWCNT). Meanwhile, heat transfer coefficient of Al<sub>2</sub>O<sub>3</sub> nanofluids is 57% higher than distilled water [2]. However, thermal performances on nanofluids still lacks the data as well as contradictory with the other researchers. Hence, investigations of thermal conductivity and heat transfer on ethylene glycol based nanofluids with seeding of hydroxyl functionalized multiwalled carbon nanotube (MWCNT-OH) are the focus of this research.

## 2. RESEARCH METHODOLOGY

### 2.1 Preparation of nanofluids

Two-step method is used in this investigation by using of MWCNT-OH, polyvinylpyrrolidone (PVP)

surfactant and ethylene glycol. The weight percentage (wt%) of PVP surfactant is 10% from wt.% of nanoparticles where range of wt% of nanoparticles is from 0.1 wt% till 1.0 wt%. These materials undergo dispersion process which were homogenized by Wise Tis HG-15D at 10000 rpm and ultrasonic by Branson 8510DTH Ultrasonic Cleaner at 40 kHz for 5 minutes. The nanofluids is next tested by a stability test rig (STR) and ZEISS inverted microscope as to ensure the stability of the dispersion. Stable nanofluids then undergoes thermal conductivity test and heat transfer test at three different temperatures (6°C, 25°C and 40°C). The thermal conductivity test uses TC-KD2 Pro thermal properties analyzer and KS-1 sensor from Decagon Devices, Inc. These devices have ASTM D5334-14 and IEEE 442-03 verification standard. Heat transfer coefficient is tested using heat transfer rig (HTR) and Pico Data Logger as to measure the values. Three best samples of nanofluids is selected to go through heat transfer coefficient test.

## 3. RESULTS AND DISCUSSION

### 3.1 Thermal conductivity

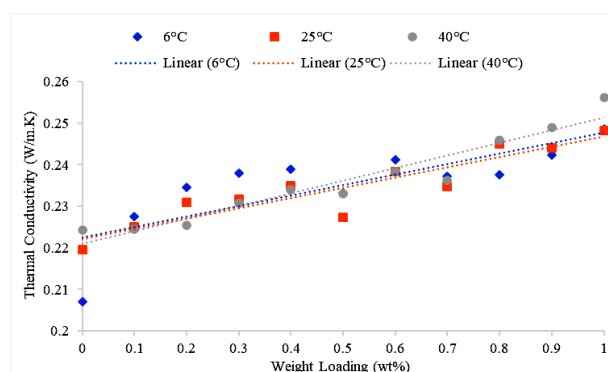


Figure 3.1 Thermal conductivity on MWCNT-OH ethylene glycol based nanofluids.

Figure 3.1 shows the thermal conductivity of MWCNT-OH ethylene glycol based nanofluids for three different temperatures. As can be seen, on 0 wt.% weight loading is the baseline values of ethylene glycol at 6°C, 25°C and 40°C which 0.2070 W/m.K, 0.2195 W/m.K and 0.2243 W/m.K. The inclusion of MWCNT-OH nanoparticles enhances the nanofluids's thermal conductivity of the ethylene glycol. Thermal

conductivity of nanofluids fluctuates with the increment of weight loading. The figure shows linear trend for all the temperatures which is in positive results with the thermal conductivity which in turn is directly proportional to weight loadings. The lowest thermal conductivity occurs on 0.1 wt.% of MWCNT-OH concentrations for each temperature. It is found that the highest thermal conductivity for 6°C, 25°C and 40°C is occurring on 1.0 wt.% concentrations. Based on the figure, the nanofluids' thermal conductivity starts to decline on concentration of 0.5 wt.% for each temperature. In this research, thermal conductivity is enhanced from 2.323% to 20.10% with the inclusion of MWCNT-OH nanoparticles in base fluid. It proved that the inclusion of nanoparticles has enhanced the thermal conductivity.

### 3.2 Heat transfer coefficient

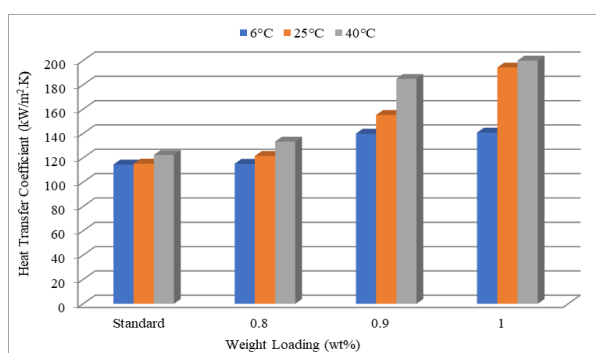


Figure 3.2 Heat transfer coefficient on MWCNT-OH ethylene glycol based nanofluids.

Heat transfer coefficient on MWCNT-OH ethylene glycol based nanofluids has been postulated in Figure 3.2. Three weight loading of nanofluids selected are 0.8 wt.%, 0.9 wt.% and 1.0 wt.% of MWCNT-OH weight loading. On standard of heat transfer coefficient for ethylene glycol are recorded at 114.49 kW/m<sup>2</sup>. K, 115.20 kW/m<sup>2</sup>. K and 122.35 kW/m<sup>2</sup>.K for 6°C, 25°C and 40°C. The highest heat transfer coefficient value is on concentration 1.0 wt.% for each temperature. Temperature 40°C (205.90 kW/m<sup>2</sup>. K) is leading the heat transfer coefficient and followed by 25°C (194.28 kW/m<sup>2</sup>. K) and 6°C (184.93 kW/m<sup>2</sup>. K). Despite that, the lowest heat transfer coefficient occurs on concentration 0.8 wt.% for each temperature which has a value of 115.15 kW/m<sup>2</sup>. K, 121.56 kW/m<sup>2</sup>.K and 133.33 kW/m<sup>2</sup>.K for 6°C, 25°C and 40°C. To sum it up, heat transfer coefficient of MWCNT-OH ethylene glycol based nanofluids increases with increment of weight loading and temperatures.

Hence, these results of thermal performances are affected by several factors. In fact, good thermal conductivity values can give greater heat transfer coefficient performance [3]. Literature stated that the inclusion of small amount of surfactant can increase thermal conductivity and heat transfer coefficient [4]. In addition, surfactant also can avoid or decreases the agglomeration form and achieve the nanofluids' stability. The stability of nanofluids is a crucial factor in thermal

performances where greater stability of nanofluids can give better thermal performance. Meanwhile, dispersion process can break down and reduce the agglomeration nanoparticles in base fluids where agglomeration nanoparticles can influence the thermal conductivity and heat transfer coefficient by decreasing the thermal performance. Moreover, small size and high surface area of nanoparticles also can enhance the thermal performance as the MWCNT-OH nanoparticles' surface area is about 40 cm<sup>2</sup>/g to 300 cm<sup>2</sup>/g [5].

### 4. SUMMARY

In this research, seeding of MWCNT-OH nanoparticles in ethylene glycol has enhanced the thermal performances specifically thermal conductivity and heat transfer coefficient. The thermal conductivity of nanofluids is enhanced by 2.232% to 20.10%. Meanwhile, heat transfer coefficient is improved with great thermal conductivity results where the three best samples of nanofluids are 0.8 wt.%, 0.9 wt.% and 1.0 wt.%. The heat transfer coefficient is improved with high weight loading and temperatures. Several factors which influence the thermal performances are surfactant, stability, dispersion process, nanoparticles size and as well as surface area of MWCNT-OH nanoparticles.

### REFERENCES

- [1] Kanagaraj, S., Varanda, F. R., Oliveira, M. S. A., & Simões, J. A. O., (2006). Theoretical model development for nanofluids thermal effectiveness. *Defect and Diffusion Forum*, 258-260, 164-171.
- [2] Albadr, J., Tayal, S. & Alasadi, M. (2013). Heat transfer through heat exchanger using Al<sub>2</sub>O<sub>3</sub> nanofluid at different concentrations. *Case Studies in Thermal Engineering*, 1(1), 38-44.
- [3] Abdullah, A., Mohamad, I.S., Bani Hashim, A.Y., Abdullah, N., & Zainal Abidin, S. (2016). Effect duration time of homogenization and sonication on stability of MWCNT-OH in ethylene glycol and deionized water," *Proceedings of Mechanical Engineering Research Day*, 171-172.
- [4] Zhou, M.Z., Xia, G.D., Chai, L.J.L., & Zhou, L.J., (2012). Analysis of factors influencing thermal conductivity and viscosity in different kinds of surfactant solutions. *Experimental Thermal and Fluid Science*, 36, 22-29.
- [5] Mohamad, I.S., Chitrabalam, S.T., Hamid, S.B.A., Chin, W.M., Yau, K.H., & Febrian, I. (2013). Comparison study on the heat transfer behavior on aqueous suspensions of rod shaped carbon nanotubes, *Advanced Materials Research*, 667, 35-42.



# A study of ultimate load of a beam under bending

Masniza Yusof <sup>1\*</sup>

<sup>1)</sup>Department of Mechanical Engineering, Politeknik Tuanku Syed Sirajuddin,  
Pauh Putra, 02600 Arau, Perlis, Malaysia

\*Corresponding e-mail: masnizayusof.poli@1govuc.gov.my

**Keywords:** Bending moment; strength; stiffness

**ABSTRACT** – Bending of beams is a frequently encountered loading situation in practice. A slender member subject to traverse loads is termed as a beam under bending. At any cross-section, the traverse loads generate shear and bending moment to maintain equilibrium. One of the common principles used to determine the loading capacity of a structure is the first yield criterion which assumes that the maximum load is reached when the stress in the extreme fabric reaches yield stress. However, the design based on this rule is not economical for a beam carrying static load, and a substantial reserve of the strength is disregarded. In order to make use of the material strength fully, the possibilities of loading the beam into the plastic region can be explored. Then, the experiment is carried out to study the ultimate load of a beam under bending. Thus, we can conclude that the solid cross section beam was the strongest and the hollow cross section beam was the weakest.

## 1. INTRODUCTION

Many structures can be approximated as a straight beam or as a collection of straight beams [1]. The bending moment, which causes the maximum stress in the beam to equal the yield stress, is known as the moment for first yield [2]. However, this is not the ultimate moment that the structural beam can sustain. This is because there is still a large elastic core capable of supporting higher loads (moments). When the stress in the entire section has reached the yield stress limit, the structure will fail. The moment, which causes this stress distribution, is the ultimate moment or the moment for full plasticity. Using this ultimate moment (ultimate load) as the design parameter, a more cost-effective and efficient design can be accomplished. The Shape Factor, which is the ratio of ultimate moment to the moment for first yield, provides an indication of the design efficiency [3]. Assume the elastic perfectly plastic material, the limit load of beams with any cross-section can be readily calculated.

One of the common principles used to determine the loading capacity of a structure is the first yield criterion which assumes that the maximum load is reached when the stress in the extreme fabric reaches yield stress [4]. While this criterion is easy to apply and safe to use, the design based on this rule is not economical for a beam carrying static load. According to the elastic flexure formula, the stress in a beam is proportional to the distance from the neutral axis [5]. When a beam is made to carry a moment causing the extreme fabric to yield, the material below this layer will still be elastic and is capable to carry further load

[6]. Therefore, if the first yield criterion is applied, a substantial reserve of the strength is disregarded. In order to make use of the material strength fully, the possibilities of loading the beam into the plastic region can be explored.

## 2. METHODOLOGY

This paper focused on the analysis of stresses in beam bending, and was carried out using various loading beams, namely 2 C-channels (thick and thin), a box beam and 2 rectangular cross-section beams. Theoretical analysis and experiments were carried out to determine the strength and stiffness of the beams, which were simply supported at 2 ends with a central load. A C-beam was chosen and a reinforcement scheme was done to prevent buckling and to increase the strength of the beam. Figure 2.1 shows the flow chart of the bending moment analysis.

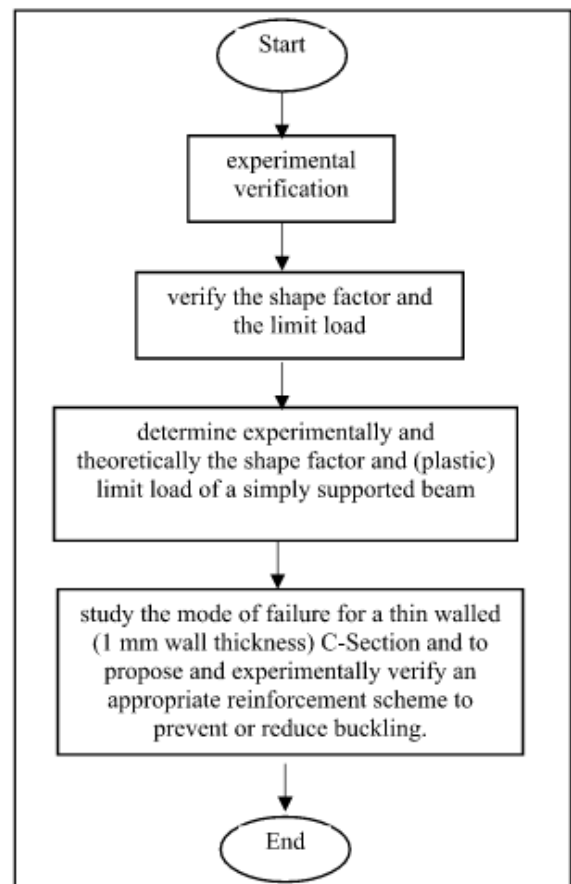


Figure 2.1 Flow chart of the bending moment analysis.

### 3. RESULTS AND DISCUSSION

Table 3.1 shows the values of the theoretical shape factors, as well as the theoretical and experimental ultimate loads experienced by beams of various cross-sections. It was observed that the experimental ultimate load was lower than that of the theoretical load, for each of the cross sections tested. One of the possible reasons for this was that failure in each of these beams occurs by other modes rather than the pure bending process stipulated. In the case of the thin C-channel, buckling and warpage of the channel occurred shortly after the application of the load force. These have resulted in the material failing, and hence the ultimate experimental load attained was lower than the theoretical calculated value. In the case of the beam with the rectangular hollow cross-section, it was observed that a region of bending occurs in the region where the roller support was placed. The deformation in that region has caused the material to fail.

Table 3.1 Result of theoretical and experimental of ultimate loads experienced by beam.

X-section	Theoretical Ultimate Load (N)	Experimental Ultimate Load (N)	Experimental Load of First Yield (N)	Theoretical Shape Factor	Experimental Shape Factor
Solid cross-section	6564	4722	3888.9	1.5	1.21
Thin C-channel	1519.25	1379.7	1207.55	1.72	1.14
Thick C-channel	5336.6	4216.9	2452.3	1.79	1.72
Hollow rectangular cross-section	7437.04	2200	1764.7	1.178	1.25

### 4. SUMMARY

Based on this study, various types of reinforcement schemes have been suggested. One of the suggestions is to use riveting joints. Theoretically, when the distance between rivets is small, the resultant stress concentration ratio is relatively small as the rivet can be taken to be over a large area. However, introducing rivets will result in stress concentration at the riveting points and this may result in material failure. Thus the modification was carried out on the thin wall C channel to reinforce the sides of the C Channel using strips bent into s-shape and adhesive bonding.

Bending of beams is a frequently encountered situation in practice. The experiment conducted was to study the ultimate load of a beam under bending. For this experiment, specimens were made of aluminum, which was a nonferrous metal; its properties differed from ferrous metals, which was iron based. As most

high stressed structures were made of ferrous metals, the correlation of the experimental results and observations were needed. Judging from the results, the solid cross section beam was the strongest and the hollow cross section beam was the weakest, which verified the theoretical calculations.

### REFERENCES

- [1] Budynas, Richard G. (2011). Shigley's Mechanical Engineering Design, 8<sup>th</sup> Ed. McGraw-Hill.
- [2] Popov, E.P. (1999). Engineering Mechanics of Solids, 2<sup>nd</sup> Ed. Chap. 20, Prentice Hall (Singapore).
- [3] Gere, James M. (2004). Mechanics of Materials, 6<sup>th</sup> Ed. Thomson Learning, USA.
- [4] Gere, J.M. and Timoshenko, S.P. (1997). Mechanics of Materials, 3<sup>rd</sup> Ed, pp. 328-340, PWS Kent Pub. Co.
- [5] Lindeburg, Michael R. (2013). Mechanical Engineering Reference Manual for the PE Exam, 13<sup>th</sup> Ed. Professional Publication.
- [6] Sugimoto, H., Arata, T., Tanaka, H., Kikumoto, K. and Sato, T. (2000). Experimental study on strengthening effects of steel reinforced concrete beams with an opening (Part 4). Summaries of Technical Papers of Annual Meeting, Architectural Institute of Japan. pp. 1127-1128.

## Specific heat capacity of carbon nanofiber nanocoolant

S. Zainal Abidin<sup>1\*</sup>, I.S. Mohamad<sup>1,2</sup>, A.Y. Bani Hashim<sup>3</sup>, N. A. B. Masripan<sup>1,2</sup> and A. Abdullah<sup>1</sup>

<sup>1</sup>) Faculty of Mechanical Engineering, Universiti Teknikal Malaysia Melaka, Hang Tuah Jaya, 76100 Durian Tunggal, Melaka, Malaysia

<sup>2</sup>) Centre for Advanced Research on Energy, Universiti Teknikal Malaysia Melaka, Hang Tuah Jaya, 76100 Durian Tunggal, Melaka, Malaysia

<sup>3</sup>) Faculty of Manufacturing Engineering, Universiti Teknikal Malaysia Melaka, Hang Tuah Jaya, 76100 Durian Tunggal, Melaka, Malaysia

\*Corresponding e-mail: syazwani2792@gmail.com

**Keywords:** Specific heat capacity; carbon nanofiber; nanocoolant

**ABSTRACT** – With the rising demand for modern technology for process intensification and device miniaturization, there was a need to develop new types of fluids that are more effective in terms of thermophysical performance. To achieve this, a new generation coolant has been proposed recently, which known as nanocoolant. However, it is evident from literature that less attention has been given to the heat capacity studies for these fluids. In this research, we have presented an experimental investigation of the specific heat ( $C_p$ ) of carbon nanofiber based nanocoolant in deionized water and ethylene glycol with a calorimeter bomb. The result indicates that the specific heat of nanocoolant decreases gradually as the nanoparticle volume fraction increases from 0.8wt% to 1.0wt%.

### 1. INTRODUCTION

Specific heat capacity determines the amounts of energy absorbed, released or even the enthalpy change in a body before changes of temperature [1]. The value of the specific heat capacity is highly crucial for evaluating the heat transfer coefficients in heat transfer studies. Very few experiments were carried out by researchers to study the specific heat capacity of CNF based nanofluids. Recently, the differential scanning calorimeter and double hot-wire methods were used to estimate the specific heat capacities of water-based silica, alumina, and copper oxide nanofluids [2]. These experimental results were well predicted by the theoretical model based on classical and statistical mechanisms. However, numerical and experimental studies for determining the specific heat capacity of nanofluids had been conducted by only a few researchers at a specific room temperature.

As a matter of fact, the accurate determination of specific heat capacity was determined in this studies in evaluating the thermal performance of nanocoolant produced from the dispersion of carbon nanofiber in deionized water and ethylene glycol based.

### 2. METHODOLOGY

Type of carbon nanofiber used in this research is Pyrograf III Carbon Nanofiber, High Heat Treated 24 (HHT24) grade. The nanocoolant was prepared using two-step method with several different concentrations of CNFs used in the base fluids. The PVP was used as the stabilizing agent. The weight percentage of CNFs varied

from 0.1wt% up to 1.0wt% with the interval of 0.1wt%. The ratio used between deionized water (DI) and ethylene glycol (EG) was set to 50:50. These mixtures were then being homogenized using the mechanical homogenizer for five minutes by using a Digital Homogenizer LHG-15 at 10000 rpm rotational speed. To ensure homogeneity and uniformity of nanocoolant, sonication was carried out using Elmasonic S30H ultrasonicator at 25°C for 5 minutes at 37 kHz frequency was used. All stabilized and adequately dispersed nanocoolant were tested for their thermal conductivity. KD2 Pro Thermal Properties Analyser (Decagon Devices, Inc.) was used to measure the thermal conductivity at three different temperatures of 6°C, 25°C and 40°C. This test was the benchmark test as the best three samples which enhance the highest thermal conductivity were chosen to undergo heat capacity test.

The usage of calorimeter bomb is to measure specific heat value for the nanocoolant. In this research, IKA C 200 (Werke GmbH & Co. KG) was used to know the heat capacity value of the formulated nanocoolant.

### 3. RESULTS AND DISCUSSION

#### 3.1 Thermal conductivity

The thermal conductivity of CNF based nanocoolant was measured at different volume fractions and various temperatures as shown in Figure 3.1.

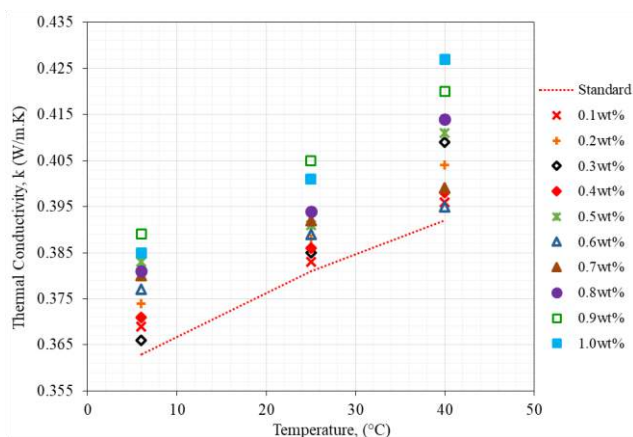


Figure 3.1 Thermal conductivity of 50DI/50EG CNF based nanocoolant.

The thermal conductivities of the sample can be seen to increase as the temperature rises as shown in

Figure 3.1. At 6°C, a sample with 0.9wt% of CNF has the highest thermal conductivity at 0.389 W/m.K, followed by 1.0wt% at 0.385 W/m.K and 0.5wt% sample recording thermal conductivity of 0.383 W/m.K. At 25°C, the sample with the highest thermal conductivity is still 0.9wt% at 0.405 W/m.K, then followed by 1.0wt% with thermal conductivity of 0.401 W/m.K and 0.8wt% with thermal conductivity of 0.394 W/m.K. However, at 40°C, the sample that shows the highest thermal conductivity is 1.0wt%, at 0.427 W/m.K. Sample with the second highest thermal conductivity is 0.9wt% at 0.420 W/m.K and thirdly, 0.8wt% with thermal conductivity 0.414 W/m.K. Hence, the addition of CNF systematically increases the thermal conductivity of the nanocoolant, as compared with the base fluid.

This fact is true at all the concentrations and temperatures investigated. The thermal conductivity of an object is carried out through the collision of the particle, hence transferring the energy from one particle to another. At higher temperature, the rate of collision is higher as the particles move at a higher average velocity. This increased rate of random collision is known as Brownian motion. The Brownian motion will result in aggregation of particle which in turn would cause the occurrence of thermal conduction [3]. This phenomenon is shown perfectly in Figure 3.1.

### 3.2 Specific heat capacity

The heat capacity was determined in order to know how much heat energy of the nanocoolant can carry out if it was used in the cooling system. Data of specific heat capacity of nanocoolant are shown in Figure 3.2.

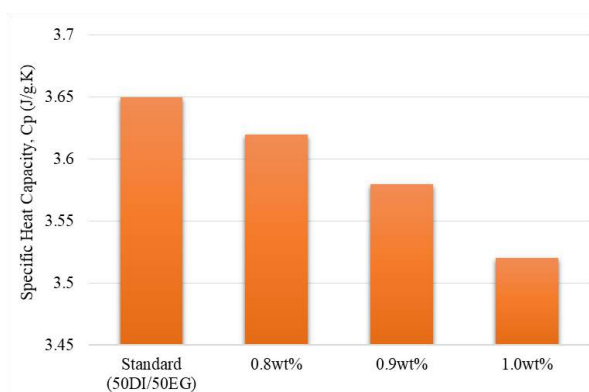


Figure 3.2 Specific heat capacity of nanocoolant.

The specific heat capacity of nanocoolant decreased when the volume fraction of CNF nanoparticles increased. The standard Cp value for 50DI/50EG without CNF addition was found to be 3.65 J/g.K and decrease to 3.62 J/g.K for 0.8wt%, 3.58 J/g.K for 0.9wt% and also 3.52 J/g.K for 1.0wt%. The result can further intercede such that low specific heat of nanocoolant can be attained in a large particle volume fraction. The decrease of specific heat capacity was reported for various water-based metallic and inorganic nanofluid systems [4]. This means that the amount of heat required to raise the temperature of the nano-

coolant is relatively lower compared to that of the base fluid.

The previous decreasing trend in specific heat is owing to the lower specific heat of solid CNF in comparison with the base fluid and surface effect such as the interaction between the base fluid and CNF that in turn forms a solid-liquid layering at the nanometric scale. The formation of these layers could reduce the energy required to raise the temperature of the nanocoolant. The formation of these layers could reduce the energy required to raise the temperature of the nanocoolant. It is construed from the previous discussion that a new model should be developed for the prediction of specific heat of the nanocoolant by considering the various mechanisms at the molecular level, particularly the nanocoolant with the suspension of CNF.

### 4. SUMMARY

In this work, the observed heat capacity was not related to the presence of a substructure. On the other hand, the agglomeration of nanoparticles and the formation of clusters can increase the thermal conductivity but, in this work, does not seem to have the same effect on the specific heat. Experimental results and the theoretical understanding of the mechanisms of the nanoparticles are needed to justify the heat capacity and fluid behavior of nanocoolant.

### REFERENCES

- [1] Gunn, D. A., Jones, L. D., Raines, M. G., Entwisle, D. C., and Hobbs, P. R. N., (2005). Laboratory measurement and correction of thermal properties for application to the rock mass. *Geotech. Geol. Eng.* 23, 773-791.
- [2] Murshed, S. M. S., Leong, K. C., and Yang, C., (2008). Investigations of thermal conductivity and viscosity of nanofluids. *International Journal of Thermal Sciences*, 47(5), 560-568.
- [3] Abidin, S.Z., Mohamad, I.S., Hashim, A.Y.B., Abdullah, N., Hafiz, M.I.M., Masripan, N.A.B., and Abdullah, A., (2016). Investigation of thermal characteristics of CNF-based nanofluids for electronic cooling applications. *Journal of Mechanical Engineering and Sciences*, 10(3), 2336-2349.
- [4] O'Hanley, H., Buongiorno, J., McKrell, T., and Hu, L. W. (2012). Measurement and model validation of nanofluid specific heat capacity with differential scanning calorimetry. *Advances in Mechanical Engineering*, 4, Article ID 181079.

# Electrical performances of Graphene with different filler loading as conductive ink

M. Mokhlis<sup>1, 2\*</sup>, M.A.Salim<sup>1, 2\*</sup>, N.A.Masripan<sup>1, 2</sup>

<sup>1</sup>) Faculty of Mechanical Engineering, Universiti Teknikal Malaysia Melaka, Hang Tuah Jaya, 76100 Durian Tunggal, Melaka, Malaysia

<sup>2</sup>) Centre for Advanced Research on Energy, Universiti Teknikal Malaysia Melaka, Hang Tuah Jaya, 76100 Durian Tunggal, Melaka, Malaysia

\*Corresponding e-mail: azli@utem.edu.my

**Keywords:** Graphene; Conductive ink; Electrical properties

**ABSTRACT** – Recent years have witnessed many breakthroughs in research on graphene for conductive ink application. This study focusing on the electrical performances of graphene as conductive ink at 10wt. %, 20wt. %, 30wt. % and 40wt. % of filler loading using a four-point probe. From the result obtained, low percentage of filler loading has no presence of conductivity while for a higher percentage of filler loading has lower resistivity and presence of conductivity. The outcome from this work would provide a convenient way to fabricate conductive ink for various printed electronics fields.

## 1. INTRODUCTION

Conductive inks, ink that developed in a printed object that can conduct electricity with widespread uses such as wearable electronics and healthcare devices, are regarded as the next generation of electronic devices [1]. In this project, graphene is a conductive material that contains superior electrical properties that draw the attention of many researchers. An effective conductive ink comprises three main components; conductive material, a polymer binder, and solvent. This study will be focusing on optimizing graphene filler loading percentage to produce a high conductive ink. The process to fabricate conductive ink includes printing procedure, ink-substrate interaction and curing process [2]. The mixing ratio of filler, binder, and hardener was a critical step to produce an ink with high conductivity, a preliminary study on the mixture of the three components was conducted. The purpose of the experiment is to identify the optimum percentage of filler loading with lower resistivity. The result obtained will bring opportunities to produce the new generation of high conductive inks. In this project, five different filler loading were prepared by manual mixing

## 2. RESEARCH METHODOLOGY

### 2.1 Formulation of graphene ink

The ink formulation of graphene, reinforced epoxy resin and hardener were achieved by a simple method involving mixing, printing and curing process. The materials were weighed using digital analytical balance (ME204E from Mettler Toledo) and the same process was repeated for each case using a different weight of the mixture. The process was continued with mixing process which took about 10 minutes at room temperature. A well-dissolved mixture was obtained

with a correct stirring technique; stir in one direction at a constant speed. The printing process was then carried out using the doctor-blading technique [3]. In this technique, the thickness of exposure ink can be controlled manually. A sharp blade was used to move the ink across the substrate at a constant speed to ensure the ink is fully exposed at the constructed gap. In the final step, curing process takes place in order to improve the bonding between the particles of filler, binder, and hardener. Curing was also applied to melt and harden the mixture with the help of the hardener so that the adhesion between ink and substrate could be improved.

Table 1 The composition of filler loading.

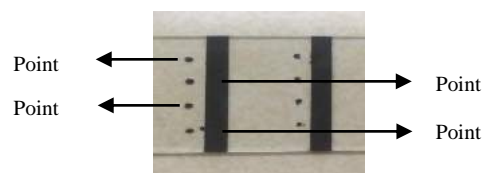
Sample	Filler		Binder		Hardener (g)	Total (g)
	(wt. %)	(g)	(wt. %)	(g)		
1	10	0.2	90	1.8	0.54	2
2	20	0.4	80	1.6	0.48	2
3	30	0.6	70	1.4	0.42	2
4	40	0.8	60	1.2	0.36	2
5	50	1.0	50	1.0	0.30	2

### 2.2 Samples characterization

The sheet resistance values of the samples were characterized in ohms-per-square was carried out using a four-point probe (RM3000 from Jandel). Four-point probe works by forcing a constant current along two outer probes and next, the voltage is read out from the two inner probes.

## 3. RESULTS AND DISCUSSION

The resistivity the ink will be discussed to find out the best ink formulation. Four points were marked and measure to determine the average of the sheet resistance.



From the results Table 1, the presence of resistivity can only be observed at 30wt. % and 40wt. %. At 10wt. % and 20wt. %, there is no resistivity present due to the insufficient amount of filler loading as a small amount of filler loading lead to agglomeration effect. Agglomeration effect can cause uneven dispersion [4]. Therefore, no electrical conductivity can be produced

due to agglomeration effect.

Table 2 Result of sheet resistance

Method	Manual mixing	Four point probe ( $\Omega/\text{sq}$ )
Sample	Filler (%)	
1	10	-
2	20	-
3	30	4862.12
4	40	7997.84
5	50	-

The conductive ink fabricated were characterized based on the electrical properties and microstructure behavior to determine the optimum ratio of filler loading. It was pointed out that the filler loading of 10wt. %, and 20wt. % did not have any presence of conductivity, while 30wt. % and 40wt. % show the existence of the conductivity, hence the decision to choose the filler loading merely based on the filler loading 30wt. % and 40wt. %.

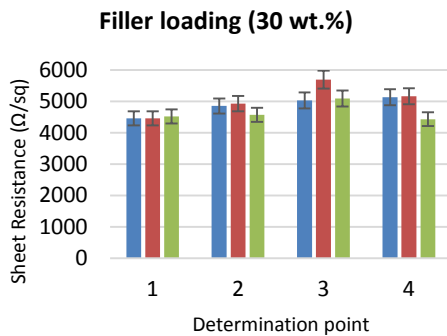


Figure 1 Graph of 30 wt. % filler loading

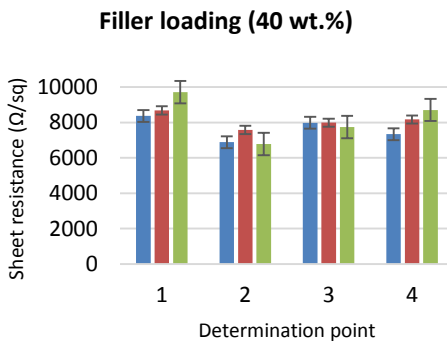


Figure 2 Graph of 40 wt. % filler loading.

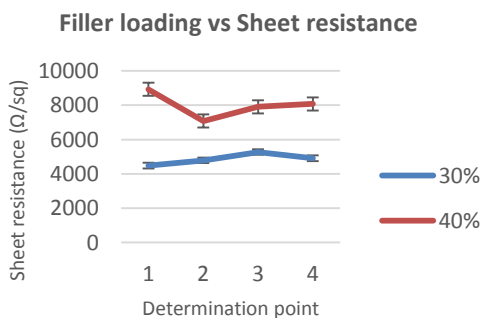


Figure 3 Graph of filler loading vs. sheet resistance

Various composition between filler, binder, and hardener was able to produce different results based on resistivity and the microstructure behavior. As for now, filler at 30% will be chosen as the base formulation to produce high conductive ink. Moreover, the process to formulate the 30 wt. % ink was easier as compared to ink that a high percentage of filler loading.

#### 4. SUMMARY

In conclusion, fabrication of conductive ink can be carried out through several processes; mixing, printing and curing process on the substrate. The conductive ink fabricated were characterized based on the electrical properties to determine the optimum ratio of filler loading. Filler loading at 30wt. % was pointed as the optimum ratio of ink mixture as its show lower resistivity and better ink dispersion.

#### REFERENCES

- [1] L. Hu *et al.*, "Stretchable, Porous, and Conductive Energy Textiles," vol. 1, pp. 708–714, 2010.
- [2] A. Mohammed, M. Pecht, A. Mohammed, and M. Pecht, "A stretchable and screen-printable conductive ink for stretchable electronics," vol. 184101, 2016.
- [3] C. Nash, Y. Spiesschaert, G. Amarandei, Z. Stoeva, R. I. Tomov, and D. A. N. Tonchev, "A Comparative Study of the Conductive Properties of Coated and Printed Silver Layers on a Paper Substrate," vol. 44, no. 1, 2015.
- [4] S. Chatterjee, F. Nafezarefi, N. H. Tai, L. Schlagenhauf, and F. A. Nu, "Size and synergy effects of nanofiller hybrids including graphene nanoplatelets and carbon nanotubes in mechanical properties of epoxy composites," vol. 0, pp. 1–7, 2012.

# Fabrication of uniaxially aligned electrospun nanofibre using a rotating collector

M. N. A. Hamzah<sup>1,2</sup> and A. H. Nurfaizey<sup>1,2\*</sup>

<sup>1</sup>) Faculty of Mechanical Engineering, Universiti Teknikal Malaysia Melaka, Hang Tuah Jaya, 76100 Durian Tunggal, Melaka, Malaysia

<sup>2</sup>) Centre for Advanced Research on Energy, Universiti Teknikal Malaysia Melaka, Hang Tuah Jaya, 76100 Durian Tunggal, Melaka, Malaysia

\*Corresponding e-mail: nurfaizey@utem.edu.my

**Keywords:** Electrospinning; electrospun nanofiber; aligned nanofiber

**ABSTRACT** – This paper is about the fabrication of aligned electrospun nanofiber based on Polyvinyl Alcohol (PVA) by using electrospinning technique with rotating collector. PVA solution was prepared by dissolved PVA powder into distilled water. This experiment was conducted at various speeds of rotating collector. PVA based nanofiber have been fabricated and characterized. The morphology of the fibres was analysed by using a Scanning Electron Microscope (SEM) and ImageJ software. From the results, 900 RPM achieved the most aligned electrospun nanofiber.

## 1. INTRODUCTION

Electrospinning is a simple technique to fabricate electrospun nanofiber from a polymer solution[1]. The outstanding small scale of fiber size make the nanofibers as the best applications in manufacturing sensors, military equipment, filtration, smart material, fuel cells and drug delivery [2]. The common electrospinning setup consists of high voltage power supply, syringe, needle, syringe pump and rotating collector as shown in Figure 1.1.

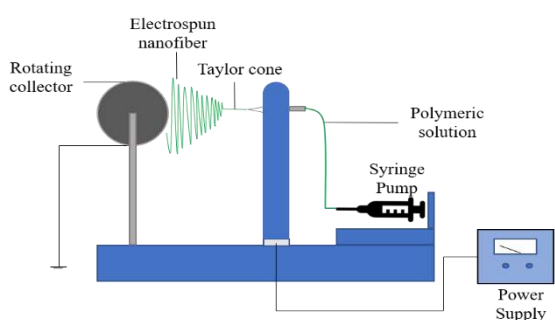


Figure 1.1 A schematic diagram of an electrospinning setup with rotating collector.

The problem that occur in common electrospinning with flat plate collector is formation of random nanofiber. Electrostatic interaction of the charge causes the whipping instability during the electrospinning process. Thus, formation of aligned nanofiber can be generated by using rotating collector with suitable speed. Nowadays, medical applications are highly on demand due to its rate of healing wound efficiency. Aligned nanofibers has highly potential as efficient cardio-inductive implant for cardiac tissue [3]. Futhermore, aligned nanofiber can also heal wound due to its rapid oxygen exchange in the nanofiber. The aim of this study

is to fabricate aligned nanofiber and investigate the suitable speed of rotating collector to get an aligned nanofiber.

## 2. METHODOLOGY

Polyvinyl Alcohol (PVA) electrospun nanofiber was produced by using electrospinning machine fabricated by UTeM students. The PVA polymer solution was prepared by dissolved 8wt% of PVA in distilled water and stirred for 4 hours by using magnetic stirrer model C-MAG HS7 (Ika Works, Malaysia). For electrospinning process, the voltage was set at 15 kV and the distance between the spinneret to the rotating collector was set at 10 cm. The speed of rotating collector was at 100, 200, 300, 400, 500, 600, 700, 800, 900 and 1000 RPM for 7 minutes to each corresponding speed. Scanning Electron Microscope (SEM) Model JSM-6010PLUS/LV (Jeol Ltd., Japan) was used to examine the morphology of the fiber. ImageJ version 1.51s software (National Institutes of Health, USA) was used to analyse the degree of oriented under SEM micrograph. The degree of oriented was measure from bottom line of the SEM image as datum as shown in Figure 2.1. The average value of the degree oriented was took as the result.

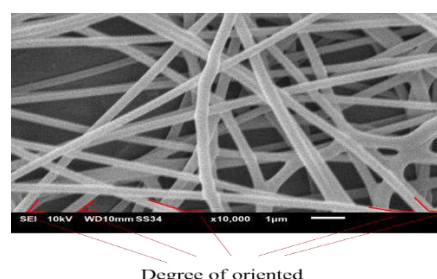


Figure 2.1 Measurement of degree of oriented.

## 3. RESULTS AND DISCUSSION

Figure 3.1 shows a graph between degree of oriented and speed of rotating collector. The lowest degree of oriented nanofiber was 200 RPM which 73.77° while the highest degree of oriented was 500 RPM which 96.22°. The main finding of this study is to obtain an aligned nanofiber which is the nearest to 90°. Based on the result, degree of oriented electrospun nanofiber at 900 RPM was the nearest to 90° which is 90.05°. However, the random oriented were still seen on the SEM image as shown in Figure 3.2.

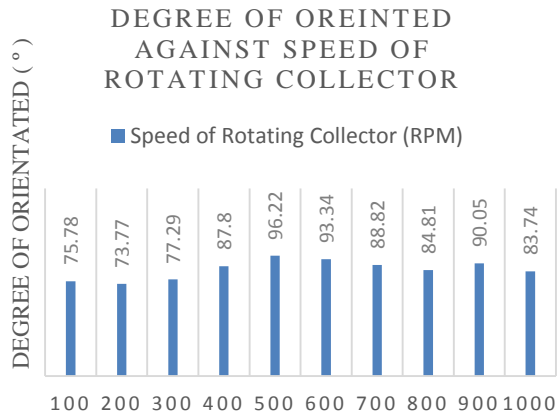


Figure 3.1 A graph between degree of oriented and speed of rotating collector.

H. Pan et al. stated that the rotating collector need to be at high speed in order to obtain aligned electrospun nanofiber, [4]. Thus, this study is complying from the previous research. However, 600 RPM it starts decreasing in degree of oriented. This problem occur probability from the accumulation of charge that increases at the collector as the speed of rotating collector increases. Accumulation of charge might cause interruption of the degree of oriented and deposition of nanofiber.

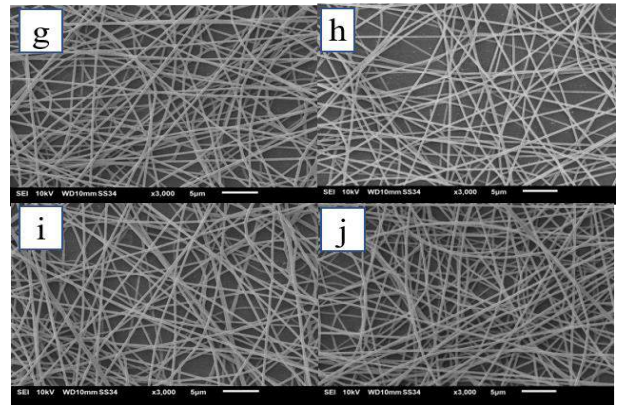
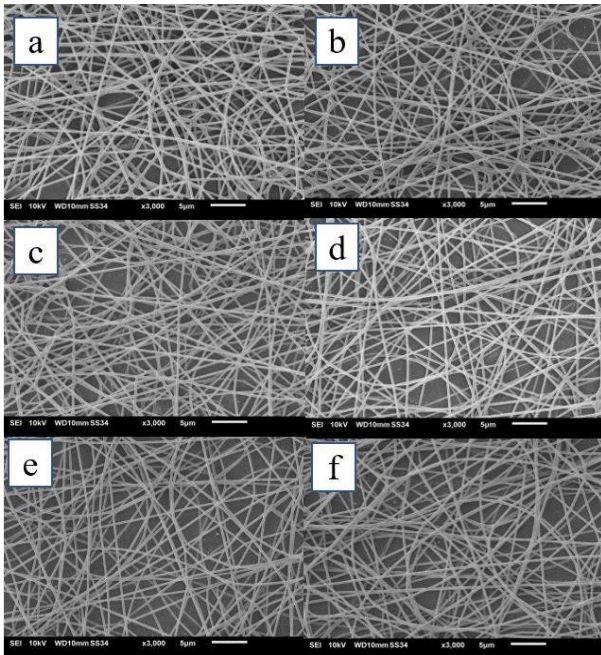


Figure 3.2 Micrograph under SEM; (a) 100 RPM (b) 200 RPM (c) 300 RPM (d) 400 RPM (e) 500 RPM (f) 600 RPM (g) 700 RPM (h) 800 RPM (i) 900 RPM (j)1000 RPM.

#### 4. SUMMARY

In this study, the aligned nanofiber was successful fabricated from PVA polymer by using electrospinning process with rotating collector. SEM and Image J software was used to scan the electrospun nanofiber and measure degree of oriented nanofiber. Based on the result, it shows that speed of rotating collector at 900 RPM is the most suitable speed to obtain aligned electrospun nanofiber as its degree oriented was nearly to 90°.

#### REFERENCES

- [1] P. Katta, M. Alessandro, R. D. Ramsier, and G. G. Chase. (2004). Continuous electrospinning of aligned polymer nanofibers onto a wire drum collector, *Nano Lett.*, Vol. 4, No. 11, pp. 2215–2218.
- [2] N. A. Munajat, A. H. Nurfaizey, S. H. S. M. Fadzullah, G. Omar, J. Jaafar, and N. S. A. Roslan. (2017). Fabrication and Characterization of Carbon Nanofibres from Polyacrylonitrile Precursor, March, pp. 1–2.
- [3] R. Safaeijavan, M. Soleimani, A. Divsalar, A. Eidi, and A. Ardeshirylajimi. (2014). Comparison of random and aligned pcl nanofibrous electrospun scaffolds on cardiomyocyte differentiation of human adipose-derived stem cells, *Iran. J. Basic Med. Sci.*, Vol. 17, No. 11, pp. 903–911.
- [4] H. Pan, L. Li, L. Hu, and X. Cui. (2006). Continuous aligned polymer fibers produced by a modified electrospinning method, *Polymer (Guildf.)*, Vol. 47, No. 14, pp. 4901–4904.



# Effects of carbon black to electrical properties on stretchable printed circuit

N.S. Rozali<sup>1</sup>, N.H. Sobri<sup>1</sup>, M.A. Suhaimi<sup>1</sup>, M.Z. Azmi<sup>1</sup> and M.Z. Akop<sup>1,2\*</sup>

<sup>1</sup>Faculty of Mechanical Engineering, Universiti Teknikal Malaysia Melaka, Hang Tuah Jaya, 76100 Durian Tunggal, Melaka, Malaysia

<sup>2</sup>Centre for Advanced Research on Energy, Universiti Teknikal Malaysia Melaka, Hang Tuah Jaya, 76100 Durian Tunggal, Melaka, Malaysia

\*Corresponding e-mail: zaid@utem.edu.my

**Keywords:** Carbon black; conductive ink; sheet resistance

**ABSTRACT** – This paper seeks to analyze the effect of type of conductive ink to stretchable printed circuit. For this study, carbon black or also can be known as CB is used as the conductive ink. This study is focus on the measurement of sheet resistance. Four-point probing system is used to measure the sheet resistance,  $R_s$  of the conductive ink. The sheet of the carbon black is measured under room temperature without any external heat or load applied. A proper printing technique must be considered to get the consistent and accurate data. The surface roughness of the different sample is determined by using 3D non-contact profilometer measuring instrument. Results shows that higher value of the surface roughness will improve the conductivity of the carbon black ink.

## 1. INTRODUCTION

Stretchable printed circuit (SPC) is a pattern of conductive traces bonded of stretchable substrates. Due to its capabilities and reliability, stretchable printed circuit has a valuable position compared to traditional printed circuit in worldwide printed circuits market. Since the stretchable printed circuit have many specialities for example high flexibility and can be fold without affecting signal transfer function, hence it has been applied in various fields such as biomedical to detect the hydration of athlete's body during training session. Next, SPC are also used in electronic devices and textile application since SPC is bendable that are anti vibration and can accommodate any design next withstand in high stress condition.

In this study, carbon black is used as conductive ink and thermoplastic polyurethane (TPU) is used as the substrate. The combination of both materials will form the stretchable printed circuit. Conductive ink can conduct electricity and compatible with substrates while SPC is pattern of conductive traces bonded on a flexible substrate.

Sheet resistance,  $R_s$  of the conductive ink can be affected by the printing technique. Different printing technique will create different surface roughness, thickness and width of the samples. For this study, the effect of different surface roughness to the sheet resistance has been considered by using

carbon black conductive ink. Sheet resistance is measured by using four-point probe system and the surface roughness of the sample is determined by using 3D non-contact profilometer instrument. Next, optical microscope is also used in this study to examine the microstructure of the samples. The objective if this study is to investigate the effects of carbon black to stretchable printed circuit at room temperature.

## 2. RESEARCH METHODOLOGY

### 2.1 Samples Preparation

There are a few materials involved to prepare the samples; carbon black conductive ink, thermoplastic polyurethanes, isopropyl alcohol and cellophane tape. Two samples are prepared and followed the dimension as in Table 2.1 below:

Table 2.1 Dimension of samples

<b>(1) Conductive ink</b>	
(a)width (mm)	3
(d)thickness (mm)	0.08
<b>(2) Substrate</b>	
(b)width (mm)	20
(c)length (mm)	30

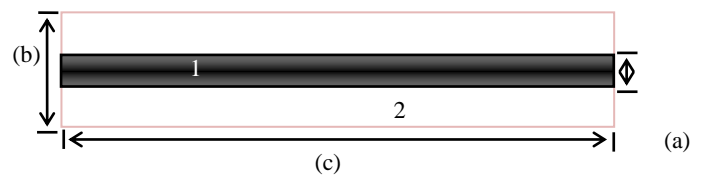


Figure 2.1 Sample's top view



Figure 2.2 Sample's side view.

The samples are printed with dimension of 3 mm width, 0.08 mm thickness and 30 mm length of conductive ink on the 20 mm width of thermoplastic polyurethane substrate as shown above. Next, the samples must be cured or dry at room temperature for 5–15 minutes. After the samples are completely cured, for accurate data purpose, the samples were

divided and marked into five points and at each point, three times readings are taken. By doing this step, the data obtain is more accurate since it is considering the average data. The samples are marked as shown in Figure 2.3 below:

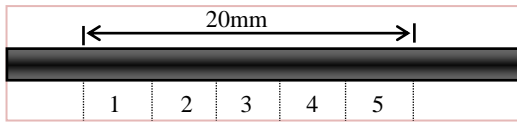


Figure 2.3 Samples divided into five points.

**2.2 Experimental**

For this study, the sheet resistance is calculated by using four-point probe technique. Figure 2.4 below shows the schematic diagram for four-point probe measuring the sheet resistance of the samples.

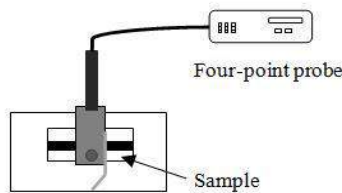


Figure 2.4 Schematic diagram top view of four-point probe measuring sheet resistance of samples setup.

**3. RESULTS AND DISCUSSION**

The average sheet resistance,  $R_s$  for Sample 1 and Sample 2 were taken at room temperature condition. Figure 3.1 below shows the total average sheet resistance for Sample 1 and 2.

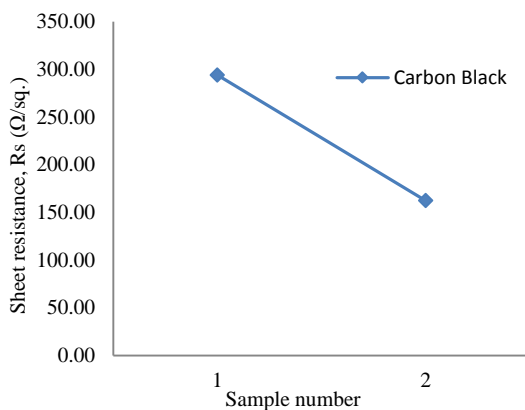


Figure 3.1 Sheet resistance versus sample number.

By referring Figure 5, the total average  $R_s$  for sample 1 and 2 when exposed in room temperature are 293.90  $\Omega/sq.$  and 162.25  $\Omega/sq.$ , the graph shows quite large different value of sheet resistance between two samples. This is due to the different surface roughness of both samples. In addition, sheet resistance also depends on the internal microstructure of the printed lines. The structure could be affected by several parameters for example

printing techniques, surface roughness and curing time [1].

By using 3D non-contact profilometer instrument, it shows that the total average surface roughness of each five points of sample 1 and 2 are 3.05 $\mu m$  and 4.59  $\mu m$  as shown in Table 3.1 below:

Table 3.1 Data for total average sheet resistance and surface roughness for sample 1 and 2.

Samples	Surface roughness ( $\mu m$ )	Total average sheet resistance, $R_s$ ( $\Omega/sq.$ )
1	3.05	293.90
2	4.59	162.25

As stated by J. Sánchez [2], the surface roughness also improve the contact between particles and will reduce the sheet resistance value and it is shows the electrical conductivity of the carbon black increased. The increasing of surface roughness not only increase the electrical conductivity, it will also will improve the mechanical properties of the conductive ink [3]. Higher surface roughness also means the sample to have more filler.

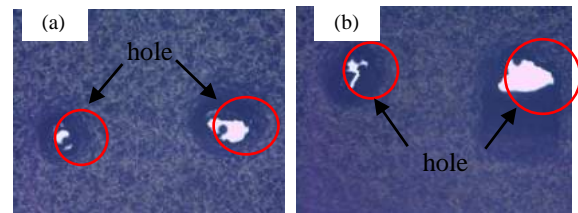


Figure 3.2 Optical microscope image for (a) sample 1 and (b) sample 2.

Figure 3.2 above presents the optical microscope image for both samples. It can be seen that the sample expose substrate (hole) when four-point probe applied to the samples. This is due to the thickness of the samples are not suitable to be measured under four-point probe. By referring the application notes of the carbon black product that has been used in this study, the sheet resistance should be lower than 55  $\Omega/sq.$  with suitable thickness printed [4].

**4. SUMMARY**

In conclusion, this study was conducted to analyze the effects of carbon black to stretchable printed circuit at room temperature. The 3D non-contact profilometer used to study the surface roughness of the sample and optical microscope is used to examine the microstructure of the carbon black. Next, higher surface roughness will give a better conductivity. To obtain a good result and consistent value of sheet resistance, the printing method must be improved and printed in a steady way. To get a better value of sheet resistance as recommended in application notes of the product, the thickness of the printed ink must be increased.

## REFERENCES

- [1] M. Žveglič, N. Hauptman, M. Maček, and M. K. Gunde. (2011). Screen-printed electrically conductive functionalities in paper substrates, *Mater. Tehnol.*, Vol. 45, No. 6, pp. 627–632.
- [2] J. Sánchez-González, A. Maclás-García, M. F. Alexandre-Franco, and V. Gómez-Serrano. (2005). Electrical conductivity of carbon blacks under compression, *Carbon N. Y.*, Vol. 43, No. 4, pp. 741–747.
- [3] J. Li, J. K. Kim, and M. Lung Sham. (2005). Conductive graphite nanoplatelet/epoxy nanocomposites: Effects of exfoliation and UV/ozone treatment of graphite, *Scr. Mater.*, Vol. 53, No. 2, pp. 235–240.
- [4] A. Notes. (2015). ELECTRIC, pp. 1–3.

# Conceptual design of stretching test rig for stretchable conductive ink

M.Z. Azmi<sup>1</sup>, N.H. Sobri<sup>1</sup>, M.A. Suhaimi<sup>1</sup>, N.S. Rozali<sup>1</sup>, and M.Z. Akop<sup>1,2,\*</sup>

<sup>1</sup>) Faculty of Mechanical Engineering, Universiti Teknikal Malaysia Melaka, Hang Tuah Jaya, 76100 Durian Tunggal, Melaka, Malaysia

<sup>2</sup>) Centre for Advanced Research on Energy, Universiti Teknikal Malaysia Melaka, Hang Tuah Jaya, 76100 Durian Tunggal, Melaka, Malaysia

\*Corresponding e-mail: [zaid@utem.edu.my](mailto:zaid@utem.edu.my)

**Keywords:** Conceptual design; stretchable conductive ink; stretchable test rig

**ABSTRACT** – With the growth of the usage of flexible and stretchable printed circuit using conductive ink in the industry, it is important to assess the reliability, performance and functionality of the flexible and stretchable printed circuit. Therefore, a stretchability test rig must be developed in order to test the stretchability of the stretchable printed circuit as well used in check the conductivity of the conductive ink when the stretchable printed circuit stretched. The stretchability test rig consist of three parts which is the main body, the secondary body and the holder. Attached to the main body is a handle which is connected with gear. The gear act as pinion for the rack which can adjust the length of the main body and the secondary body. Two holders will be used to clamp both end of the sample conductive printed circuit which then one holder will be attach to main body and another attached to secondary body.

## 1. INTRODUCTION

Conductive ink has a vary properties in which some of the conductive ink can be stretch, flex, bend, as well as other various properties [1]. With the various kind of usage of the products which use the conductive ink as well as the printed circuit, the need for performance and functionality of these conductive inks and printed circuit need to be conduct [2].

In this paper, the detail design of the stretchable test rig was made to perform the strain test on the stretchable printed circuit as well as the conductive ink. This stretchable test rig will allow the access on the performance of the printed circuit under strain test, which also include the conductivity of the conductive ink, the allowable of the four-point probe device to check the conductivity of the conductive ink and also the adhesion of the conductive ink on the stretchable circuit [3].

The objective of this paper is to design a stretchable test rig which will be used to determine the conductivity of the conductive ink under strain test of the stretchable printed circuit. The process involves in completing this paper are the detail designs of the stretchable test rig which also include the schematic diagram and 3D modeling.

## 2. RESEARCH METHODOLOGY

### 2.1 Product Design Specification (PDS)

In order to produce a product which satisfy the key requirement of the design functionality, PDS were made to ensure all the features need in the product design meet with all the requirements. Table 2.1 shows the PDS need in the stretchable test rig.

Table 2.1 PDS of stretchable test rig.

Product design specification	
Stretchable test rig	
No.	Requirements
	Performance
1	1.1 Able to do stretchable motion
	1.2 Can allow four-point probe device to collect data on the circuit
	Dimension
2	2.1 Maximum height : 40mm
	2.2 Maximum width : 110mm
	2.3 Maximum length : 400mm
	Weight
3	3.1 Total weight : 0.07kg
	Material
4	4.1 Should be lightweight and corrosion resistance
	Safety
5	5.1 No sharp edge from the body of the test rig
	Ergonomic
6	6.1 Simple and easy to use
7	Cost
	7.1 Depend on the material cost
	7.2 Low maintainance cost

For the set up of the experiment, the stretchable printed circuit is attached with two holders from both two body. The holder is detachable from the body which allow ease of install the circuit with the holder. Figure 2.1 shows the set up of the circuit for testing.

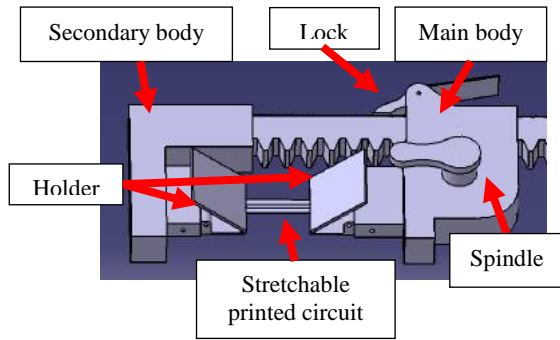


Figure 2.1 Set up of stretchable printed circuit for strain testing.

During the testing, both holder will clamp both side of the circuit. When the spindle is turn, the main body will push the secondary body causing the printed circuit stretched. The lock mechanism will allow the test rig to hold the position when needed.

### 2.2 Detail Design of Test Rig

The test rig consists of three main part which is the main body, secondary body and holder.

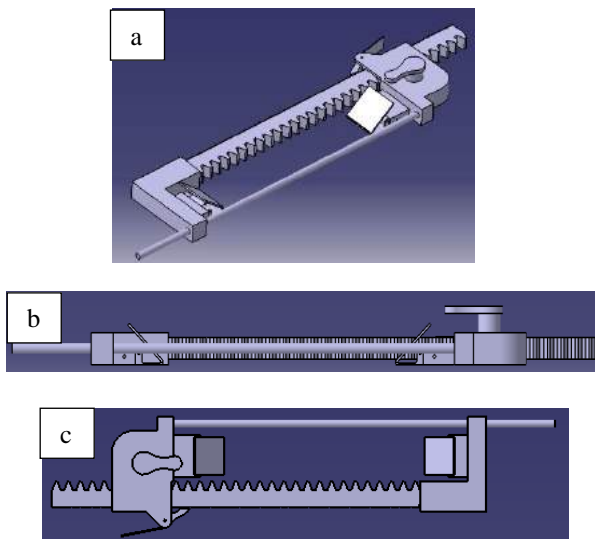


Figure 2.2 3D modeling of test rig (a) isometric view, (b) side view and (c) top view.

Inside the main body, there are gear which attached with the spindle which allow the user to rotate. The gear is connected with the rack from secondary body where the body can push each other using the gear. A lock mechanism is used to hold down the rack from retract back the rig from the stretch from the circuit.

The secondary body only consist of rack, a slot for the holder and slot for a rod from main body. These rod function is to balance the rig when performing the strain test.

The holder function is straight forward where it will hold the circuit. It is detachable from the circuit for ease of install the circuit. When the suitable

length of the circuit obtains, the holder can be install to both body with a rod.

## 3. DESCRIPTION OF PROPOSED DESIGN

### 3.1 Advantages of Detail Test Rig

The stretchable test rig help in strain test as it is hard to constantly pull the circuit and maintain the length at same length. Without a proper tool, the data obtain cannot be consistent thus will lead to unreliable data.

The stretchable test rig is small and compact in size which easy to mobilize. The lock mechanism also important as it can hold the stretch of the circuit in the length needed.

## 4. SUMMARY

In this paper, the design of stretchable test rig was meant to be used for strain test on stretchable printed circuit and conductive ink to see whether there is conductivity change in the circuit when there is present of strain in the circuit. Ideally this test rig was designed to be used in a small and compact scale of circuit.

## REFERENCES

- [1] Tuomas, H. (2016). Reliability studies on printed conductors on flexible substrates under cyclic bending (Doctoral dissertation).
- [2] Norhidayah, A. A., Saad, A. A., Sharif, M. F. M., Ani, F. C., & Ali, M. Y. T. (2017). Stress Analysis of a Stretchable Electronic Circuit. *Procedia Engineering*, 184, 625–630.
- [3] Yu, X., Mahajan, B. K., Shou, W., & Pan, H. (2017). Materials , Mechanics , and Patterning Techniques for Elastomer-Based Stretchable Conductors,22–31.

# Electrothermal performance of Ag-filled stretchable conductive ink

A.A. Ashikin<sup>1,2</sup>, G. Omar<sup>1,2,\*</sup>, N. Tamaldin<sup>1,2</sup>, M.N.A. Nordin<sup>1,2</sup>, M. Z. Akop<sup>1,2</sup>,  
S.H.S.M Fadzullah<sup>1,2</sup>, S. Jasmee<sup>1</sup>

<sup>1</sup>) Faculty of Mechanical Engineering, Universiti Teknikal Malaysia Melaka,  
Hang Tuah Jaya, 76100 Durian Tunggal, Melaka, Malaysia

<sup>2</sup>) Centre for Advanced Research on Energy, Universiti Teknikal Malaysia Melaka,  
Hang Tuah Jaya, 76100 Durian Tunggal, Melaka, Malaysia

\*Corresponding e-mail: [ghazali@utem.edu.my](mailto:ghazali@utem.edu.my)

**Keywords:** Thermal; Ag particles; sintering process

**ABSTRACT** – The purpose of this investigation is to explore the relationship between thermal effect and sheet resistance of conductive ink. Scanning Electron Microscopy (SEM) is used to study the microstructure when the ink was exposed to heat. The SCI specimen was exposed to high temperature has low resistance compared to the specimen at room temperature (RT). Morphology SCI will be observed using Scanning Electron Microscopy (SEM) to investigate the thermal effect on microstructure.

## 1. INTRODUCTION

Nowadays, electronic industries focus on Stretchable Conductive Ink (SCI) technology to replace with the conventional printed circuit board technology. One of an advantages using SCI is low fabrication cost compare to the conventional printing method [1]. A screen printing method is used for printing the SCI on the substrate and a stainless stencil or screen mesh to form conductive line.

This paper investigates the thermal effect of SCI to examine the effect of sheet resistance of SCI at variant temperature on SCI surface. The aim of this investigation is to assess the effects of thermal in electrical properties of SCI and to study the microstructure of SCI when ink surface exposed to heat.

## 2. RESEARCH METHODOLOGY

### 2.1 Samples preparation

Commercial SCI was required in this experiment. The SCI ink was printed as a specimen as shown in Figure 2.1 by screen printing method. The length of specimen is 20.0 mm and 0.15mm of ink thickness. The specimens need to cure in oven at 80°C for 1 hour. Three times of reading were taken at 5 points.

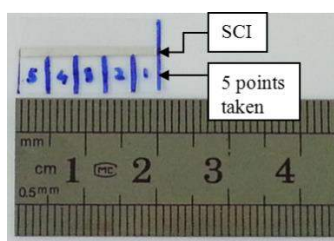


Figure 2.1 Specimen.

The specimens were exposed to heat at 40°C, 60°C and 100°C and the specimen in room temperature (RT) condition was provide as a control data for this experiment. The experimental setup was arranged as shown in Figure 2.2.

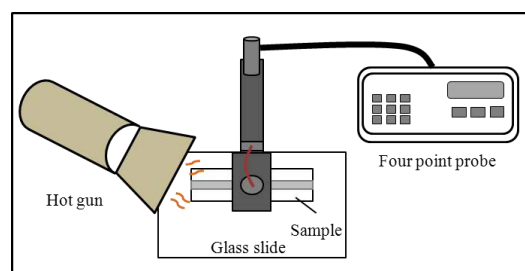


Figure 2.2 Experimental setup.

### 2.2 Samples characterization

A four point probe technique was performed to observe the electrical properties of specimens at different room temperature. The probe head have four pins with spacing 1.00 mm. A hot gun was used to provide heat on the specimens and thermal image analyzer was used to identify the surface temperature of ink when heat applied onto the ink. Scanning Electron Microscopy (SEM) was used to analyze microstructure of SCI in each specimen.

## 3. RESULTS AND DISCUSSION

A decrease pattern in resistivity shows in figure 3.1. The sheet resistance for the specimen at RT was 0.09  $\Omega$ /sq., 0.12  $\Omega$ /sq. for specimen at 40°C, 0.11  $\Omega$ /sq. for specimen exposed to 60°C and lastly 0.05  $\Omega$ /sq. for the sample subjected to 100°C. The decrease resistivity occurs due to coefficient of thermal expansion of Ag particles.

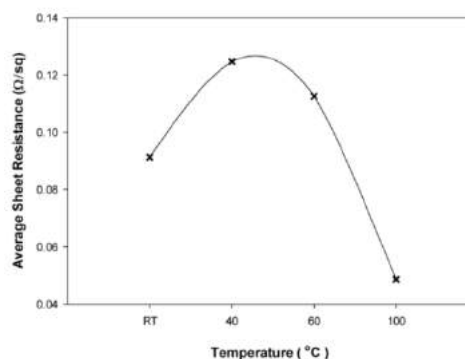


Figure 3.1 Sheet resistances versus temperature.

The Ag particles in the SCI were expanding [2] when the particles exposed to the heat. Based on [3], the CTE value for Ag is 19.68 ppm/°C. During expansion process, the Ag particles became larger and it helps to cover a gap between Ag particles. An increasing of

particles contact between Ag particles to particles is simply created electrical paths compare with Ag particles at RT condition [4].

From the SEM images in Figure 3.2 until 3.5, the morphology shows that the gaps between Ag particles become closer and decrease when the SCI exposed to high temperature. It is because Ag molecule will expand the particles sizes and the gaps between Ag particles to particles were covered. For sintered specimen, the sintered Ag particles mixed with larger particles and touched each other. In SCI, the electrical paths are useful to allow electrons to flow from negative to positive charges [5]. The increasing of electrical paths on SCI will reduce the sheet resistance and improved the conductivity of SCI. But, fewer electrical paths in SCI will increase the value of sheet resistance and the conductivity of ink.

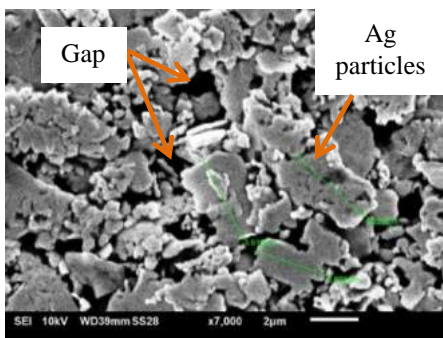


Figure 3.2 SEM image of Ag particles exposed on RT condition. Many gaps appear on the ink surface.

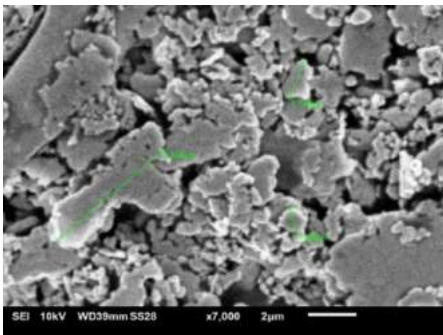


Figure 3.3 SEM image of Ag particles exposed to heat at 40°C.

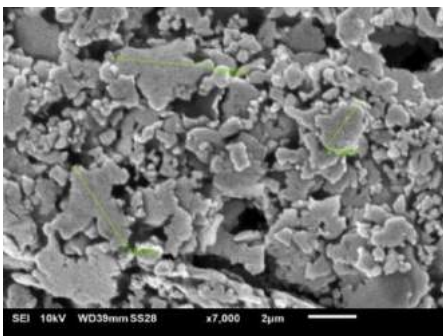


Figure 3.4 SEM image of Ag particles exposed to heat at 60°C.

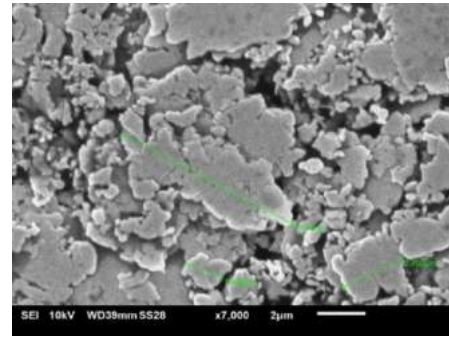


Figure 3.5 SEM image of Ag particles exposed to heat at 100°C shows that the gap become closer and decreased.

#### 4. SUMMARY

This experiment was performed to study the effects of electrothermal on SCI. The electrical properties of the SCI were measured by a four probe point and SEM micrograph shows the microstructure of SCI at different temperature condition. The sheet resistance of SCI at high temperature is lower compared to RT due to coefficient thermal expansion of Ag and decreased the gap between Ag particles to particles.

#### REFERENCES

- [1] Yung, L. C., Fei, C. C., Mandeep, J. S., Abdullah, H. B., & Wee, L. K. (2014). Synthesis of a nano-silver metal ink for use in thick conductive film fabrication applied on a semiconductor package. *PloS one*, 9(5), e97484.
- [2] Anuar, S. K., Mariatti, M., Azizan, A., Mang, N. C., & Tham, W. T. (2011). Effect of different types of silver and epoxy systems on the properties of silver/epoxy conductive adhesives. *Journal of Materials Science: Materials in Electronics*, 22(7), 757-764.
- [3] Agilent Technologies. (2002). *Laser and Optics User's Manual*. Chapter 17 Material Expansion Coefficients, 17-11.
- [4] Galagan, Y., Coenen, E. W., Abbel, R., van Lammeren, T. J., Sabik, S., Barink, M., ... & Blom, P. W. (2013). Photonic sintering of inkjet printed current collecting grids for organic solar cell applications. *Organic Electronics*, 14(1), 38-46.
- [5] Banfield, D. (2000). Understanding and measuring electrical resistivity in conductive inks and adhesives. *SGIA Journal*, 6, 29-36.

# Hydrophobicity performance of thermoplastic polyurethane coated with TiO<sub>2</sub> under thermal aging effect

S. Jasmee<sup>1,2,\*</sup>, G. Omar<sup>1,2</sup>, M.N.A. Nordin<sup>1,2</sup>, N.A.B. Masripan<sup>1,2</sup>, A. A. Kamarolzaman<sup>1,2</sup>

<sup>1</sup>) Faculty of Mechanical Engineering, Universiti Teknikal Malaysia Melaka, Hang Tuah Jaya, 76100 Durian Tunggal, Melaka, Malaysia

<sup>2</sup>) Centre for Advanced Research on Energy, Universiti Teknikal Malaysia Melaka, Hang Tuah Jaya, 76100 Durian Tunggal, Melaka, Malaysia

\*Corresponding e-mail: [solehahjasmee@gmail.com](mailto:solehahjasmee@gmail.com)

**Keywords:** TPU; contact angle; RMS roughness

**ABSTRACT** –Water repellent characteristics using ceramic-based coating may protect the surface from degradation, moisture absorption and corrosion due to the hydrophobicity behavior of the surface after coating. This paper seeks to provide insight into characterization and understanding on the effect of thermal aging on the hydrophobic performance of polymer substrate (TPU) with and without coated of Titanium Dioxide (TiO<sub>2</sub>). The results reveal that hydrophobicity of TPU increases on coated and thermally aged. Although the contact angle does not differ much after coated with TiO<sub>2</sub>, the substrate still behaves as hydrophobic. Surface roughness was found to be one of the factors affecting the hydrophobicity of the surface.

## 1. INTRODUCTION

Printed Flexible Circuits (PFC) is currently gained a lot of interest in electronic application due to its flexibility and elasticity. PFC based normally comes from polymer-based materials [1-2]. However, polymer materials could suffer from high moisture absorption that can degrade the performance of the PFC [3].

Coating is one of the solutions that could be used to provide a protective layer from moisture absorption [4]. Ceramic is found as one of the promising water repellency coatings such as Titanium dioxide (TiO<sub>2</sub>) [5].

The ability of a surface to repel water can be expressed in three different categories which are hydrophilic, hydrophobic and superhydrophobic. The contact angle for hydrophilic is  $\theta \leq 90^\circ$ , hydrophobic is  $\theta \geq 90^\circ$  and superhydrophobic is  $\theta \geq 150^\circ$ .

It has been reported that surface energy and surface roughness play an important role in wettability. Wenzel and Cassie-Baxter theory has shown the effect of roughness on contact angle. According to Wenzel, a hydrophilic surface will become more hydrophilic while hydrophobic surface will become more hydrophobic when roughness increases. Cassie- Baxter further explained that liquid droplet cannot diffuse between rough structures due to air trap [6].

Thermoplastic Polyurethane (TPU) is a well-known polymer for its flexible and stretchable properties. The water repellency performance and the acceptance of coating on TPU are expected to be one of the most promising flexible substrates for electronics packaging.

This paper investigates the hydrophobicity performance of TPU and the impact of temperature on the polymer hydrophobicity. Besides, TiO<sub>2</sub> will be used as a coating material on TPU in order to understand the

effect of water repellency at elevated temperature. This study will also find the correlation of the surface roughness created by thermal aging on surface hydrophobicity.

## 2. RESEARCH METHODOLOGY

### 2.1 Sample Preparation

Thermoplastic Polyurethane (TPU) was used as a polymer substrate meanwhile TiO<sub>2</sub> as a coating material. The substrate was cut into small pieces (50mm x 15mm x 0.1mm: length x width x thickness) and cleaned with liquid detergent before ultrasonicated with distilled water. Later, the sample was keep dried at ambient temperature.

### 2.2 Experimental

This study was done at three different conditions. Firstly, the contact angle of the as-received sample was measured. After that, the sample undergoes heat treatment at room temperature (RT), 40°C, 60°C, and 80°C. Lastly, the sample was coated with TiO<sub>2</sub> by using spin coating method at 300 r.p.m and followed by heated at RT, 40°C, 60°C, and 80°C. The contact angle and surface roughness for all samples at different conditions were measured.

The contact angle measurement was done by using self-fabricated contact angle measurement tools for three-time at six different determinations to ensure its accuracy and precision while the surface roughness was done by using Profilometer Surfatest SJ-410.

## 3. RESULTS AND DISCUSSION

### 3.1 Contact Angle

Figure 3.1 shows the contact angle of uncoated and coated TPU after heated. From the graph, the contact angle of as received TPU at RT shows hydrophobic behavior with contact angle larger than 90° (CA: 98°±1.74). According to Hejda et. Al, the surface energy is one of the factors influencing the CA [7]. TPU is a polymer that comes from urethane based which basically attributed to the lower surface energy of the polymer due to the polar/dispersion interaction. The lower surface energy of the surface cause higher in surface tension of the liquid and higher CA. Gooch (2011) shows that TPU has a surface energy that does not exceed the level of 40 mJ/m<sup>2</sup> which is the reason of TPU behaves as hydrophobic [8].

Further heating for both coated and uncoated cause the contact angle to increase. However, TPU/



TiO<sub>2</sub> shows higher hydrophobicity compared to TPU/UC.

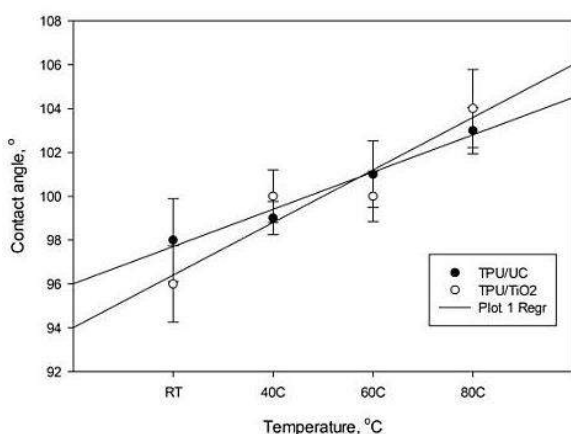


Figure 3.1 contact angle of TPU and TPU/TiO<sub>2</sub> at RT, 40°C, 60°C, and 80°C.

### 3.2 Surface Roughness

It has been reported that the wetting behavior of liquid on a solid surface depends on the surface morphology (i.e. surface roughness) [9]. Figure 3.2 shows the surface roughness of TPU and TPU/TiO<sub>2</sub> against temperature.

Overall, both sample shows increment in surface roughness as temperature increase. With regard to the contact angle shown in Figure 3.1, the effect of the surface roughness of the samples on the contact angle is quite noticeable. Increasing the surface roughness will cause the contact angle to be larger, according to Wenzel. This is because the water droplet does not diffuse easily on the rough surface which leads to the larger contact angle [10]. Rough surface also increases the air trap between roughness which causes the geometry of solid-liquid area to decrease, thus enhance the contact angle as stated in Cassie-Baxter.

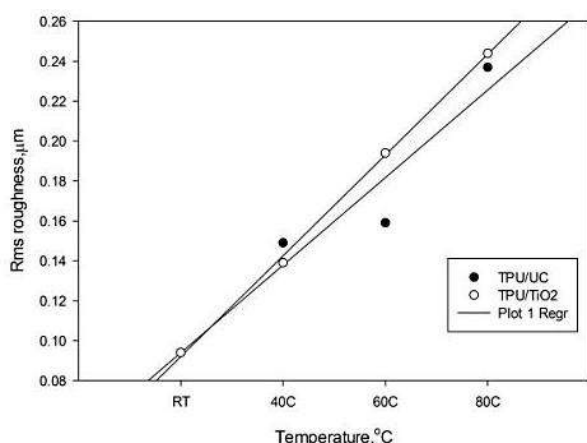


Figure 3.2 surface roughness of TPU and TPU/TiO<sub>2</sub> at RT, 40°C, 60°C, and 80°C.

## 4. SUMMARY

This paper has successfully demonstrate the hydrophobicity behavior of the TPU coated and uncoated. The hydrophobicity of both surface have increase after heat treatment due to increase in surface roughness. The results obtained consistence with the

Wenzel and Cassie- Baxter theory when surface energy, roughness and air-trap between the liquid-air interface does effect the hydrophobicity.

## REFERENCES

- [1] H.K. Seung et al. (2007). "All-inkjet-printed flexible electronics fabrication on a polymer substrate by low-temperature high-resolution selective laser sintering of metal nanoparticles," *Nanotechnology*, vol. 18, no. 34.
- [2] P. McLeod (2003). *A Review of Flexible Circuit Technology and its Applications.*: PRIME Faraday Partnership.
- [3] W. Hans, D. Eirini, W. Bernhard, and M. Bernd (2010). "Influence of moisture on humidity sensitive material parameters of polymers used in microelectronic applications," in 2010 3rd Electronic System-Integration Technology Conference (ESTC), Berlin, Germany.
- [4] L. Ziyin, L. Yan, L. Zhou, and W. Ching-ping (2011). "Novel preparation of functionalized graphene oxide for large scale, low cost, and self-cleaning coatings of electronic devices," in 2011 IEEE 61st Electronic Components and Technology Conference (ECTC), Lake Buena Vista, FL, USA .
- [5] O. Simona, L.C. Anna, and D. Michele (2015). "TiO<sub>2</sub> Nanosols Applied Directly on Textiles Using Different Purification Treatments," *Materials (Basel)*, vol. 8, no. 11, pp. 7988-7996.
- [6] Y. Wan, J. Luo, J. Xu, X Zhang, and H. Yu (2013). "Experimental study of surface roughness effects on wettability," in Proceedings of the International Conference on Manipulation, Manufacturing and Measurement on the Nanoscale, IEEE, Piscataway, pp. 97-100.
- [7] F. Hejda, P. Solar, and J. Kousal (2010). "Surface Free Energy Determination by Contact Angle," in WDS'10 Proceedings of Contributed Papers, Prague, Czech Republic, pp. 25-30.
- [8] J. W. Gooch (2011). *Encyclopedic Dictionary of Polymers*, 2nd ed. New York: Springer.
- [9] J. T. Simpson, S. R. Hunter, and T. Aytug (2015). "Superhydrophobic materials and coatings: A review," *Reports on Progress in Physics*, vol. 78, no. 8, p. 086501, July.
- [10] L. F. Wang and Z. D. Dai (2016). "Effects of the natural microstructures on the wettability of leaf surfaces," *Biosurface and Biotribology*, vol. 2, pp. 70-74.

# The Effects of Line Width Cross-Sectional Geometry to Stretchable Printed Circuit

N.H. Sobri<sup>1</sup>, N.S. Rozali<sup>1</sup>, M.A. Suhaimi<sup>1</sup>, M.Z. Azmi<sup>1</sup> and M.Z. Akop<sup>1,2,\*</sup>

<sup>1</sup>Faculty of Mechanical Engineering, Universiti Teknikal Malaysia Melaka, Hang Tuah Jaya, 76100 Durian Tunggal, Melaka, Malaysia.

<sup>2</sup>Centre for Advanced Research on Energy, Universiti Teknikal Malaysia Melaka, Hang Tuah Jaya, 76100 Durian Tunggal, Melaka Malaysia.

\*Corresponding e-mail: zaid@utem.edu.my

**Keywords:** Line width; conductive ink; stretchable printed circuit

**ABSTRACT** – The purpose of this study is to investigate the effects of line width cross-sectional geometry to stretchable printed. Four-point probes are used to measure resistivity of the conductive ink. Different width of ink was used. As a result, the higher width conductive ink content gave lower resistance than using lower width conductive ink content.

## 1. INTRODUCTION

Stretchable printed circuit board (SPCB) also known as elastic circuits or elastic electronics is a technology for building electronic circuits by depositing stretchable electronic devices and circuits onto stretchable substrates or embed them completely in a stretchable material. The structures are nevertheless exposed to mechanical stress and no wiring is required because of their elastic behaviour. It can eliminate wire connections failures and increase the reliability of the devices. There are many type of substrate that can be used in stretchable printed circuit. For this research Thermoplastic polyurethane (TPU) was used to conduct the experiment. There are many characteristic make TPU extremely popular across a range of application and market. For example is famed for many things including its ability to resist oil, solvents, chemical, grease and abrasion, its high elongation and tensile strength its elasticity and to varying degrees [1].

Conductive ink is the ink that can conduct electricity. As stated above, when used the substrate that flexible, no wiring is required as it replace to conductive ink to conducts electricity. Conductive inks are manufactured by blending conductive fillers with resin, solvents and additive. Fillers are usually pigments, which differentiate the graphic ink from the functional ink. Conductivity of ink depends largely on the amount of metal filler loaded in the ink, particle size of the fillers, percentage and quality of binder used and continuity of the printed layer after printing and drying [2].

There are several having various type of ink for conductive ink such as silver and carbon. In this research, carbon was used as conductive. Carbon inks are providing low friction and excellent thermal stability. The properties of carbon ink are good adhesion to different substrates, high mechanical and chemical resistance and favourable curing conditions (lowest possible curing temperature and short curing times) [3]. There are also chemically inert with low reactivity to solvent and other chemical. Carbon inks are very

resistant to flexing. It also is environmentally friendly. The objective of this study is to identify the sheet resistance due to width of ink. The resistance will measure by using four point probes.

## 2. RESEARCH METHODOLOGY

### 2.1 Sample Preparation

To run the experiment, there are four main components in screen printing which is commercialize carbon ink paste, cellophane tape for the pattern design, TPU as the substrate and razor blade as the squeegee which to spread ink paste through two lines of cellophane tape marked.

After all of them were prepared, the width on the glass slide or TPU was measured and placed the tape in the mark. Then, ink was slide until the end of the path by using razor blade as shown in Figure 2.1. Ink cure in room temperature before the resistance measure by using four point probes. Sample marked as shown in Figure 2.2 before measurement of resistivity.

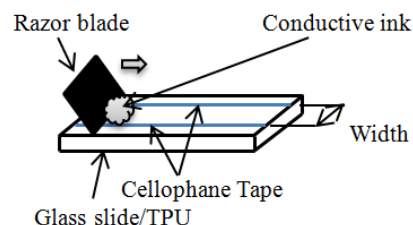


Figure 2.1 Illustration diagram printing process.

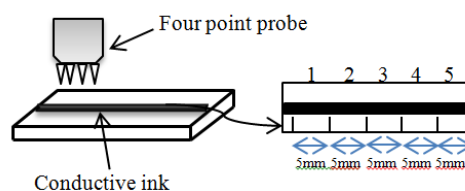


Figure 2.2 Marked sample.

## 3. RESULTS AND DISCUSSION

In this section, results from the resistance due to different width will be discussed in detail. The width that were investigates are 3mm, 6mm and 9mm. Based from, initially the width of the ink printed on the substrates is less than 1mm but the width dimension were change after few attempt on taking the data due to the ink does not attach on the substrate when measure with four point probe.

The reasons printing the conductive ink on the glass slides are to focusing the result on the effect of the different width of the conductive ink to the resistivity and be a baseline data for TPU. This is the result obtains from different width printing on glass slides and TPU by measured using four point probe.

Table 3.1 Glass slide as substrate

Width (mm)	Average Resistance (ohm/sq)
3	332.08
6	239.6
9	76.67

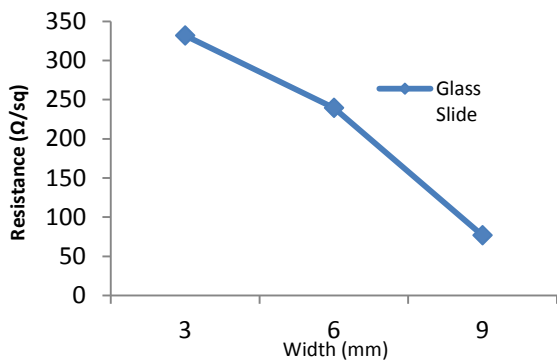


Figure 3.1: Glass slide as substrate

Based on Figure 3.1, the graph resistance versus width shown rapidly decrease. When width of ink increased the resistance value will be decrease. The lowest data and the highest data are 76.67Ω/sq and 332.08Ω/sq. The highest resistance occurs when the width measured at 3mm and the lowest resistance occurs when the width at 9mm. The resistance value for width 6mm is 239.6Ω/sq. The results shows obtain can be supported by previous journal from other researchers [4].

Table 3.2 TPU as substrate

Width (mm)	Average Resistance (ohm/sq)
3	410.36
6	266.31
9	177.53

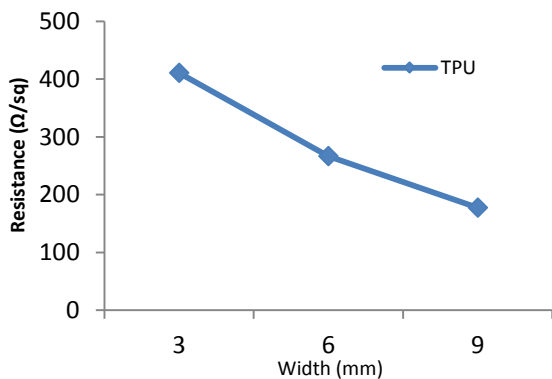


Figure 3.2: TPU as substrate

Based on graph in Figure 3.2, the pattern of the data of TPU is quite same with the glass slide data which is when the width of the ink increase, the reading of the sheet resistance will be the lowest. The pattern of the graph is constantly decreasing from the smallest width of conductive ink which is 3mm until the highest width taken as 9mm. As can be seen the highest sheet resistance is 410.39Ω/sq for width 3mm and the lowest sheet resistance is 177.5Ω/sq.

**4. SUMMARY**

The purpose of this study is to investigate the effects of line width cross-sectional geometry to stretchable printed. Obviously the decreases trend appears when width of ink increase. It can conclude that when the width of the ink increasing, the sheet resistance obtain will be decreasing.

**REFERENCES**

[1] Huntsman (2010).“A guide to thermoplastic polyurethanes (TPU),” *Huntsman*, p. 26.  
 [2] S. S. Bhore (2013).“Formulation and Evaluation of Resistive Inks for Applications in Printed Electronics,” pp. 1–94.  
 [3] A. Dipl, R. Dietrich, and D. J. Tekath, “Report 148 : Carbon-conductive inks – Fields of application and potential for rationalisation and cost reduction.”  
 [4] C. Phillips, A. Al-Ahmadi, S. J. Potts, T. Claypole, and D. Deganello (2017), “The effect of graphite and carbon black ratios on conductive ink performance,” *J. Mater. Sci.*, vol. 52, no. 16, pp. 9520–9530.

# The preparation and morphological investigation of polyacrylonitrile electrospun nanofibre with different loading of carbon nanotube

N.A. Munajat<sup>1</sup>, A.H. Nurfaizey<sup>1,2,\*</sup> and S. H. S. M. Fadzullah<sup>1,2</sup>

<sup>1</sup>) Faculty of Mechanical Engineering, Universiti Teknikal Malaysia Melaka, Hang Tuah Jaya, 76100 Durian Tunggal, Melaka, Malaysia

<sup>2</sup>) Centre for Advanced Research on Energy, Universiti Teknikal Malaysia Melaka, Hang Tuah Jaya, 76100 Durian Tunggal, Melaka, Malaysia

\*Corresponding e-mail: nurfaizey@utem.edu.my

**Keywords:** Electrospinning; nanofibre; polyacrylonitrile; carbon nanotube

**ABSTRACT** – Polyacrylonitrile (PAN) electrospun nanofibres with different loading of multi-walled carbon nanotube (MWCNT) were successfully prepared using electrospinning method. PAN powder was dissolved in dimethylformamide and the solution was electrospun under constant electrospinning parameters. The morphological structure and average fibre diameter of the nanofibres were examined using electron scanning microscopy. It was found that the solution with a higher content of MWCNT produced fibres with thicker fibre diameter. It was also observed that the surfaces of the fibres were rougher compared to control fibres. The results suggest that the inclusion of MWCNT reduced the electrospinnability of the PAN polymer solution.

## 1. INTRODUCTION

In the recent years, studies on conductive nanomaterials have gained a significant amount of interest from researchers due to their unique properties such as high surface area, high electrical conductivity and superior mechanical properties[1]. As a result, various new nanomaterials have been introduced and proposed for a wide range of applications in industries such as textile, composites, biomedical, aerospace, and electronic industries [2].

Electrospinning process is one of the most versatile and cost effective methods for preparing polymeric nanofibres [3]. A basic electrospinning setup consists of a high voltage power supply, polymer solution, spinneret tip and a grounded collector. The high voltage power supply is used to charge the polymer solution with a high amount of electrostatic forces, causing a jet of polymer to be ejected from the pipette tip flying towards the grounded collector. During the flight, fibre thinning process takes place which is due to stretching as the result of applied electric forces and solvent evaporation. The typical average fibre diameter is about 80 nm and the length was about higher than a kilometer [4].

Previously, filler materials have been incorporated to further enhance the properties of the nanofibres. For example, it was reported that a small addition of MWCNT into the nanofibre could improve the mechanical and electrical properties of the nanofibres [5]. However, the fabrication process of the fibre is quite challenging due to the hydrophobicity nature of the MWCNT. This could cause agglomeration of the solution and subsequently producing fibres with

defects such as beads and ribbons. The focus of this study was to investigate the effects of different MWCNT loading on morphological structure and fibre diameter of PAN electrospun nanofibres.

## 2. RESEARCH METHODOLOGY

### 2.1 Samples preparation

The PAN polymer which has an average molecular weight of 124,000-130,000 g/mol and N,N-Dimethylformamide (DMF) was purchased from Sigma Aldrich. The MWCNT used was an industrial-grade from Nanostructured & Amorphous Materials, Inc. (USA). A control PAN polymer solution was prepared by dissolving 10 wt% of PAN into N,N-Dimethylformamide (DMF) and stirred for 6 hours at room temperature using a magnetic stirrer model C-MAG HS7 (Ika Works, Malaysia).

The preparation of polymer solution with the addition of MWCNT was slightly different. Firstly, the MWCNT was added to the DMF and sonicated for 1 hour to break the bundles of MWCNT. After that, the solution was transferred to the magnetic stirrer to disperse the solution. PAN powder was added carefully by a small amount at a time to avoid agglomeration. The solution was stirred for 24 hours until a clear and homogeneous solution was obtained. Different weight percentage of the MWCNT were used to produce samples of NF1 to NF4, as shown in Table 2.1.

Table 2.1 Different weight percentage of MWCNT.

Sample	MWCNT concentration (wt.%)
NF 1	0.0 (control)
NF 2	0.3
NF 3	0.5
NF 4	1.0

The electrospun nanofibres were produced by using Electrospin Model ES1a (Electrospin Ltd., NZ). Throughout electrospinning process, the voltage was set at 18 kV whilst the distance between the spinneret to the collector was set at 13 cm. All the electrospun nanofibres collected were stored in vacuum for 24 hours to ensure the solvent has completely vaporized.

### 2.2 Samples characterization

Scanning electron microscope (SEM) Model JSM-5010PLUS/LV (Jeol Ltd., Japan) was used to examine the morphology of the fibres and ImageJ version 1.50

software (National Institutes of Health, USA) was used to measure fibre diameter based on the SEM micrographs.

### 3. RESULTS AND DISCUSSION

The as-spun electrospun nanofibre samples are showed in Figure 3.1. The NF 1 (control) sample appeared white in appearance. However, for NF 2, NF 3 and NF 4, the samples turned greyish. The darkest sample was NF 4 which contains the highest amount of MWCNT (1.0%).

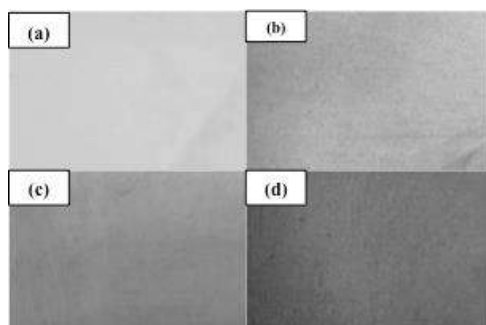


Figure 3.1 Physical appearance of as-spun electrospun nanofibre with different loadings of MWCNT (a) NF 1 (0.0%), (b) NF 2 (0.3%), (c) NF 3 (0.5%) and (d) NF 4 (1.0%), respectively.

SEM micrographs of electrospun nanofibres are showed in Figure 3.2. The average fibre diameters of the samples are presented in Table 3.1. It was clearly shown that the fibre diameter increased as the weight percentage of MWCNT increased.

Table 3.1 Different weight percentage of MWCNT.

Sample	Fibre diameter (nm)
NF 1	868.72±79.03
NF 2	1731.64±54.10
NF 3	2515.08±196.02
NF 4	2732.73±159.33

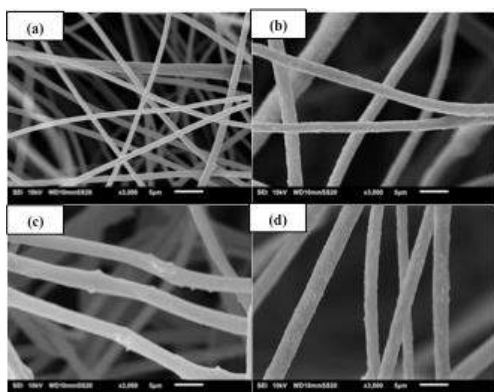


Figure 3.2 SEM image of electrospun nanofibre with a different weight percentage of MWCNT (a) NF 1, (b) NF 2, (c) NF 3 and (d) NF 4, respectively.

The control sample NF 1 produced smooth and uniform fibres (Figure 3.3). However, the formation of

beads was obvious as the amount of MWCNT increased.

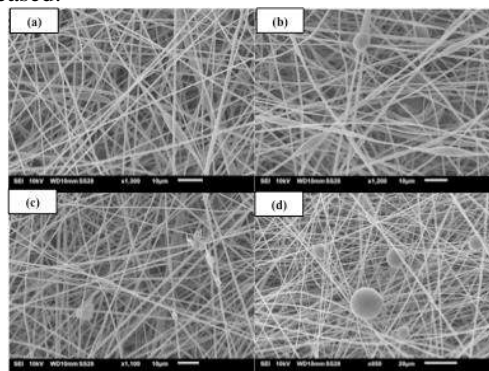


Figure 3.3 SEM image of deformation in electrospun nanofibre with a different weight percentage of MWCNT (a) NF 1, (b) NF 2, (c) NF 3 and (d) NF 4, respectively.

The results suggest that the electrospinnability of PAN solution was reduced as the amount of MWCNT increased. This is evidenced by the formation of thick fibres with rough surfaces and beads. Another reason for this was due to inhomogeneous dispersion of MWCNT of the PAN solution causing inconsistency in electrospinning process.

### 4. SUMMARY

In this study, MWCNT filled PAN electrospun nanofibres were prepared and investigated. The inclusion of MWCNT reduced the electrospinnability of the PAN polymer solution, producing thick and beaded fibres. Further studies on mechanical, chemical and electrical properties are needed to better understand the effects of MWCNT loading on the properties of the nanofibres.

### REFERENCES

- [1] J. K. Pandey (2015). *Handbook of Polymer Nanocomposites. Processing, Performance and Application*.
- [2] S. K. Nataraj, K. S. Yang, and T. M. Aminabhavi (2012). "Polyacrylonitrile-based nanofibers - A state-of-the-art review," *Prog. Polym. Sci.*, vol. 37, no. 3, pp. 487–513.
- [3] N. A. Munajat, A. H. Nurfaizey, S. H. S. M. Fadzullah, G. Omar, J. Jaafar, and N. S. A. Roslan (2017). "Fabrication and Characterization of Carbon Nanofibres from Polyacrylonitrile Precursor," no. March, pp. 1–2.
- [4] A. H. Nurfaizey, N. Tucker, J. Stranger, and M. P. Staiger (2012). "Functional nanofibers in clothing for protection against chemical and biological hazards," Woodhead Publishing, pp. 62–86.
- [5] H. Guo, M. L. Minus, S. Jagannathan, and S. Kumar (2010). "Polyacrylonitrile/carbon nanotube composite films," *ACS Appl. Mater. Interfaces*, vol. 2, no. 5, pp. 1331–1342.

# Effect of the contact angle between mass and finite rod in transverse vibration using Laminated Rubber-Metal Spring (LR-MS) Model for automotive absorber

S.R. Ruslan<sup>1</sup> and M.A. Salim<sup>1,2,\*</sup>

<sup>1</sup>Faculty of Mechanical Engineering, Universiti Teknikal Malaysia Melaka, Hang Tuah Jaya, 76100 Durian Tunggal, Melaka, Malaysia

<sup>2</sup>Centre for Advanced Research on Energy, Universiti Teknikal Malaysia Melaka, Hang Tuah Jaya, 76100 Durian Tunggal, Melaka, Malaysia

\*Corresponding e-mail: azli@utem.edu.my

**Keywords:** Laminated rubber metal-spring, vibration, suspension system

**ABSTRACT** – This paper presents the effect of the contact angle between mass and finite rod in transverse vibration using LR-MS model for automotive absorber. The mathematical model for transmissibility are developed by using two different approaches. The first approach using assumption of massless suspension absorber where the system are modelled by using spring and damper. The second approach employs the impedance technique that derived from wave propagation method. The contact angle will effect to the transmissibility graph either offset to upper or lower side. Furthermore, the parametric study also been discussed in this paper in order to get the transmissibility correlation.

## 1. INTRODUCTION

The suspension demonstrations in the axial direction as well as in the transverse direction. Since the transverse solidness is not unbounded, the system has a resonance in the transverse direction and the transverse movement at this frequency causes an undesired sensor yield and this blunder in the alignment. Then, by using the transverse vibration model, there need to consider the longitudinal excitation, orientation of moment and also wave effect [1-3]. The equation of motion and the free-vibration solution of the system are found by assuming the mass, damping and stiffness of the system in harmonic motion. Additionally, the governing equation of automotive absorber in transverse direction had been developed using wave propagation method. In addition, the wave effect is proposed with the purpose of making comparison with previous model [4-5].

## 2. RESEARCH METHODOLOGY

This study is focused on the mathematical model technique that can be utilized for finding estimated answer for transverse vibration issues for the suspension system. This technique utilized for create suspension model and recreate the transmissibility performance in transverse vibration [6]. Another working hypothesis brought up in this research is that the whole suspension system can be changed into finite rod system, by the end goal to get the contact angle relationship between mass and finite rod for LR-MS model. It was present a study on the effects of contact angle by changing its parameters where four important parameters are evaluated, which are mass density, young's modulus,

length of suspension absorber and radius of finite rod. Figure 2.1 shows the partial displacement in finite rod model and Figure 2.2 shows the transmissibility comparison between lumped parameter and transverse model for single degree-of-freedom system, respectively.

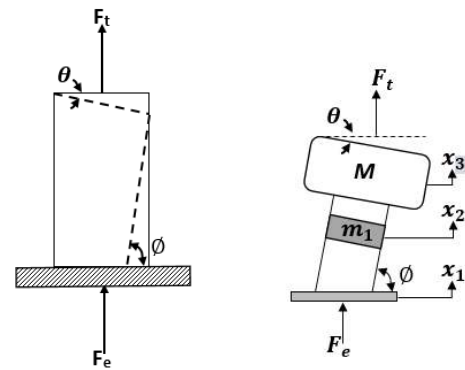


Figure 2.1: Partial displacement in finite rod model

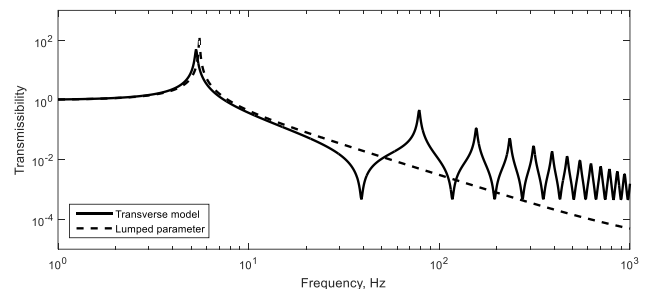


Figure 2.2: Transmissibility comparison between lumped parameter and transverse model for single-degree-of-freedom

The equation of motion of the mathematical model can be represented as

$$Z_{11} = \frac{2EIk_b^3 \cos(k_b L) \cosh(k_b L)}{j\omega(\sin(k_b L) \cosh(k_b L) - \cos(k_b L) \sinh(k_b L))} \quad (1)$$

$$Z_{22} = \frac{EIk_b^3 (1 + \cos(k_b L) \cosh(k_b L))}{j\omega(\sin(k_b L) \cosh(k_b L) - \cos(k_b L) \sinh(k_b L))} \quad (2)$$

$$Z_{12} = Z_{21} = \frac{EIk_b^3 (\cos(k_b L) + \cosh(k_b L))}{j\omega(\sin(k_b L) \cosh(k_b L) - \cos(k_b L) \sinh(k_b L))} \quad (3)$$

The transmissibility for the transverse vibration in the impedance equation:

$$T_\gamma = \left| \frac{F_t}{F_e} \right| = \left| \frac{-\omega^2(M)x_1 + j\omega(Z_{11}^{(1)}x_1) - j\omega(Z_{12}^{(1)}x_2)}{-j\omega Z_{21}^{(2)}x_2} \right| \quad (4)$$

The relationship of contact angle between mass and finite rod is

$$T_\gamma = \frac{F_t \times \left( \frac{\theta\pi}{180} \right)}{F_e \times \left( \frac{\phi\pi}{180} \right)} \quad (5)$$

For the rotation angle, there have two which are represented in Table 2.1 and 2.2.

Table 2.1: Fixed value of  $\theta$ , variable value of  $\phi$

$\theta$	$\frac{\theta\pi}{180}$ (rad)	$\phi$	$\frac{\phi\pi}{180}$ (rad)
5°	0.08727	5°	0.08727
5°	0.08727	10°	0.17453
5°	0.08727	15°	0.26180
5°	0.08727	20°	0.34907
5°	0.08727	25°	0.43633
5°	0.08727	30°	0.52360

Table 2.2: Fixed value of  $\phi$ , variable value of  $\theta$

$\theta$	$\frac{\theta\pi}{180}$ (rad)	$\phi$	$\frac{\phi\pi}{180}$ (rad)
5°	0.08727	5°	0.08727
10°	0.17453	5°	0.08727
15°	0.26180	5°	0.08727
20°	0.34907	5°	0.08727
25°	0.43633	5°	0.08727
30°	0.52360	5°	0.08727

### 3. RESULTS AND DISCUSSION

The results for this study shows in Figures 3.1 and 3.2. According to these two figures, it shows that by increasing the frequency, the transmissibility going near to the unity, and by increasing the frequency, the anti-resonance peaks were appeared in small gap.

In addition, when the angle  $\theta$  increase ( $\phi$  fix at 5°) the transmitted force is greater than excitation force. In others word, the transmissibility is greater than 1. Next, if the angle  $\phi$  increase ( $\theta$  fix at 5°) the transmitted force is less than excitation force, indicate the effective isolation for the system. The value of natural frequency are same at any angle combination. That mean, the contact angle ( $\theta, \phi$ ) only effect to the value of transmissibility which is offset to upper or lower side. Four parameters were taken into accounts which are density, young's modulus, length of suspension absorber and radius of finite rod. From the density analyses, there are show that the natural frequency still at same value (6.25Hz) even the value of density increased. The natural frequency will increased when the young's

modulus increased. The resonance frequency shift right due to the effect of the elastic properties. The natural frequency will decreased when the length is increased. When the radius increased, the natural frequency had also increased

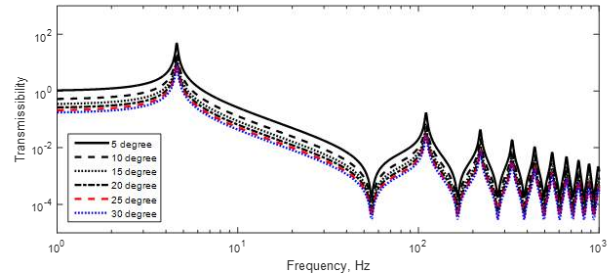


Figure 3.1: Transmissibility for variable value of  $\phi$

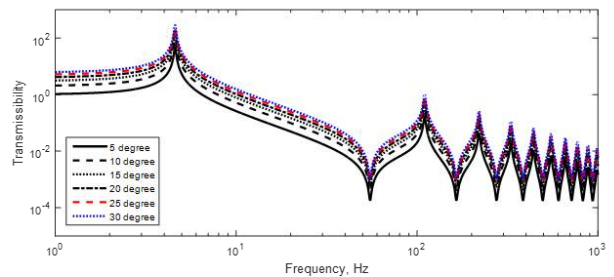


Figure 3.2: Transmissibility for variable value of  $\theta$

### 4. SUMMARY

At the end of this study, several conclusion were obtained. Generally, the study of transverse vibration model has provided some basic theory and understanding on how it influences the performance of the suspension absorber.

### REFERENCES

- [1] Agharkakli, A., Sabet, G. S., and Barouz, A. (2012). Simulation and Analysis of Passive and Active Suspension System Using Quarter Car Model for Different Road Profile. *International Journal of Engineering Trends and Technology*, Vol. 3 (5), pp. 636-644.
- [2] Parekh, A., Kumbhar S. B. and Joshi, S. G. (2014). Transmissibility Analysis of a Car Driver's Seat Suspension System with an Air Bellow Type Damper. *International Journal on Recent Technologies in Mechanical and Electrical Engineering*, Vol. 1 (3), pp. 12– 19.
- [3] Forsen, A. (1997). Road-Induced Longitudinal Wheel Forces in Heavy Vehicles. Sae Transactions, Paper No. 973260.
- [4] Oluwole O. O. (2012). Matlab and Simulink Use in Response Analysis of Automobile Suspension System in Design. *International Journal of Traffic and Transportation Engineering*, Vol. 1 (2), pp.19-31.
- [5] Ungar, E. E. (1991). Equality of Force and Motion Transmissibilities. *Journal of the Acoustical Society of America*, Vol. 90(1), pp. 596-597.
- [6] Galanti, F. (2013), Modelling, Simulation and Control For A Skyhook Suspension. *Journal of Automotive*. pp 1-39





1<sup>st</sup> Colloquium Paper:

# ADVANCED MATERIALS AND MECHANICAL ENGINEERING RESEARCH (CAMMER'18)



PENERBIT UTeM Press  
Website : [www.utm.edu.my/penerbit](http://www.utm.edu.my/penerbit)  
Books Online : [utembooks.utm.edu.my](http://utembooks.utm.edu.my)  
Email : [penerbit@utm.edu.my](mailto:penerbit@utm.edu.my)

ISBN 978-967-2145-13-4



9 789672 145134